MERLIN/*NF2*-MEDIATED TUMOR SUPPRESSION: FROM MECHANISM TO TRANSLATION

A Dissertation

Presented to the Faculty of the Weill Cornell Graduate School

Of Medical Sciences

in Partial Fulfillment of the Requirements for the Degree of

Doctor of Philosophy

by

Jonathan Eric Cooper

February 2016

MERLIN/*NF2*-MEDIATED TUMOR SUPPRESSION: FROM MECHANISM TO TRANSLATION

Jonathan Eric Cooper, Ph.D.

Cornell University 2016

The FERM domain protein Merlin, encoded by the *NF2* tumor suppressor gene, regulates cell proliferation in response to adhesion signaling. The growth inhibitory function of Merlin is induced by intercellular adhesions and inactivated by joint integrin/receptor tyrosine kinase signaling. Merlin contributes to the formation of cell junctions in polarized tissues, activates anti-mitogenic signaling at tight-junctions, and inhibits oncogenic gene expression. Thus, inactivation of Merlin causes uncontrolled mitogenic signaling and tumorigenesis. The underlying molecular mechanisms driving Merlin's tumor suppressive functions have remained largely elusive since its discovery over two decades ago. We show that Merlin's predominant tumor suppressive functions are attributable to its inhibition of the $CRL4^{DCAF1}$ E3 ubiquitin ligase in the nucleus. These findings are supported using *in vitro* and *in vivo* binding assays, multiple lines of genetic evidence, *in vitro* mouse models, and freshly explanted NF2 patient samples. We subsequently show that Merlin's nuclear translocation and inhibition of $CRL4^{DCAF1}$ suppresses inhibition of the Hippo tumor suppressor pathway kinases Lats1 and 2. Merlin's inhibition of $CRL4^{DCAF1}$ therefore promotes inhibition of the YAP and TAZ transcriptional coactivators and abrogates oncogenic signaling. I further develop a conditional *Dcaf1* allele to assess the *in vivo* role of $CRL4^{DCAF1}$ in

Merlin-deficient mouse models. A rapid non-germline genetically engineered mouse model using fetal liver progenitor cells shows that DCAF1 is necessary for Merlin-deficient tumorigenesis. However, *Dcaf1* deletion in the adult liver exacerbates hepatomegaly and tumorigenesis, which likely stems from the expansion of a bipotential hepatobiliary niche. I also set out to develop a rapid malignant pleural mesothelioma (MPM) mouse model using virally delivered constructs to simultaneously recombine conditional alleles and inhibit or somatically mutate cooperating tumor suppressors. Finally, I show that $CRL4^{DCAF1}$ inhibition using the NEDD8 Activating Enzyme inhibitor MLN4924 reduces oncogenic signaling in Merlin-deficient MPM. Combining MLN4924 with traditional chemotherapy or mechanism-based therapy significantly delays the growth of Merlin-deficient MPM, a cancer that is highly refractory to standard chemotherapeutics. These latter findings support the use of MLN4924 in combination with mTOR/PI3K inhibitors for the treatment of Merlin-deficient tumors.

BIOGRAPHICAL SKETCH

Jonathan Cooper was born in 1984 in Livingston, New Jersey, close to his home town of West Caldwell. Jon became interested in science at a young age due to the influence of his father, Alan, a medicinal organic chemist. Jon also received formative inspiration from the popular science fiction series *Star Trek: The Next Generation*, which glamorized the concepts of exploration and scientific pursuit. In high school, Jon's interests shifted towards molecular and cellular biology when he attended the Waksman Student Scholars Program, a summer research program at Rutgers University. From then on, Jon focused strongly on pursuing research, which he promptly took up while attending Lehigh University. While working as an undergraduate researcher in the laboratory of Dr. Colin Saldanha at Lehigh University's Department of Biological Sciences, Jon became more familiar with the techniques necessary to ask and address scientific questions. After receiving a Bachelors of Science in Molecular Biology, Jon continued his exploration of biology at Weill Cornell Graduate School of Biomedical Sciences, where he soon joined the laboratory of Dr. Filippo Giancotti in the Cell Biology Program at the Sloan Kettering Institute. There, Jon studied the molecular pathogenesis of *NF2/*Merlin-deficient tumorigenesis.

This work is dedicated first and foremost to my family who always motivated me to effectively pursue my goals, my friends and colleagues for providing personal and professional support, the teachers and mentors who shaped my scientific trajectory, and Ralitsa for being a source of pragmatic optimism and sometimes baked goods.

ACKNOWLEDGEMENTS

I'd like to thank my advisor and mentor Dr. Filippo Giancotti for his unconditional support and guidance throughout my graduate career. My thesis work would not have been possible without the help and support from my special committee members Drs. Xuejun Jiang, Michael Overholtzer, and Pengbo Zhou. I would also like to thank Dr. Wei Li for serving as a mentor and courteous colleague who helped guide me in our shared endeavors and my development as a scientist.

Current and past members in the Giancotti lab have made for a collaborative and fun atmosphere. I'd like to especially thank Dr. Kelly Gillen and Mayur Gadiya for being comrades in times of need, Drs. Young-Mi Kim and Javier Otero for being excellent listeners and sources of wisdom, and Drs. Goutam Chakraborty and Surajit Sinha for always being candid with scientific advice. I would like to thank Dr. Hediye Erdjument-Bromage for providing an optimistic perspective and an open-door policy. Lastly, I'd like to thank Dr. Andy Koff for guiding my progress as a graduate student at several milestones.

This work was supported by a NIH T32 Molecular and Cellular Biology Training Grant, P30 CA08748 (to MSKCC), and R01 CA152975 (to Filippo Giancotti).

TABLE OF CONTENTS

LIST OF FIGURES

LIST OF TABLES

Chapter One

Introduction

1.1: A primer on *NF2*/Merlin

The ability of normal cells to survive and proliferate is dictated by environmental cues including intercellular and matrix adhesions as well as the presence of growth factors. Normal cells undergo growth arrest when detached from the extracellular matrix or when they come into contact with adjacent cells and form intercellular junctions (1). Neoplastic cells evade contact inhibition of proliferation, which leads to the disruption of tissue organization - a distinguishing event in cancer (2). The *NF2* (Neurofibromatosis Type 2) tumor suppressor gene encodes the FERM (4.1 protein/Ezrin/Radixin/Moesin) domain protein Merlin, which is coordinately regulated by intercellular adhesion and attachment to the extracellular matrix (3-7). Cadherin engagement inactivates PAK, causing an accumulation of the active, dephosphorylated form of Merlin. Notably, since integrin attachment to the extracellular matrix activates PAK, Merlin can therefore be regulated independently of contact-mediated signaling events (7).

Neurofibromatosis type 2 patients carry a single mutated *NF2* allele and develop a highly specific subset of central and peripheral nervous system tumors. NF2-associated tumors include schwannomas, meningiomas, and ependymomas, which arise from the Schwann cells comprising the myelin sheath surrounding sensory and motor neurons, arachnoid cap cells within the arachnoid villi in the meninges, and ependymal cells lining the CSF-filled

ventricles of the brain and central spinal canal, respectively. In addition to the autosomal dominant NF2 disorder, non-germline Merlin deficiency is a driving force in sporadic occurrences of nearly all vestibular schwannomas, a majority of meningiomas, and a notable fraction of ependymomas. Moreover, Merlin was found to be inactivated in a large proportion of malignant mesotheliomas (8, 9) and to a lesser extent in other solid tumors (10-13).

Due in large part to Merlin's high sequence homology to the ERM (Ezrin/Radixin/Moesin) family of cytoskeletal linker proteins (Figure 1.1), it was widely assumed that Merlin suppresses mitogenic signaling at the cell cortex to mediate contact inhibition and tumor suppression (14). Active Merlin suppresses Rac-PAK signaling (7, 15-17), restrains activation of mTORC1 independently of Akt (18, 19), inhibits PI3K-Akt and FAK-Src signaling (20, 21), and negatively regulates the EGFR-Ras-ERK pathway (22, 23). However, the mechanisms by which Merlin inhibits these pathways remain unclear, and furthermore, the relative contribution of these pro-mitogenic signals to various Merlin-deficient malignancies is unknown. Interestingly, Merlin activates the Hippo tumor suppressor pathway to suppress the transcriptional coactivators YAP/TAZ in mammals or the *Drosophila* ortholog Yorkie, revealing a conserved role for Merlin in regulation of organ size, stem cell behavior, and cell proliferation (24-26). Notably, few germline or somatic mutations of Hippo pathway components have been discovered in human tumors - the exception being Merlin, which remains as one of the only bona fide tumor suppressors in the Hippo pathway (27).

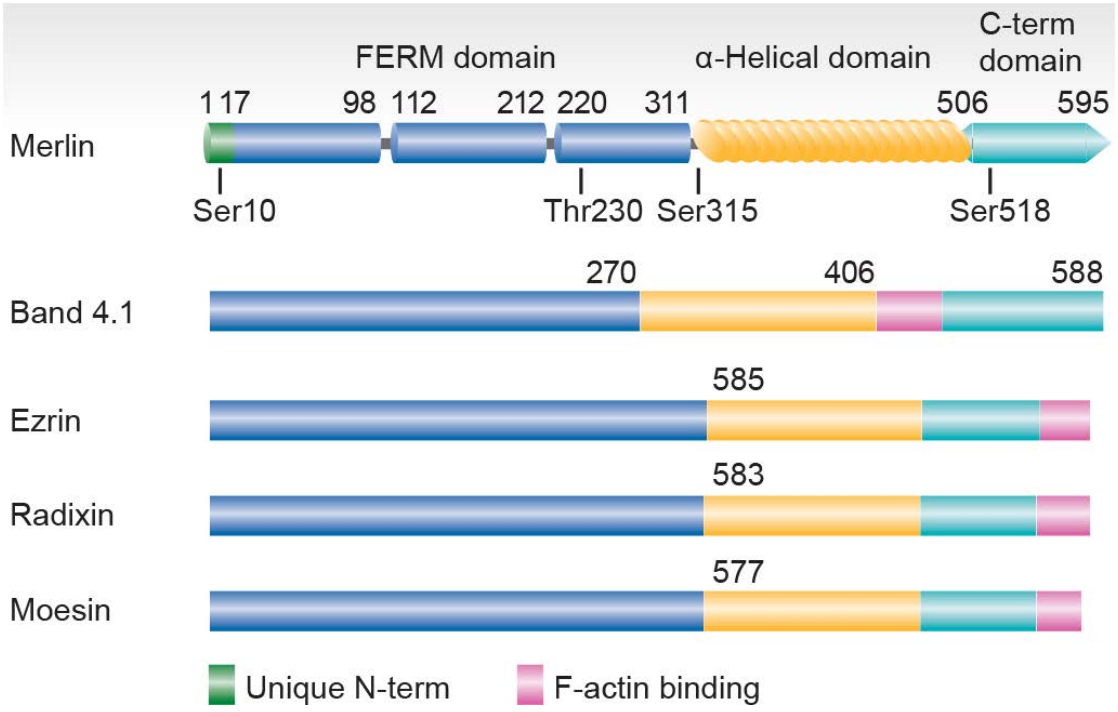

Figure 1.1: Overview of Merlin and ERM domain organization
Merlin and other canonical ERM proteins have a similar domain organization consisting of an N-terminal FERM domain that is divided into three subdomains. The following 150-200 residues consist of an α-helical rich coiled coil domain, and the proteins terminate with a hydrophilic tail. Whereas canonical ERM proteins contain an actin-binding carboxy-terminal ERM-associated domain (C-ERMAD; purple), Merlin contains no canonical actin-binding domain and, further, has an extended N-terminal 17 residues (green) unique among ERM proteins, illustrating divergent functions with other ERM proteins. Merlin's phosphorylation sites are indicated.

Post-translational modification of Merlin is vitally important to its conversion between dormant and growth-inhibitory states, where the dephosphorylated and more open state is now considered to be active in contact inhibition and tumor suppression (28). However, without crystallographic analyses of full-length Merlin in both its active and inactive conformations, structural inferences drawn from biochemical experiments must be approached with caution. Apropos of the myriad upstream signals and modifications affecting Merlin, the downstream biochemical functions of Merlin have been the subject of intensive research for over two decades, yet a consensus mechanism for Merlin's function in normal tissues has not been reached. It is becoming apparent that Merlin functions primarily in two branches – contact inhibition of proliferation and tumor suppression. Although these branches are naturally intertwined, the distinct locations of Merlin function and respective interactors in those subcellular compartments lend credence to a concept of a bimodal function.

Recent studies among the ever-increasing breadth of NF2 literature have revealed important high-affinity interactors governing Merlin's biochemical function. Notably, Merlin regulates tight junction-associated Angiomotin to inhibit Rac signaling (29), and nuclear-localized Merlin inhibits the $CRL4^{DCAF1}$ E3 ubiquitin ligase to suppress oncogenic gene expression (30). Moreover, Merlin's regulation of YAP/TAZ is a burgeoning and highly provocative field due to the multifarious roles of Hippo signaling in organ growth, stem cell maintenance, and cancer. Recent studies have also shed light on Merlin's conformational changes that regulate its intramolecular associations and downstream signaling, providing

fundamental insight into Merlin's regulation and biochemical function. In this chapter, we will explore Merlin's rich biochemical background and examine new insights that are shaping our understanding of Merlin's role in normal biology and how its loss leads to the deregulation of a multitude of signaling pathways leading to tumorigenesis.

1.2: The *NF2* gene

NF2 maps to the long arm of chromosome 22 and encodes two Merlin isoforms. The longer, dominant Merlin isoform 1 (Merlin-1 or Merlin), has an extended carboxy-terminal tail that is encoded by exon 17 (Figure 1.2). Merlin isoform 2 (Merlin-2), on the other hand, contains the alternatively spliced exon 16 which ends in a stop codon, encoding 11 unique residues following amino acid 579 as compared to Merlin-1 (10). Notably, Merlin-2 lacks carboxy-terminal residues required for intramolecular binding between the amino-terminal FERM domain and the carboxy-terminal tail, possibly leading to a constitutively open conformation (31, 32). Recent studies have found that Merlin-2 inhibits cell proliferation and attenuates downstream mitogenic signaling to the same extent as Merlin-1 (28, 33). Recent mouse genetics studies comparing *Nf2* isoform 1 and isoform 2 knockout animals revealed Merlin-1 and Merlin-2 are both fully functional tumor suppressors since knockout of either singly does not result cause tumorigenesis (34).

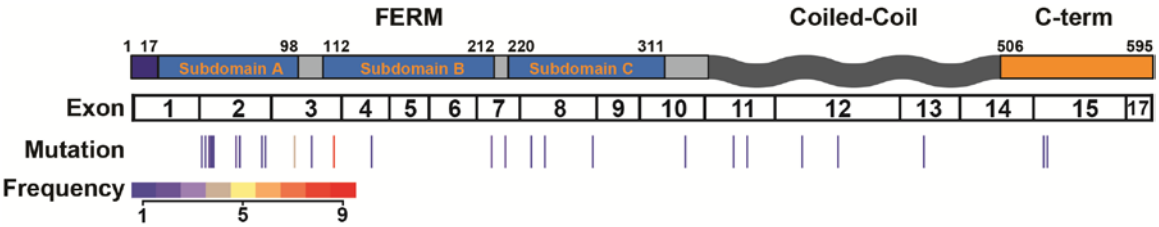

Figure 1.2: Merlin structure and overview of pathogenic mutations

Merlin is a 595-residue protein divided into three structurally distinct regions – an amino-terminal FERM domain, an α-helical coiled-coil domain, and a carboxy-terminal hydrophilic tail. Merlin's FERM domain is further subdivided into three globular subdomains. *NF2* encodes 16 exons, terminating with exon 17 in the canonical Merlin isoform. The positions of patient-derived missense mutations or single residue deletions are indicated below the exon schematic, with mutation frequency indicated by a heat map. Either these mutations underlie NF2 tracked within a family, were found in two or more unrelated patients, or experimental evidence was obtained to confirm their pathogenicity. Mutational data were obtained from Ahronowitz *et al*, 2007 (35) and Li *et al*, 2010 (30).

1.3: Merlin protein structure and intramolecular association

The biochemical functions of Merlin are imparted by three mechanisms - post-translational modification, localization, and interaction with downstream effectors. Merlin is composed of a globular amino-terminal FERM domain and a carboxy-terminal hydrophilic tail joined by a flexible coiled-coil segment, displaying structural resemblance to the FERM domain-containing ERM proteins (Figure 1.1) (36, 37). This resemblance is most apparent in the first 300 residues of Merlin's FERM domain, which share ~65% sequence identity with canonical ERMs. However, Merlin has several notable differences in its primary sequence that distinguish it in form and function from its ERM counterparts. Merlin's amino-terminus contains a 7-residue conserved Blue box motif and 17 unique amino-terminal residues (38, 39). Importantly, Merlin lacks a canonical actin-binding motif that is otherwise conserved among ERMs and paramount to their function at the cortical cytoskeleton (14).

A central mechanism in Merlin and ERM function is the formation of homo- and heterotypic interactions that regulate their activity. The majority of ERMs within cells are held in a dormant state imparted by an intramolecular association between the FERM domain and the C-terminal tail (40-42). Disruption of this association and subsequent activation is achieved by phosphorylation of an ERM C-terminal threonine residue by Rho kinase (Figure. 1.3). Active ERMs bind to cytoplasmic domains of cell-adhesion receptors such as CD44 and ICAM via their FERM domains while their C-termini interact with and regulate the cortical actin cytoskeleton (43, 44). Furthermore, once opened, active ERM proteins may

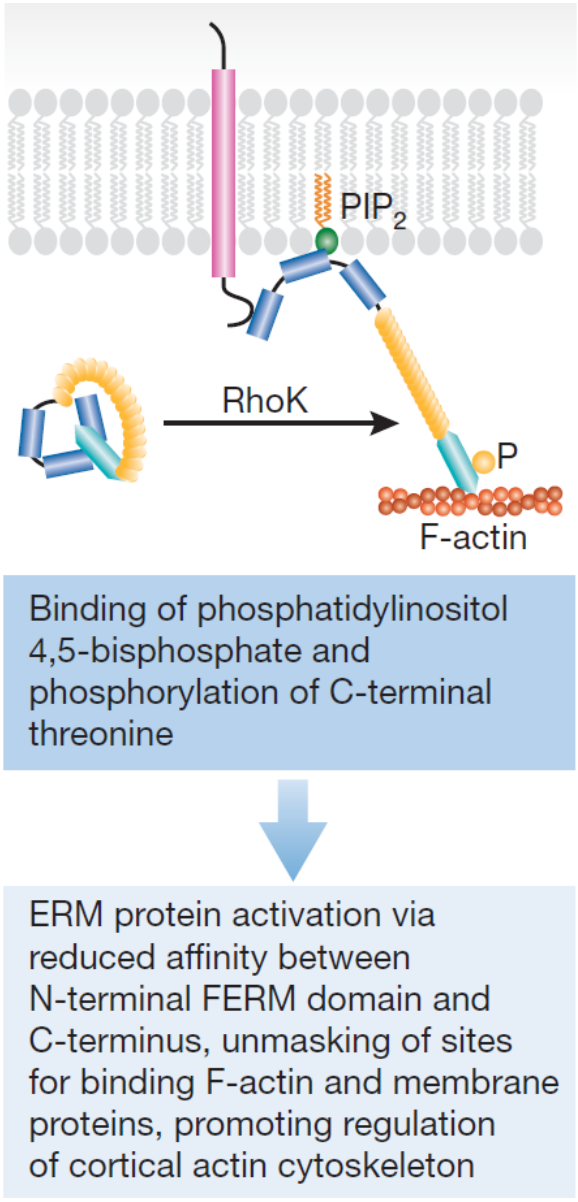

Figure 1.3: Phosphoregulation of ERM proteins
Canonical ERM proteins are maintained in an inactive state by intramolecular interaction between the C-terminal tail and FERM domain. Phosphorylation of a c-terminal threonine by Rho kinase - which may be aided by recruitment to membrane regions rich in phosphatidylinositol 4,5-bisphosphate - activates canonical ERM proteins by disrupting the head-to-tail interaction.

form interactions amongst themselves and with Merlin (40). Merlin's intramolecular associations and subsequent activation states have been a subject of intensive study for nearly 20 years (28, 31, 32, 41, 45-47), yet a consensus model to explain the relationship between its phosphorylation and interdomain binding in the context of seemingly contrary genetic evidence has only recently been uncovered.

It is well established that Merlin switches from an active state to an inactive state by phosphorylation at serine 518 (Figure 1.4A) (48). Phospho-mimetic (S518D) or phospho-deficient (S518A) permutations strongly correlate with Merlin's growth-permissive or growth-inhibitory functions, respectively (28, 30, 49). Essentially, serine 518 phosphorylation acts as a binary switch in which dephosphorylated Merlin functions in adhesion signaling while phosphorylated Merlin remains dormant, although studies within the last five years have shown this to be an oversimplified interpretation. Several lines of evidence suggest that Merlin exists in multiple states that vary between "fully open" and "fully closed" forms which are regulated primarily by S518 phosphorylation, and moreover, FRET studies reveal that Merlin's FERM domain and carboxy-terminus are constitutively held in close proximity, undergoing only subtle changes upon post-translational modification (28, 50). A classic study found that Merlin-2 – which lacks the carboxy-terminal residues necessary for intramolecular interaction – is unable to function in contact inhibition or tumor suppression (31). This

Figure 1.4: Adhesion-mediated regulation of the Merlin activation cycle
(**A**) In proliferating cells, integrin-mediated anchorage to the cell matrix and stimulation of receptor tyrosine kinases (RTKs) activate Rac, in turn activating PAK and leading to phosphorylation of Merlin at Serine 518. In response to high cyclic AMP levels, PKA also phosphorylates Merlin at serine 518. Serine 518 phosphorylation increases the interdomain binding between Merlin's carboxy-terminus and FERM domain, maintaining Merlin in a more closed, inactive form.
(**B**) Conversely, in contact-inhibited cells, dephosphorylated Merlin accumulates as a result of intercellular adhesions which lead to PAK inhibition. Merlin may also be activated via MYPT1-mediated dephosphorylation.

A

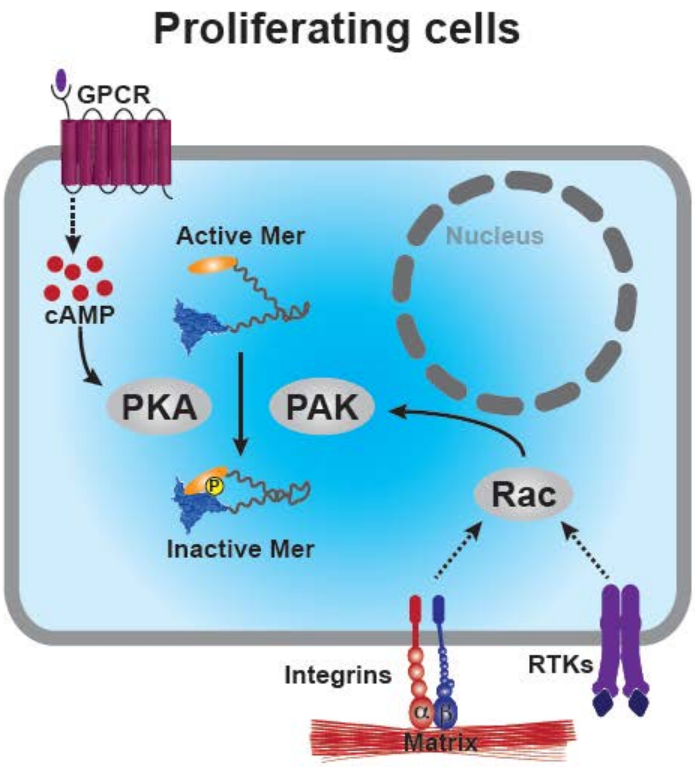
Proliferating cells
GPCR
Active Mer
Nucleus
cAMP
PKA
PAK
Rac
Inactive Mer
Integrins
RTKs
Matrix

B

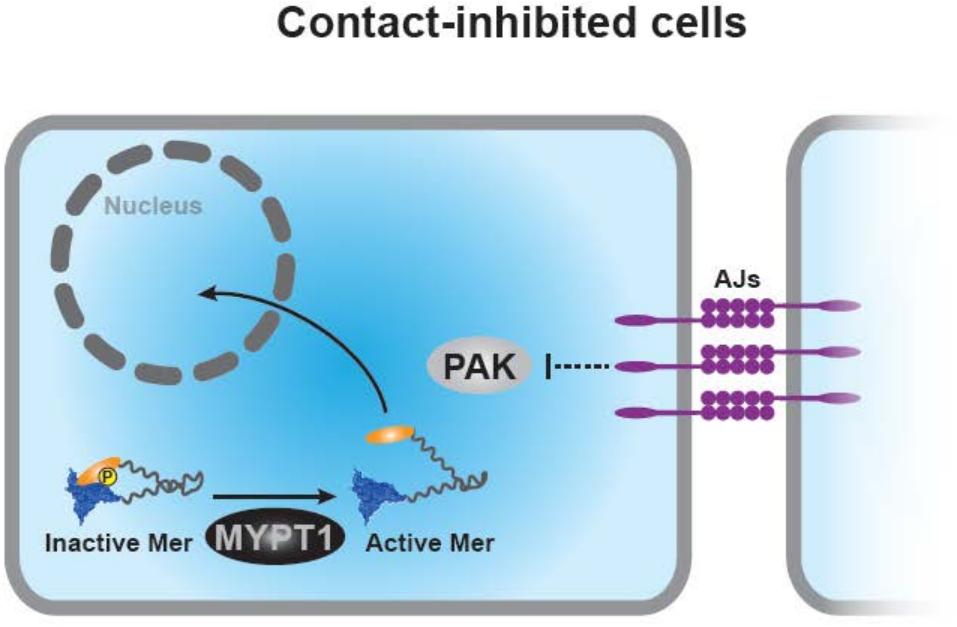
Contact-inhibited cells
Nucleus
AJs
PAK
Inactive Mer
MYPT1
Active Mer

observation led to a hypothesis that was held for over a decade positing that dephosphorylated and active Merlin functions in a closed conformation.

Recently, two independent laboratories found that Merlin-2 suppresses growth in mammalian cell lines, suggesting that interdomain binding is dispensable for Merlin's adhesion signaling (28, 33). Through comprehensive biochemical investigation, Anthony Bretscher's group reported that phosphorylated Merlin displays higher interdomain binding and that Merlin therefore inhibits cell growth in its open state (28). These results are underscored by the observation that a stably closed Merlin mutant does not suppress cell growth, whereas Merlin-2 and the S518A mutant - which are both defective in interdomain binding and therefore more open - suppress growth to the same extent as wild-type Merlin. Cumulatively, these results reveal that S518 phosphorylation and mutations that cause Merlin to become more closed result in decreased growth inhibition, whereas more open forms of Merlin – those that are increasingly defective in interdomain binding – are more active in growth inhibition. This finding contributes greatly to a consensus of Merlin structure and function as it relates to normal biology and tumor suppression, resolving a decade-old schism between biochemical observations and in vivo genetic studies.

Biochemical studies have provided essential insight into Merlin's conformational changes and resulting activation, which are now largely corroborated by genetic data. Most patient-derived truncations and a vast majority of non-truncating mutations occur within the FERM domain (Figure 1.2),

lending credence to its quintessential role in anti-mitogenic signaling and tumor suppression (35). Initially discovered in *Drosophila*, the “Blue box motif” is a conserved region within the FERM subdomain F2 corresponding to residues 177-183 in human Merlin. Substitution of these residues with alanines imparts loss of contact inhibition and promotes tumorigenesis in NIH-3T3 cells (51). Mutations in the Blue box act in a dominant negative manner in both *Drosophila* and mammals, displaying the importance of the FERM domain in Merlin’s tumor suppressive function. As compared to the FERM domain, mutations are scarce in Merlin’s carboxy-terminal tail and are dramatically reduced in the central α-helical domain, again implying that Merlin’s downstream tumor suppressive functions are imposed by the FERM domain (Figure 1.2) (35). Notably, replacement of Merlin’s F2 subdomain with that of the ERM protein Ezrin abolishes its growth suppressive activity, while individual or combined replacement of subdomains F1 and F3 do not affect proliferation (33). These results imply that subdomain F2 of Merlin’s FERM domain is largely responsible for Merlin’s growth inhibitory effects. Truncating mutations correlate with increased NF2 severity and predominate among NF2 patients, while missense mutations – although more rare - allow for a more systematic interpretation of Merlin’s biochemical role in tumor suppression. Merlin’s FERM domain interacts directly with the $CRL4^{DCAF1}$ E3 ubiquitin ligase, inhibiting its ubiquitylation activity and downstream oncogenic signaling. Multiple patient-derived missense mutants, including those mapping to subdomain F2, are defective in $CRL4^{DCAF1}$ interaction, despite the fact that some of these mutations were predicted to cause little structural perturbation (30, 37).

Recent biochemical insights combined with more than a decade of patient-derived genetic data provide crucial insight into Merlin's normal biochemical function and role in tumor suppression. Merlin's α-helical domain and carboxy-terminus function in maintaining Merlin in an inactive conformation during normal biological function, and may further be necessary for functions underneath the cell cortex in the organization of cell junctions and in contact inhibition. However, while interdomain binding is an important part of Merlin's regulation and normal cellular functions, the overall structure and specific protein-interacting domains within Merlin's amino-terminal FERM domain are essential for contact inhibition and tumor suppression.

1.4: Post-translational modification of Merlin

Merlin is regulated by multiple post-translational modifications downstream of an ever-expanding array of intracellular and extracellular cues. Receptor tyrosine kinases and integrins relay pro-mitogenic signals by activating CDC42 and Rac, which in turn activate p21-activated kinase (PAK) (Figure 1.4A). Activated PAK directly phosphorylates Merlin at serine 518, leading to an increase in carboxy-terminal association with the FERM domain and subsequent inactivation, presumably through masking of protein-interacting domains on the FERM domain which are necessary for downstream signaling or occlusion of a nuclear localization signal (30, 36). Since Merlin has a long half-life within cells, it is a compelling hypothesis that phosphatases exist to dephosphorylate Merlin at serine 518 and dynamically control levels of the dephosphorylated active form.

MYPT1-PP1δ (MYPT1) is a phosphatase that was shown to dephosphorylate Merlin (22) (Figure 1.4B), and recent evidence revealed that it may be inhibited by Integrin-linked kinase (ILK) (52). It remains to be determined whether MYPT1-mediated Merlin activation via dephosphorylation is a major mechanism in NF2 pathogenesis and Merlin-deficient tumors, or whether nascent and dephosphorylated Merlin largely functions in this capacity.

The phosphorylation status of serine 518 drives Merlin's activation cycle, although other modifications modulate Merlin's conformation and downstream biochemical functions. Phospho-peptide mapping and band-shift experiments revealed that Merlin is phosphorylated at multiple sites and that serine 518 phosphorylation may be necessary for subsequent phosphorylation at other residues (17, 53). In addition to PAK-mediated phosphorylation, PKA was shown to independently phosphorylate Merlin at serine 518 and serine 10, the latter modification affecting the actin cytoskeleton (54, 55). Merlin's phosphoregulation by PKA may be an important mechanism in cells which are sensitive to the cyclic AMP-PKA signaling axis, including the pathogenically relevant Schwann cells (56). AKT phosphorylates Merlin at two additional sites – threonine 230 and serine 315 – and this phosphorylation causes decreased interdomain binding, intermolecular binding to phosphoinositides and PIKE-L (a GTPase that enhances PI3K activity), and ubiquitylation (57). The observation that AKT-mediated phosphorylation blocks Merlin's interaction with PIKE-L supports an inhibitory role for this interaction (20, 57). This finding also raises the possibility that constitutive activation of the PI3K-Akt pathway resulting from PTEN loss or

activating PI3K mutations would lead to Merlin inactivation, imparting a PI3K feed-forward mechanism. However, speculation that Merlin is inactivated by decreased interdomain binding conflicts with the recent observations that the open form of Merlin is active (28, 33). Moreover, the importance of the ubiquitin-proteasome system in Merlin's degradation is debatable, as cycloheximide chase experiments revealed that Merlin has a half-life exceeding 24 hours (30), although this does not rule out other ubiquitylation-mediated effects on Merlin function. Akt- and PAK-mediated phosphorylation of Merlin was recently shown to promote its sumoylation - an ubiquitin-like modification - which was found to affect Merlin's subcellular localization, interdomain binding, and growth-inhibitory activity (58). However, the requirement for sumoylation in Merlin's normal function and in tumor suppression remains incompletely understood since serine 518 phosphorylation, which renders Merlin inactive, appears to promote its sumoylation.

1.5: Merlin functions at the plasma membrane, cell cortex, and cytoskeleton

As cells become confluent, Merlin interacts with membrane-associated proteins where it regulates the formation of membrane domains (59). Merlin's organization of intercellular contacts is central to its normal function in contact inhibition, which is disrupted in Merlin-deficient tissues (60). Indeed, Merlin was initially interpreted as functioning at the cell cortex due to its homology to ERM proteins and its localization by immunostaining (61). This notion was supported in *Drosophila* by the observation that nascent Merlin is recruited to the plasma

membrane (39, 62). These observations were corroborated by Merlin's role in the establishment of adherens junctions in confluent cells and localization in lamellipodia and membrane ruffles (5, 7, 63-65). Merlin interacts with a number of proteins that are localized at or underneath the plasma membrane, including other ERMs, NHERF, the intracellular domain of CD44, α-catenin at maturing adherens junctions, and Angiomotin at tight junctions (6, 29, 60, 61, 66).

In keratinocytes and skin epithelium, Merlin is recruited to α-catenin and promotes its binding to Par3, aiding in the maturation of adherens junctions (Figure 1.5) (60). This is consistent with the disruption of adherens junctions in Merlin-deficient primary fibroblasts and keratinocytes (5). Interestingly, α-catenin can bind to 14-3-3 protein, which sequesters phosphorylated YAP in the cytoplasm and suppresses YAP-mediated transcription (67, 68). Moreover, it was recently discovered that α-catenin interacts with the APC tumor suppressor to promote the ubiquitylation and degradation of β-catenin as well as repression of Wnt target genes in the nucleus (69). Since Merlin's interaction with α-catenin and its role in junction formation was exclusively studied in skin and fibroblasts, it is difficult to put this mechanism in the context of NF2 pathogenesis and other Merlin-deficient malignancies. It will be of great interest to see whether Merlin's interactions with α-catenin leads to the suppression of YAP- and β-catenin-mediated oncogenic gene expression in pathogenically-relevant tissues.

Merlin interacts with the scaffold and signaling protein Angiomotin at mature tight junctions, regulating contact inhibition and potentially tumor suppression (Figure 1.6) (29). Angiomotin exists in two isoforms - both of which

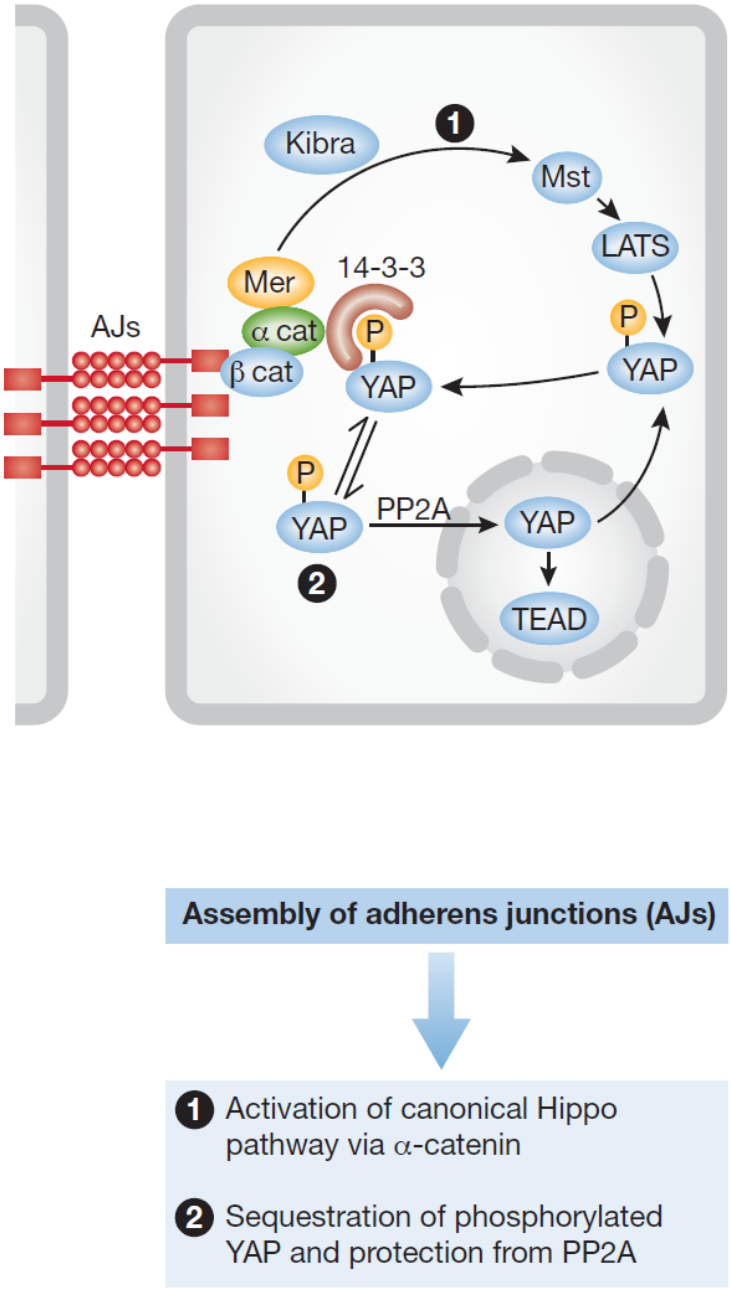

Figure 1.5: Merlin functions in the assembly of adherens junctions
Merlin is recruited to nascent adherens junctions by α-catenin and contributes to the activation of Hippo signaling by cooperating with Kibra to activate the classical core kinase cascade, or by enabling α-catenin to sequester phosphorylated Yap in the cytoplasm through 14-3-3 proteins.

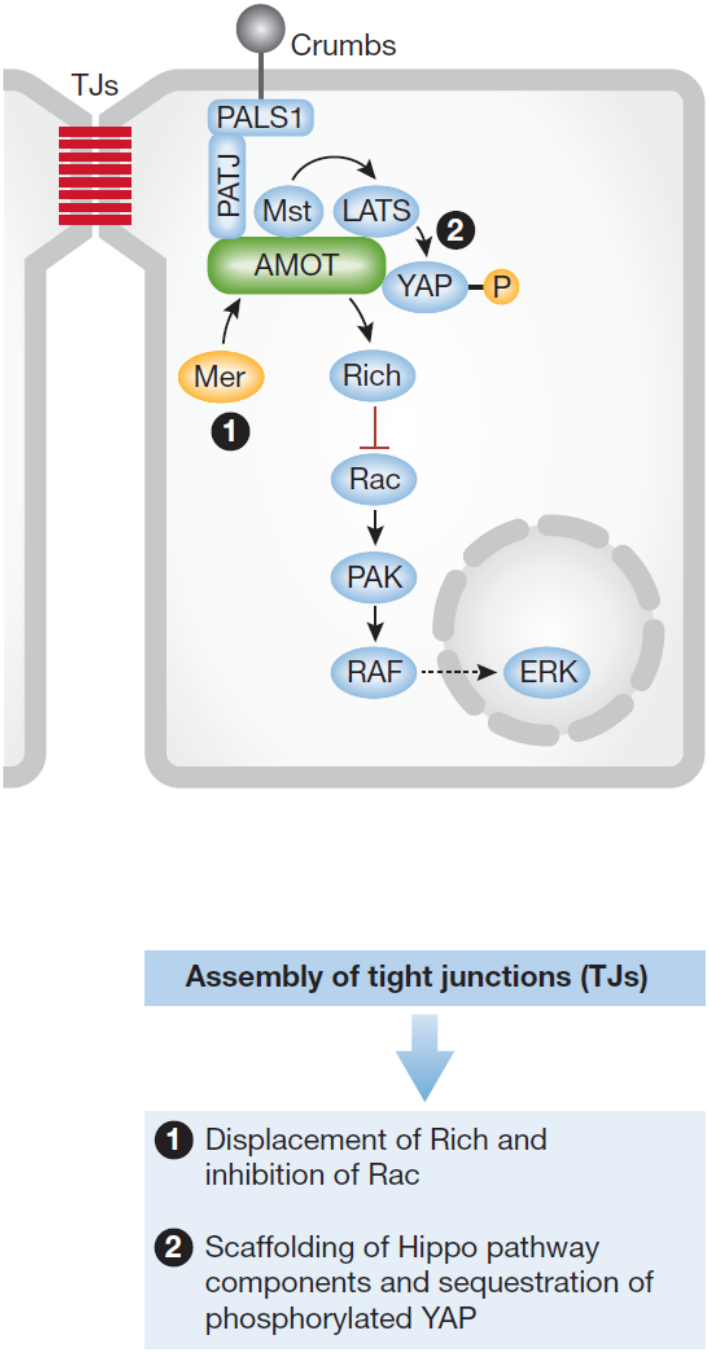

Figure 1.6: Merlin regulates Angiomotin
Upon assembly of tight junctions, Merlin binds to Angiomotin and displaces the Rac GAP Rich, thereby inhibiting Rac. In addition, Merlin might assist Angiomotin in coordinating the activation of the Hippo core kinase cascade.

interact with Merlin - and associate with tight junctions through interactions with Patj, Pals1, and Mupp1 (70, 71). At assembled tight junctions, Merlin binds to Angiomotin and displaces Rich - a GTPase Activating Protein for Rac - thus suppressing Rac-PAK signaling (29). Therefore, Merlin's inhibition of Rac at tight junctions promotes contact inhibition and acts as a barrier to mitogenic signaling (7). One major caveat to this finding is that Angiomotin interacts not only with Merlin's α-helical and carboxy-terminal domains, but also with phospho-deficient and phospho-mimetic Merlin mutants (29). These results strongly imply that Merlin binds to Angiomotin regardless of its activation status, and therefore, independently of growth suppressive stimuli. Further work is needed to fully understand the role of Angiomotin in Merlin's function in normal cells and in Merlin-deficient tumorigenesis.

A fraction of Merlin has been found to localize to cholesterol-dependent membrane domains - which were interpreted as lipid rafts - as a result of phosphoinositide binding (72, 73). Active Merlin was shown to bind phosphoinositides in several studies, although there is contradicting evidence as to whether this occurs in Merlin's active or inactive forms (73, 74), raising uncertainty over the relevance of this interaction to adhesion signaling. However, a Merlin mutant lacking residues necessary for phosphoinositide binding – K79, K80, K269, E270, K278, and K279 – was significantly defective in suppressing growth of Merlin-deficient cells (73). This observation was supported by experiments confirming that the Merlin mutant retained normal folding. However, the ability of the phosphoinositide-binding mutant to interact with other proteins

that were previously shown to mediate Merlin's function was not tested. Notably, mutation of Merlin E270 abolishes interaction with $CRL4^{DCAF1}$, which could explain the growth-suppression defects of the phosphoinositide-binding mutant (30). Merlin's phosphoinositide binding and potential localization to lipid rafts requires further scrutiny to determine its relevance both in normal biological function and in Merlin-deficient pathogenesis.

In addition to Merlin's localization at the cortex and contact-dependent membrane domains, Merlin functions in the cytoplasm to control cytoskeletal dynamics and vesicular transport. Merlin associates with actin and tubulin in the cytoplasm (33, 75, 76), although Merlin's association with the actin cytoskeleton is dispensable for tumorigenesis (33, 77). Merlin migrates along microtubules in a kinesin-1- and dynein-dependent manner (76), and Merlin was recently found to slow the turnover of microtubules, thus stabilizing them (78). In addition, Merlin has been found to promote microtubule-mediated anterograde transport of vesicles (79), which could function in promoting the transport of anti-mitogenic biomolecules or regulating the availability of growth factors at the plasma membrane. Merlin's effects on the actin cytoskeleton do not appear to be pathogenically relevant, and it remains to be demonstrated whether regulation of microtubule dynamics is necessary in Merlin-mediated contact inhibition and tumor suppression in vivo. Therefore, current models imply that Merlin largely enforces contact inhibition and the organization of membrane domains by acting at the plasma membrane or cortex, while Merlin's strongest tumor suppressive functions are enforced in another cellular compartment.

1.6: Merlin interacts with the CRL4^{DCAF1} E3 Ubiquitin ligase in the nucleus

Prior research in our lab led to the discovery that wild-type Merlin, but not a patient-derived missense mutant, interacts with the CRL4^{DCAF1} E3 ubiquitin ligase (Figures 1.7A and B) (30). Wild-type Merlin and the phosphorylation-resistant mutant S518D, canonically interpreted as the active conformer, preferentially interact with DCAF1 while phospho-mimetic and patient-derived mutants lack binding (Fig. 1.7C). Immunoblotting Flag-HA-tagged (FH) DCAF1 precipitates with an antibody recognizing phosphorylated Merlin confirmed that de-phosphorylated Merlin preferentially interacts with DCAF1 (Figure 1.7D). Wei Li, a former postdoctoral fellow who spearheaded this project following the departure of his co-author Liru You, carried out further experiments to identify the cellular compartment in which Merlin and CRL4^{DCAF1} interact. He found that DCAF1 can localize to the nucleus (Figures 1.8A and B), as might be expected based on the localization and function of other CRL4 ligases (80, 81). Notably, Wei found that Merlin can localize in the nucleus (Figures 1.8A and B) and that Merlin interacts with DCAF1 specifically in this compartment despite these proteins' ability to localize in both the cytosolic/crude membrane and nuclear soluble fractions (Figure 1.8D) (30). Importantly, these observations constituted the first identification of a nuclear binding partner for Merlin.

Further observation that the dephosphorylated form of Merlin preferentially translocates to the nucleus while the phosphorylated form is largely excluded is consistent with the long-standing observation that Merlin suppresses tumorigenesis in its dephosphorylated form (28, 30, 33, 51). Moreover, several

Figure 1.7: Merlin associates with CRL4^{DCAF1}
Modified from Li et al. 2010 (30). Experiments performed by Liru You and Wei Li.
(**A**) COS-7 cells were transfected with the indicated FH-tagged (FH; FLAG-HA) forms of Merlin and subjected to TAP. Proteins were separated by SDS-PAGE and stained with Colloidal Blue. Dots point to the FH-tagged baits and asterisks to the 169 and 127 kD bands identified by mass spectrometry as DCAF1 and DDB1, respectively.
(**B**) 293T cells were transfected with moderate amounts of FH-tagged DCAF1 or empty vector. Total lysates and Flag-immunoprecipitates (M2) were subjected to immunoblotting with antibodies to the indicated proteins.
(**C**) As in (**B**), with transfection of moderate amounts of the indicated constructs and immunoprecipitation with anti-FLAG (M2) or control (C) antibodies.
(**D**) As in (**B**), with co-transfection of Myc-Merlin or empty vector and immunoprecipitation with anti-FLAG (M2) or control (C).To control for the specificity of the anti-p-Merlin antibodies, the indicated sample was treated with calf intestinal alkaline phosphatase (CIP) prior to SDS-PAGE. Endogenous Merlin was detected upon longer exposure.

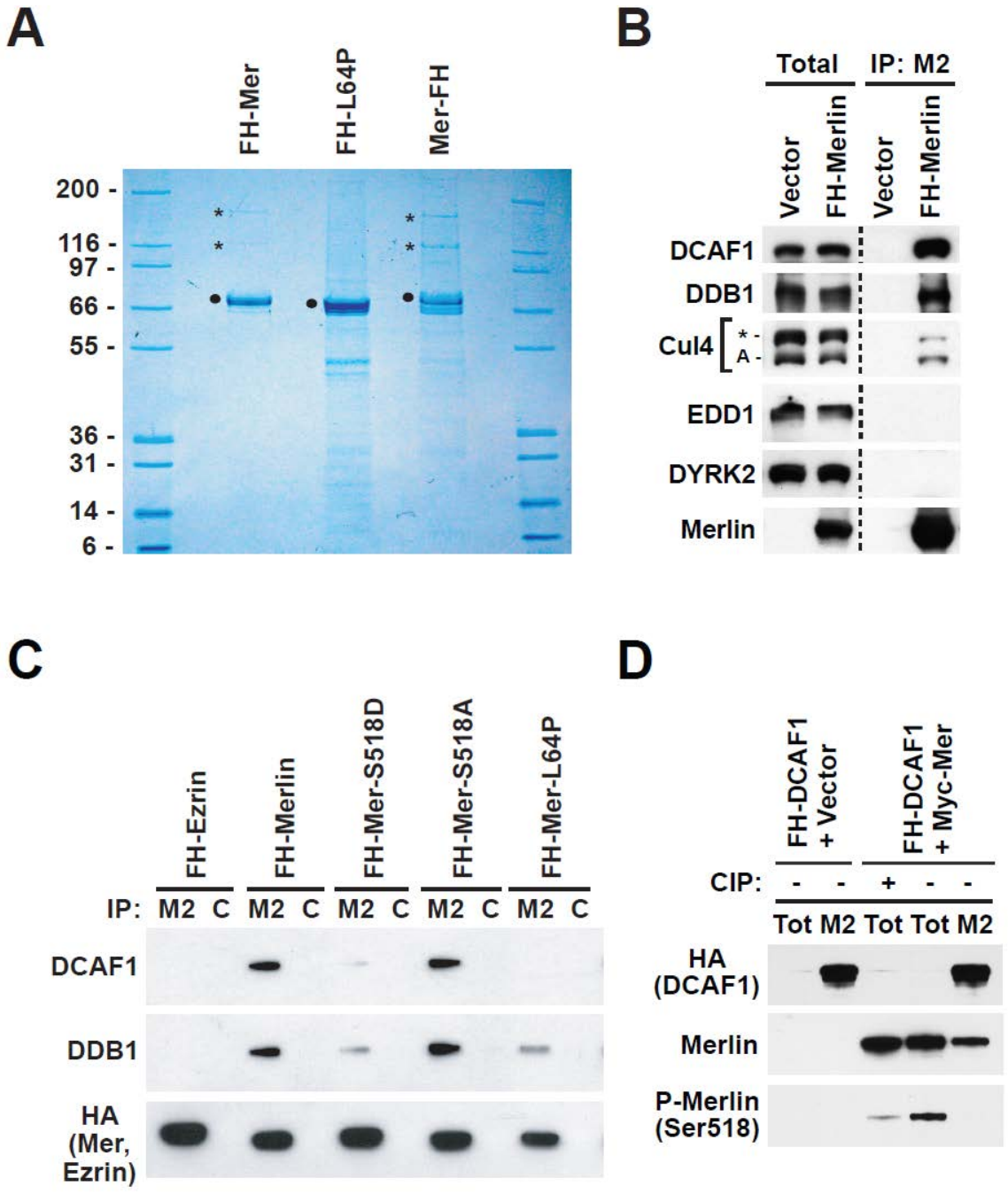
A
FH-Mer
FH-L64P
Mer-FH
200 -
116 -
97 -
66 -
55 -
36 -
31 -
14 -
6 -
B
Total
IP: M2
Vector
FH-Merlin
Vector
FH-Merlin
DCAF1
DDB1
Cul4
* -
A -
EDD1
DYRK2
Merlin
C
FH-Ezrin
FH-Merlin
FH-Mer-S518D
FH-Mer-S518A
FH-Mer-L64P
IP: M2 C M2 C M2 C M2 C M2 C
DCAF1
DDB1
HA (Mer, Ezrin)
D
FH-DCAF1 + Vector
FH-DCAF1 + Myc-Mer
CIP: - - + - -
Tot M2 Tot Tot M2
HA (DCAF1)
Merlin
P-Merlin (Ser518)

Figure 1.8: Merlin interacts with $CRL4^{DCAF1}$ in the nucleus

Modified from Li et al. 2010. Experiments performed by Wei Li.

(**A**) Meso-33 cells were transiently transfected with moderate amounts of the indicated constructs and subjected to double immunofluorescent staining with anti-HA and anti-Myc followed by DAPI.

(**B**) MCF-10A cells were subjected to subcellular fractionation. Equal amounts of proteins from the nuclear (NF) and non-nuclear (CM; cytosol + crude membranes) fraction were subjected to immunoblotting with antibodies to the indicated proteins.

(**C**) HEI286 untransformed Schwann cells, LP9 untransformed mesothelial cells, and MCF-10A untransformed mammary epithelial cells were stained with affinity-purified antibodies to the N-terminal segment of Merlin followed by DAPI.

(**D**) Equal amounts of proteins from the non-nuclear (CM) and nuclear-soluble (NS) fraction of HeLa cells and Merlin-immunoprecipitates were immunoblotted as indicated. Anti-Cul4 recognizes Cul4A and a higher molecular weight band, possibly corresponding to Neddylated Cul4A or Cul4B (asterisk).

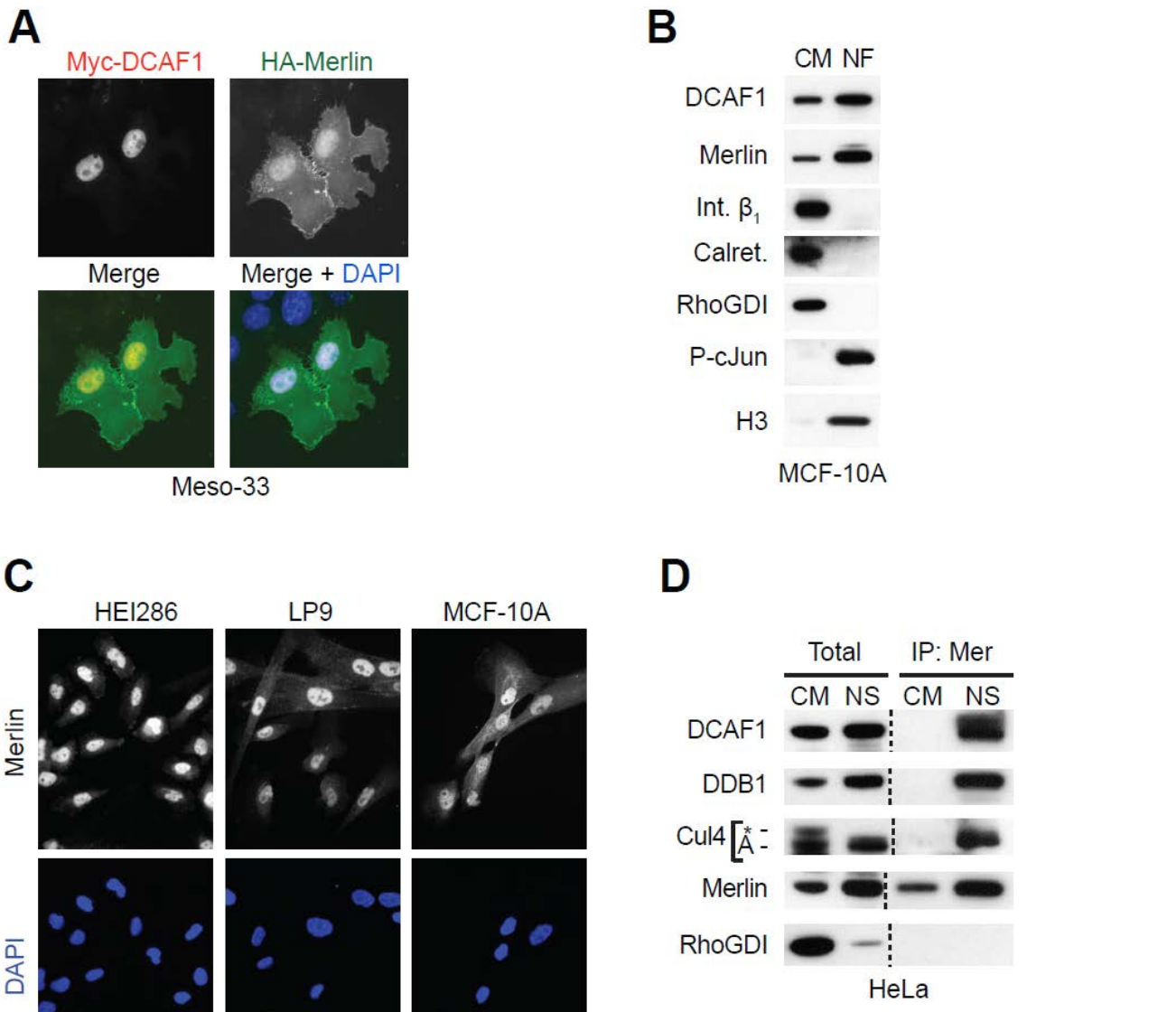
A
Myc-DCAF1
HA-Merlin
Merge
Merge + DAPI
Meso-33
B
CM NF
DCAF1
Merlin
Int. β1
Calret.
RhoGDI
P-cJun
H3
MCF-10A
C
HEI286
LP9
MCF-10A
Merlin
DAPI
D
Total
IP: Mer
CM NS CM NS
DCAF1
DDB1
Cul4
Merlin
RhoGDI
HeLa

reports have characterized Merlin's localization in the nucleus, and Merlin migrates towards the nucleus by microtubule-based transport in *Drosophila* (58, 76, 82, 83). Although Merlin lacks a canonical nuclear localization sequence, it contains a motif on its carboxy-terminus that promotes nuclear export by the CRM1-exportin pathway (83) and truncations that remove these residues show increased nuclear localization (30, 33). Interestingly, the isolated FERM domain of Merlin is necessary and sufficient for nuclear localization, once again highlighting the importance of Merlin's FERM domain in its normal function (30). Moreover, the dephosphorylated form of Merlin preferentially localizes to the nucleus in confluent and growth factor-deprived cells, when Merlin's anti-mitogenic effects would be most active (30). As the phosphorylated, more closed form of Merlin is excluded from the nucleus, interdomain binding imposed by S518 phosphorylation may occlude the FERM domain residues necessary for nuclear translocation (28, 30). Since a large proportion of Merlin shuttles to the nucleus in contact-inhibited cells, Merlin's nuclear function – particularly inhibition of the oncogenic $CRL4^{DCAF1}$ ubiquitin ligase – may be vital for growth suppression (30). Understanding more about $CRL4^{DCAF1}$ biology and its interaction with Merlin and other binding partners is an important step in conceptualizing how Merlin's inhibition of this E3 ligase is an important stepping stone in the control of multiple pro-oncogenic signaling pathways.

DCAF1 (DDB1 and Cul4-Associated Factor 1) was originally identified as VprBp (Vpr-binding protein) – a cytoplasmic protein that binds to the HIV-1 viral accessory protein Vpr (84, 85), before it was found to function as the substrate

recognition subunit of the $CRL4^{DCAF1}$ E3 ubiquitin ligase (86). Viral Vpr and the related Vpx proteins promote HIV and SIV infection by functioning as adaptors that bind to DCAF1 and usurp its recruitment of substrates to degrade proteins that normally suppress viral infectivity (87, 88). In fact, viral subversion of E3 ubiquitin ligases occurs in a number of human diseases (34, 86, 89-91). SAMHD1 is a viral restriction factor that functions in myeloid-lineage cells and resting $CD4^+$ T-cells by reducing the concentration of cellular dNTPs and thus inhibiting the viral reverse transcriptase. In HIV-2 and SIV, Vpx binds to DCAF1 and acts as an adaptor to co-opt the ubiquitin-conjugating machinery to target and degrade SAMHD1 (92-97). A recent landmark study found that Vpx binds the WD40 domain of DCAF1 to produce a new surface that recruits SAMHD1, providing the first structural elucidation of lentiviral hijacking of the cell's ubiquitin-proteasome system (98). These studies provide a starting point to understand how $CRL4^{DCAF1}$ binds its targets.

Structural analysis of the DCAF1-Vpx-SAMHD1 complex revealed that Vpx creates a new binding surface by enclosing a portion of the DCAF1 WD40 domain. The WD40 domain of DCAF1, near the carboxy-terminus, is a seven-bladed β-propeller that forms an overall fan shape (98). Residues within the WD40 domain are necessary for interacting with DDB1 and therefore docking to the CRL4 complex (86). As Vpx-associated DCAF1 is able to recruit SAMHD1 and mediate its ubiquitylation (98), it is plausible that DCAF1 uses portions of its WD40 domain to bind native targets. A recent study found that DCAF1 can recruit mono-methylated proteins using the hydrophobic pocket within its chromo

domain, which resides in the amino-terminal half of the protein (99). In addition to the role of $CRL4^{DCAF1}$ in ubiquitylation, DCAF1 has a putative kinase domain near the amino-terminus which imparts intrinsic kinase activity towards histone H2A to downregulate anti-mitogenic genes (100). Combined, these studies reveal that DCAF1 can interact with multiple target proteins using several distinct regions spanning its primary sequence. However, without further structural characterization of full-length DCAF1, it cannot be ruled out that these domains are juxtaposed, and that one or more protein-interacting regions act in a single multifunctional recruitment domain.

DCAF1 was established as the substrate recognition component of the $CRL4^{DCAF1}$ E3 ligase nearly ten years ago (86), and several $CRL4^{DCAF1}$ targets have been discovered. Vpr- and Vpx-mediated targeting of SAMHD1 and the uracil DNA glycosylase UNG2 direct these proteins to proteasomal degradation (93, 101). Moreover, it was found that $CRL4^{DCAF1}$ is recruited by Vpr to activate the SLX4 complex, a structure-specific endonuclease whose ectopic activation results in G2/M arrest and evasion of innate immunity in HIV-infected cells (102). Native DCAF1-binding proteins include Merlin, the nuclear orphan receptor Rorα, histones H2A and H3, HDAC, the polarity protein Lgl, the lymphoid cell-specific V(D)J recombination protein RAG1, the protein phosphatase PPP2R1A, and the replication factor Mcm10 (30, 99, 103-107). Several of these proteins – particularly the histones and HDAC – can broadly affect epigenetics, suggesting that Merlin's inhibition of $CRL4^{DCAF1}$ can greatly alter gene expression. It was recently observed that $CRL4^{DCAF1}$ interacts with and promotes activation of TET

proteins, a family of enzymes that convert 5-methylcytosine to 5-hydroxymethylcytosine (5hmC) (108). These conversions cause epigenetic modifications that regulates DNA demethylation and therefore gene transcription, which were shown to have dramatic effects during embryonic development and tumorigenesis. Notably, loss of TET2 is a common occurrence in myeloid leukemia and 5hmC reduction is a distinguishing feature of melanoma and is observed in a range of other solid tumors (109). However, the mechanism by which $CRL4^{DCAF1}$ regulates TET proteins – whether by ubiquitylation or another modification – is currently unknown. Indeed, the mechanism by which $CRL4^{DCAF1}$ modulates several bona fide interactors remains elusive, and it is unclear whether ubiquitylation of these targets is necessary or sufficient for their regulation. Regardless, these findings suggest that CRL^{DCAF1} can multifariously modulate epigenetics.

1.7: Convergence on YAP and TAZ

The size of multicellular organisms and their composite tissues is tightly regulated by restricting cell size and proliferation (93, 94). The Hippo pathway has emerged as a potent regulator of organ size throughout the animal kingdom. Notably, genetic experiments in *Drosophila* and mice revealed that the Hippo pathway controls cell proliferation and promotes apoptosis, and disruption of the pathway at multiple levels leads to tissue overgrowth and tumorigenesis (110, 111). This is particularly evident in mouse genetic models, where dysregulation of Hippo pathway proteins in the liver elicits dramatic hepatomegaly and

development of a range of tumors (24, 112-115). The Hippo pathway is canonically driven by a core kinase cascade consisting of the Ste20-like kinases Mst1 and Mst2 (Mst1/2), which in conjunction with Sav1, phosphorylate and activate the NDR family kinases Lats1 and Lats2 (Lats1/2) along with cofactors Mob1A and Mob1B. Active Lats kinases phosphorylate and inactivate the YAP and TAZ transcriptional coactivators (Figure 1.9A). In the absence of Hippo signaling, active YAP and TAZ translocate to the nucleus to promote transcription of genes that drive proliferation, evasion of apoptosis, and stemness (Figure 1.9B) (26, 116). The atypical cadherin Fat, along with the apical polarity protein Crumbs, function in *Drosophila* to activate the Hippo pathway. These proteins activate the FERM domain protein Expanded, which complexes with Merlin and Kibra to activate the core kinase cascade (96, 97, 117, 118). Although the core kinase cascade is evolutionarily conserved between Mammals and *Drosophila*, the upstream signaling promoting activation of the Hippo pathway has diverged.

It has recently become evident that some of the key proteins regulating the core Hippo cascade in *Drosophila* evolved after the divergence of arthropods. It is unclear whether *Drosophila* Expanded (Ex) and Fat have orthologs in vertebrates, and the mammalian proteins which bare closest resemblance appear to function primarily through Hippo-independent mechanisms (119-122). The adherens junction protein Echinoid and the unconventional myosin Dachs - a downstream target of Fat - regulate the *Drosophila* Hippo pathway but are absent in vertebrates. Angiomotin was retained during the evolution of chordates as a

Figure 1.9: The core Hippo pathway kinase cascade

(**A**) The Hippo tumor suppressor pathway was originally identified in flies and in the past decade has emerged as a regulator of several mechanisms of cancer progression, regulation of organ development, regeneration, and stemness. The Hippo pathway consists of a kinase module that is regulated by upstream signaling and a transcription module that can drive oncogenesis in many tissues. In canonical Hippo signaling, the STE2-like kinases MST1 and 2 and their adaptor protein Sav1 activate the NDR-like kinases LATS1 and 2 along with their adaptors MOB1A and B. The LATS proteins phosphorylate YAP and TAZ, leading to their cytosolic sequestration which simultaneously excludes them from functioning as co-transcriptional activators along with TEAD family proteins but also primes them for degradation.

(**B**) In the absence of active LATS1 or 2, YAP and TAZ translocate to the nucleus where they bind to and activate TEAD-dependent transcription of pro-proliferative and anti-apoptotic genes. Since both DCAF1 and Merlin appear to affect Hippo pathway target genes, we wanted to know whether expression of Merlin and DCAF1 regulate the activity of YAP.

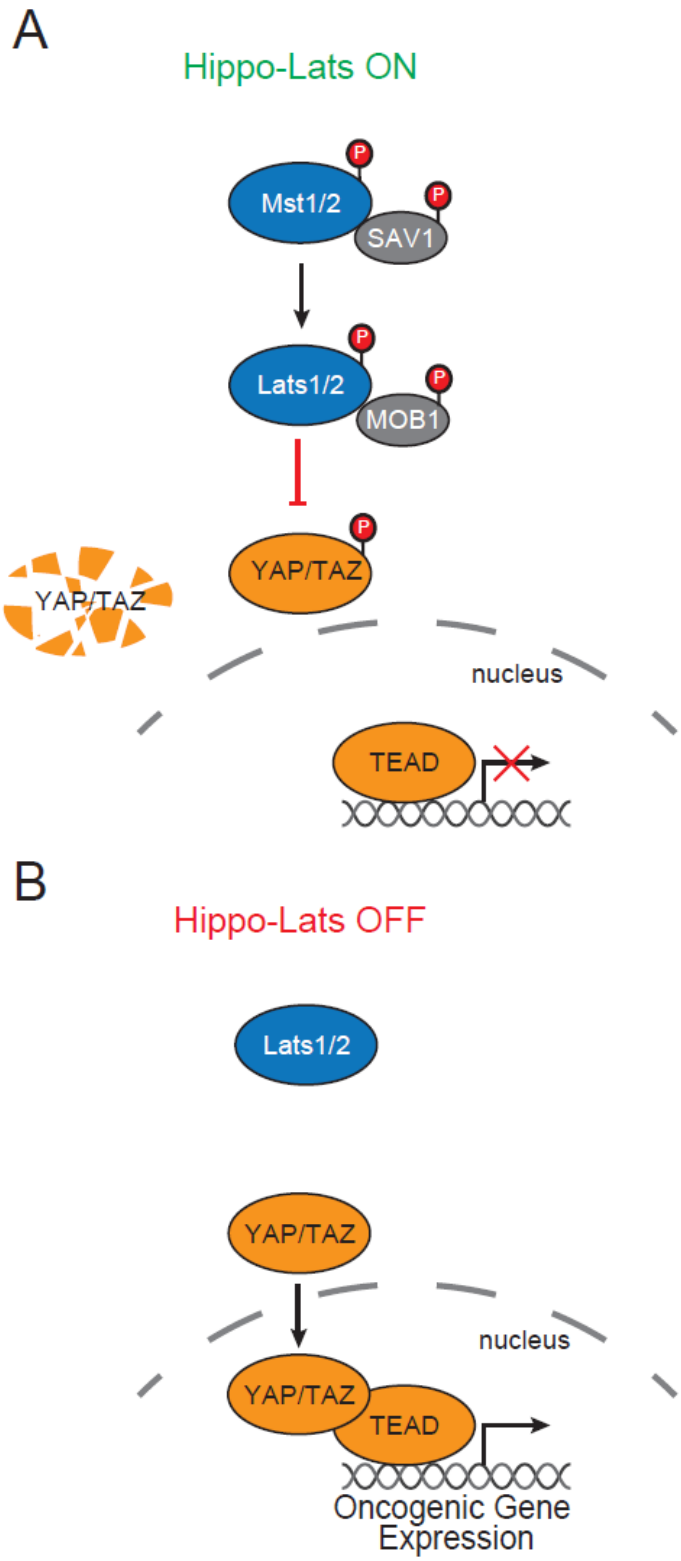
A
Hippo-Lats ON
Mst1/2
SAV1
Lats1/2
MOB1
YAP/TAZ
YAP/TAZ
nucleus
TEAD
B
Hippo-Lats OFF
Lats1/2
YAP/TAZ
nucleus
YAP/TAZ
TEAD
Oncogenic Gene
Expression

regulator of Hippo signaling but was replaced with Ex at the base of the arthropod lineage (122). The evolution of a novel domain in Ex to bind Yki – the *Drosophila* ortholog of YAP - reestablished Crumbs-mediated regulation of Hippo signaling which was uncoupled when the PDZ-binding motif of Yki was lost during arthropod evolution. In addition to these evolutionary shifts in regulation of Hippo signaling, Merlin's input into the pathway appears to be more complicated in mammals.

It is becomingly increasingly clear in mammals that multiple signals converge to affect the Hippo core kinase cascade in addition to canonical Hippo signaling (116). Upstream of the core cassette, Merlin can interact with Kibra to activate the Hippo kinase cascade, although the biochemical mechanism is unclear (24, 96). Merlin is recruited to tight junctions by Angiomotin, which serves as a scaffold for PDZ- and WW-domain- containing proteins including Hippo pathway components (Figure 1.6) (123-126). Interestingly, tight junction-associated Angiomotin directly binds phosphorylated YAP and TAZ and retains them at the cortex (123, 126) and also serves as a scaffold for activation of the Hippo core kinases Mst2 and Lats2, promoting canonical YAP/TAZ inhibition (124). Since Merlin binds to Angiomotin and displaces other complexed proteins, it is plausible that Merlin's binding could modulate Angiomotin recruitment of Hippo components. It remains to be tested whether Merlin promotes or inhibits Angiomotin's direct effects on Hippo signaling. Recently it was found that the p130 isoform of Angiomotin promotes YAP function by disrupting its association with Lats1 in the cytoplasm, and furthermore, by binding to YAP in the nucleus to

drive expression of a subset of YAP target genes to drive tumorigenesis (Figure 1.6) (127). It will be of great interest to determine whether Angiomotin is shuttled to the nucleus to promote YAP function in sparse cells or cells that have had their tight junctions disrupted. Combined, these results suggest Angiomotin has tumor suppressive and growth-promoting functions, which may depend on the tissue, cellular, or biochemical environment. Identification of the contexts in which Angiomotin functions to inhibit or promote Hippo signaling - including the biochemical function of Merlin in these processes – will provide important mechanistic insight into both Merlin function and Hippo signaling.

1.8: Questions to address

Merlin inhibits several important pro-mitogenic pathways and its inactivation drives tumorigenesis in multiple tissues. Despite decades of research, the biochemical mechanism underlying Merlin's regulation of oncogenic signaling remained elusive. During my thesis studies, I set out to determine how Merlin suppresses tumorigenesis and whether we could use our findings to derive mechanistic-based therapies for Merlin-deficient malignancies.

In the following chapter, I will discuss how Merlin suppresses tumorigenesis in the nucleus by inhibiting $CRL4^{DCAF1}$, an oncogenic E3 ubiquitin ligase. I will subsequently reveal a direct link between Merlin's inhibition of $CRL4^{DCAF1}$ in the nucleus and regulation of the Hippo tumor suppressor pathway. Subsequently, I will address the *in vivo* role of $CRL4^{DCAF1}$ in mouse models of Merlin-deficient

tumorigenesis. Lastly, I will show how we exploited the mechanisms we uncovered for preclinical therapy of Merlin-deficient tumorigenesis.

Chapter Two

Merlin/*NF2* suppresses tumorigenesis by inhibiting the E3 ubiquitin ligase $CRL4^{DCAF1}$ in the nucleus

2.1: Merlin inhibits $CRL4^{DCAF1}$-dependent ubiquitylation

Initial experiments revealed that Merlin is not a ubiquitylation target of the $CRL4^{DCAF1}$ ligase, raising the possibility that Merlin functions upstream of the ligase (30). I set up an *in vivo* ubiquitylation assay to examine the effect of Merlin expression on the ubiquitin conjugating activity of $CRL4^{DCAF1}$. I transfected COS-7 cells with Flag-HA-tagged DCAF1 (FH-DCAF1) and Myc-ubiquitin, treated the cells with the proteasome inhibitor MG132 to accumulate ubiquitylated species, and immunoprecipitated $CRL4^{DCAF1}$ and its associated ubiquitylated products using anti-Flag. Myc immunoblotting revealed that FH-DCAF1 isolated from MG132-treated cells coprecipitates ubiquitylated species of apparent molecular weight ranging from 55 to 300 kDa. This implies that $CRL4^{DCAF1}$ targets one or more substrates which remain associated with the complex through the immunoprecipitation (Figure 2.1A, top). FH-DCAF1 isolated from untreated cells coprecipitated only a modest amount of ubiquitylated species ranging from 180 to 250 kDa. Importantly, co-transfection of increasing concentrations of HA-tagged Merlin caused a dose-dependent suppression of the recruitment of ubiquitylated products. These results suggest that Merlin suppresses the ubiquitin conjugating activity of $CRL4^{DCAF1}$. Re-probing the blot with anti-HA indicated that the fraction of recombinant Merlin coprecipitated by FH-DCAF1 does not noticeably become

Figure 2.1: Merlin inhibits $CRL4^{DCAF1}$

(**A**) COS-7 cells were transfected with 3 µg of FH-DCAF1 and 2 µg of Myc-Ubiquitin in combination with the indicated amounts of HA-Merlin, treated with 25 µM MG132 for 6 hours or left untreated. Flag- or control-immunoprecipitates (M2 and C, respectively) were subjected to immunoblotting with anti-Myc to visualize ubiquitylated proteins (top) or anti-HA to visualize DCAF1 and Merlin (bottom). Upper arrow points to DCAF1 and lower arrow to Merlin.

(**B**) Total lysates from (**A**) were blotted to verify expression levels.

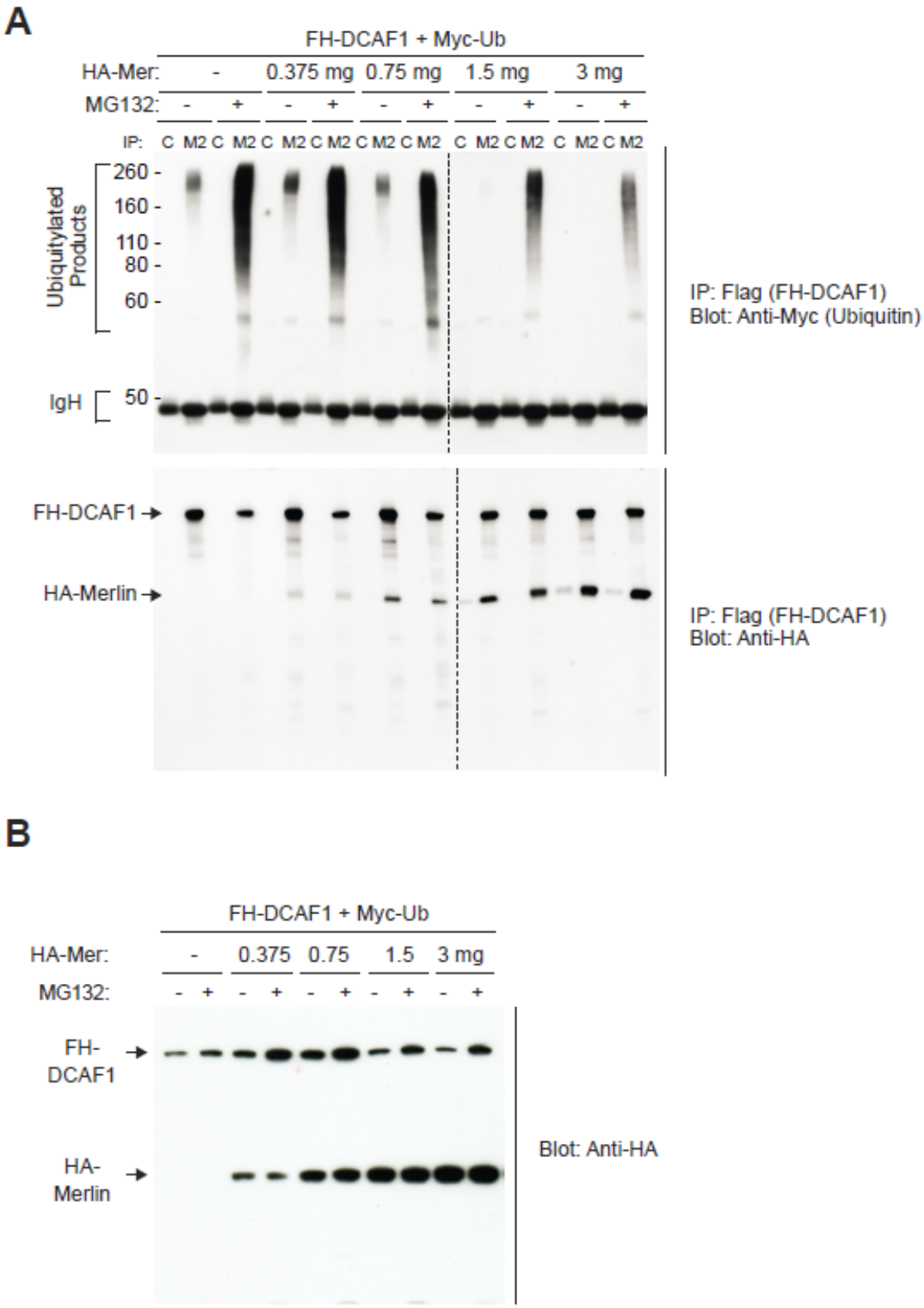
A
FH-DCAF1 + Myc-Ub
HA-Mer:
-
0.375 mg
0.75 mg
1.5 mg
3 mg
MG132:
IP:
C M2 C M2 C M2 C M2 C M2 C M2 C M2 C M2 C M2 C M2
Ubiquitylated Products
260
160
110
80
60
IgH
50
IP: Flag (FH-DCAF1)
Blot: Anti-Myc (Ubiquitin)
FH-DCAF1
HA-Merlin
IP: Flag (FH-DCAF1)
Blot: Anti-HA
B
FH-DCAF1 + Myc-Ub
HA-Mer:
-
0.375
0.75
1.5
3 mg
MG132:
FH-DCAF1
HA-Merlin
Blot: Anti-HA

ubiquitylated *in vivo*, supporting the notion that Merlin acts upstream of $CRL4^{DCAF1}$ rather than serving as a substrate of the ligase (Figure 2.1A, bottom). Immunoblotting the input revealed similar expression levels for the recombinant proteins but indicated that proteasome inhibition partially stabilizes DCAF1 (Figure 2.1B). These observations suggest that Merlin binds to $CRL4^{DCAF1}$ and suppresses its ability to mediate ubiquitin conjugation of its targets.

I subsequently tested the effect of Merlin depletion on $CRL4^{DCAF1}$ activity. I infected COS-7 cells with control or Merlin shRNA-encoding lentivirus and then subjected the resulting lysates to an *in vivo* ubiquitylation assay. This assay indicated that Merlin depletion causes a dramatic increase in $CRL4^{DCAF1}$ ubiquitin conjugating activity (Figure 2.2). This effect was specific since was suppressed by overexpression of Merlin but not Ezrin, the latter of which does not associate with FH-DCAF1 (30). These results of positive expression and depletion provide compelling evidence that Merlin negatively regulates $CRL4^{DCAF1}$ (Figure 2.3A). We hypothesized that in Merlin-deficient cells or when Merlin is inactive, $CRL4^{DCAF1}$ ubiquitylates proteins and elicits growth-promoting or oncogenic signaling (Figure. 2.3B).

2.2: DCAF1 mediates hyperproliferation in Merlin-deficient cells

Prior studies in our lab revealed that loss of Merlin promotes progression through G1 (19), raising the possibility that DCAF1 affects this specific phase of the cell cycle. BrdU incorporation assays performed by Wei Li confirmed that DCAF1 depletion inhibits the ability of G0 synchronized Meso-33 – a Merlin-

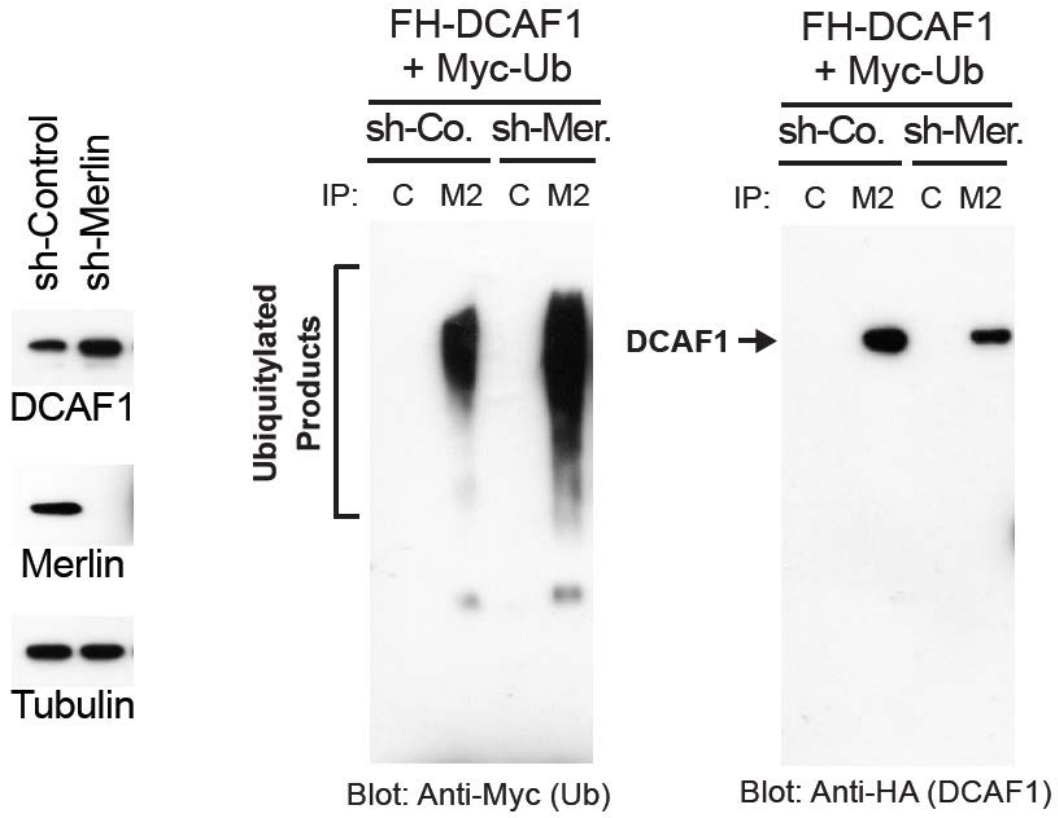

Figure 2.2: Merlin depletion promotes CRL4^{DCAF1}-mediated ubiquitylation
Cos7 cells stably infected with lentiviral vectors encoding a control shRNA or a shRNA targeting Merlin were subjected to immunoblotting (**left**) or transfected with FH-DCAF1 and Myc-Ubiquitin followed by immunoblotting of Flag- or control-immunoprecipitates with anti-Myc (middle) or anti-HA (**right**).

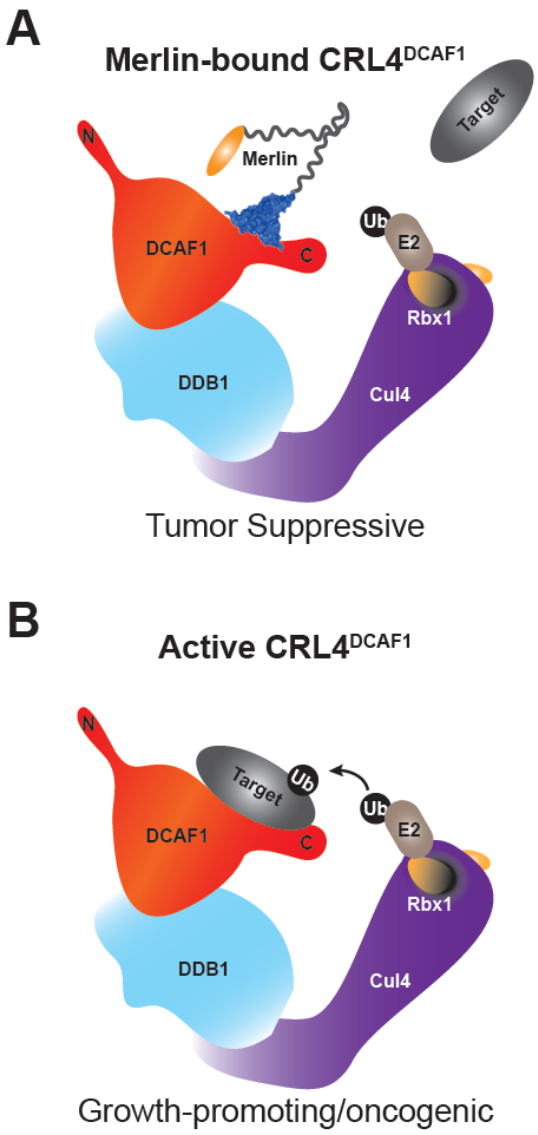

Figure 2.3: A hypothetical model of Merlin-mediated inhibition of CRL4^{DCAF1}
(**A**) Active Merlin translocates to the nucleus and binds to the carboxy-terminus of DCAF1, acting as a pseudo-substrate to block CRL4^{DCAF1} from recruiting and ubiquitylating target proteins. We propose Merlin's inhibition of CRL4^{DCAF1} suppresses oncogenic gene expression.
(**B**) CRL4^{DCAF1} is an E3 ubiquitin ligase consisting of the substrate-recruiting DCAF1 protein that is linked to the amino-terminal domain of a cullin (Cul4A/B) backbone through DDB1, which is itself a large multi-domain protein. Bound to the cullin carboxy-terminal domain, Rbx1 uses its RING domain to recruit a ubiquitin-charged E2, which directs conjugation of ubiquitin to a DCAF1-bound target protein.

deficient mesothelioma cell line – to progress through G1 and enter S phase in response to mitogens (30). This effect appeared to be specific since DCAF1 depletion in the Merlin-positive mesothelial line Met5a had only a modest effect on progression through G1. These results suggested that Merlin-deficient cells are more sensitive to DCAF1 inactivation than their normal counterparts. FACS analysis confirmed that DCAF1 depletion primarily inhibits progression through G1 (30). As these results suggest that Merlin suppresses cell proliferation by inhibiting $CRL4^{DCAF1}$, we reasoned that expression of a mutant form of DCAF1 that is unable to interact with Merlin should counteract Merlin's antimitogenic effects. To test this hypothesis, I transfected Meso-33 cells with FH-Merlin, alone or in combination with wild-type DCAF1 or DCAF1-1417X (Figure 2.4A). DCAF1-1417X is a mutant that lacks a distal carboxy-terminal motif which is bound by Merlin, making this mutant Merlin-resistant. Wei Li found that that expression of Merlin-resistant DCAF1-1417X in these samples fully rescued Meso-33 cells from undergoing growth arrest upon introduction of Merlin (Figure 2.4B). Wild-type DCAF1 exhibited only a moderate growth rescue. We noted that despite a higher level of Merlin expression in these samples (Figure 2.4A), Merlin does not bind stoichiometrically to wild-type DCAF1 in this experiment (Figure 2.4C). We speculate that overexpressed Merlin may saturate the cellular machinery required for modification of Merlin to enable its binding to $CRL4^{DCAF1}$ in this cell line. Taken together, these data provide compelling evidence that Merlin suppresses cell proliferation by inhibiting $CRL4^{DCAF1}$.

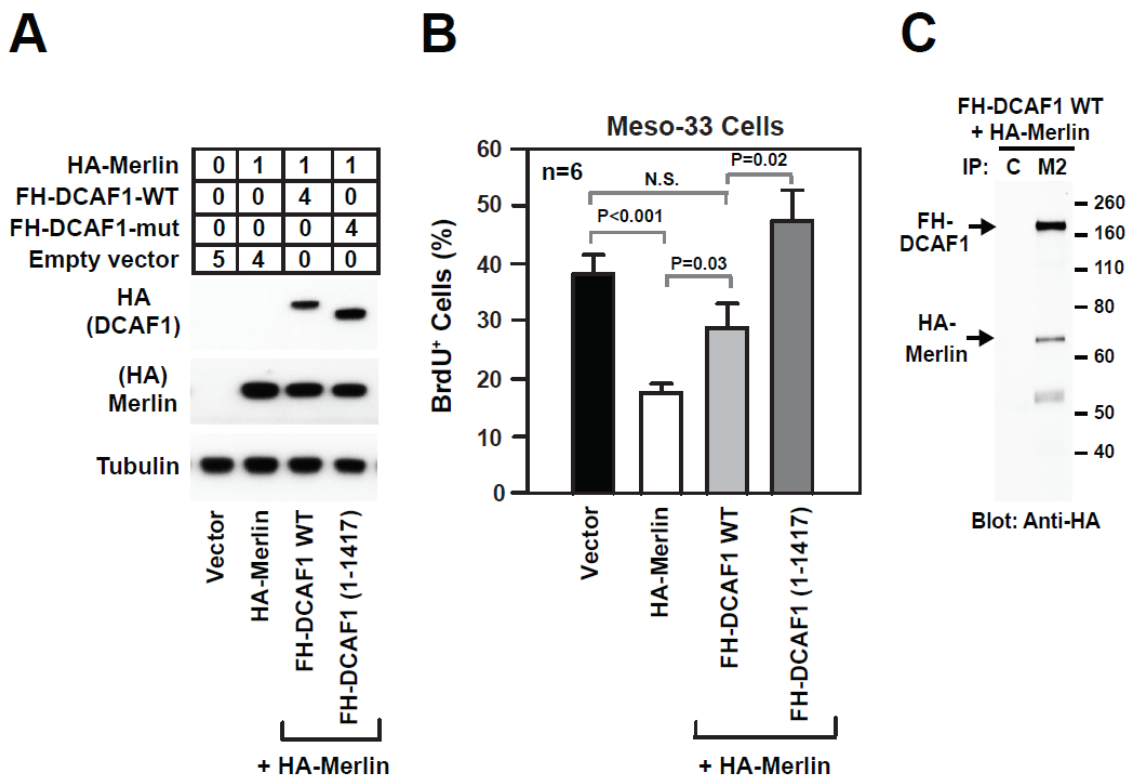

Figure 2.4: DCAF1 mediates hyperproliferation in Merlin-deficient cells

The experiment in figure (**B**) was performed by Wei Li.

(**A**) Meso-33 cells were transiently transfected with the indicated micrograms of vectors encoding HA-Merlin, alone or in combination with FH-DCAF1 or FH-DCAF1 (1-1417), and subjected to immunoblotting as indicated. The anti-HA blots including FH-DCAF1 and HA-Merlin were exposed for the same time.

(**B**) The cells in (**A**) were subjected to a BrdU incorporation assay by Wei Li. The graph shows the percentage (± SEM) of BrdU+ cells.

(**C**) Flag (M2) or control (C) immunoprecipitates from lysates containing 0.3 mg of total proteins from Meso-33 cells transfected with FH-DCAF1 WT and HA-Merlin (same treatment as lane 3 from (**A**)) were immunoblotted with anti-HA. Note that DCAF1 is not saturated by Merlin under these experimental conditions.

2.3: Tumor-derived mutations prevent Merlin's ability to interact with or to inhibit CRL4^{DCAF1}

A majority of *NF2* missense mutants map to the amino terminal FERM domain (Figure 1.2) (35). To further study the relevance of Merlin's interaction with CRL4^{DCAF1} for tumor suppression, we examined a panel of tumor-derived missense mutants. The Merlin mutations L46R, F62S, L64P, L141, A211D, and E270G are likely bona fide pathogenic mutations since they were found in two or more unrelated NF2 patients or were known to track with disease in individual families. In contrast, G197C, which was identified in a single patient affected by mild bilateral Schwannoma, may represent a polymorphism or a passenger mutation (35). Structural analyses by Stephen B. Long on a published crystal structure of the Merlin FERM domain (37) suggested that L46R, F62S, L64P, L141, and A211D disrupt the hydrophobic core of two subdomains of the FERM domain in which they reside. Notably, E270G simply removes a surface charge from a surface-exposed loop on a FERM subdomain. Wei Li evaluated the growth suppressive function of the panel of Merlin missense mutants in the Merlin-deficient Meso-33 cell line and found that all of the bona fide pathogenic mutants were devoid of growth inhibitory activity, whereas the putative passenger mutant G197C suppressed proliferation to the same extent as wild type Merlin (30). Wei reasoned that structural defects elicited by pathogenic missense mutations may affect their ability to interact with CRL4^{DCAF1}, as the FERM domain directly interacts with the carboxy terminus of DCAF1 (30). Strikingly, immunoprecipitations using FH-Merlin and its mutants revealed that none of the

bone fide tumor-derived missense mutants associated with $CRL4^{DCAF1}$ (30). This provided preliminary evidence that Merlin needs to combine with $CRL4^{DCAF1}$ to suppress tumorigenesis.

To assess the ability of tumor-derived Merlin missense mutants to directly interact with $CRL4^{DCAF}$, I engineered each mutation into a GST fusion protein comprising the isolated FERM domain of Merlin, which we had found to bind efficiently to *in vitro* translated DCAF1 (30). GST-FERM-A211D bound DCAF1 *in vitro* almost as efficiently as wild type GST-FERM or GST-FERM-G197C, suggesting that the A211D mutant does not interact *in vivo* with $CRL4^{DCAF1}$ due to an alternative mechanism (Figure 2.5A and B). The remaining mutant FERM domains displayed decreased binding to recombinant DCAF1 - L46R, L64P, and E270G did not bind at all under my experimental conditions, whereas F62S and L141P displayed defective binding. Subcellular fractionation experiments performed by Wei Li revealed that the A211D mutant which displayed abrogated *in vivo* interaction with $CRL4^{DCAF1}$ but retained *in vitro* binding was defective in nuclear translocation (30). Additionally, since F62S and E270G were able to accumulate in the nucleus to normal or near normal levels, we inferred that they do not combine *in vivo* with $CRL4^{DCAF1}$ because they are unable to directly interact with DCAF1. Of particular note, the E270G mutation was predicted to not overtly affect the overall structure of the FERM domain since it can theoretically be accommodated by a small adjustment of the surface loop in which it resides. This implicated the loop containing residue 270 as a surface that may be involved in direct interaction with DCAF1 and also confirmed the high specificity

Figure 2.5: Pathogenic mutations disrupt the ability of Merlin to bind to DCAF1 or to inhibit CRL4^{DCAF1}

The experiment in (**D**) was performed by Liru You.

(**A**) *In vitro* translated and TNT-labeled DCAF1 was incubated with 0.5, 1, and 2 µg of GST fusion proteins comprising the FERM domain of wild type Merlin or indicated mutants. GST-bound DCAF1 was detected by blotting with Streptavidin-HRP.

(**B**) Densitometric analysis of (**A**). The graph shows the binding values in arbitrary units.

(**C**) COS-7 cells were transfected with the indicated FH-tagged forms of Merlin and subjected to immunoprecipitation with control (C) or anti-Flag (M2) antibodies followed by immunoblotting.

(**D**) COS-7 cells were transfected with FH-DCAF1 and HA-Ubiquitin in combination with Myc-tagged Merlin wild type, Merlin-339X, Ezrin, or empty vector and treated with 25 µM MG132. Flag- or control-immunoprecipitates were immunoblotted with anti-HA (**left**). Total lysates were immunoblotted with anti-Myc (**right**).

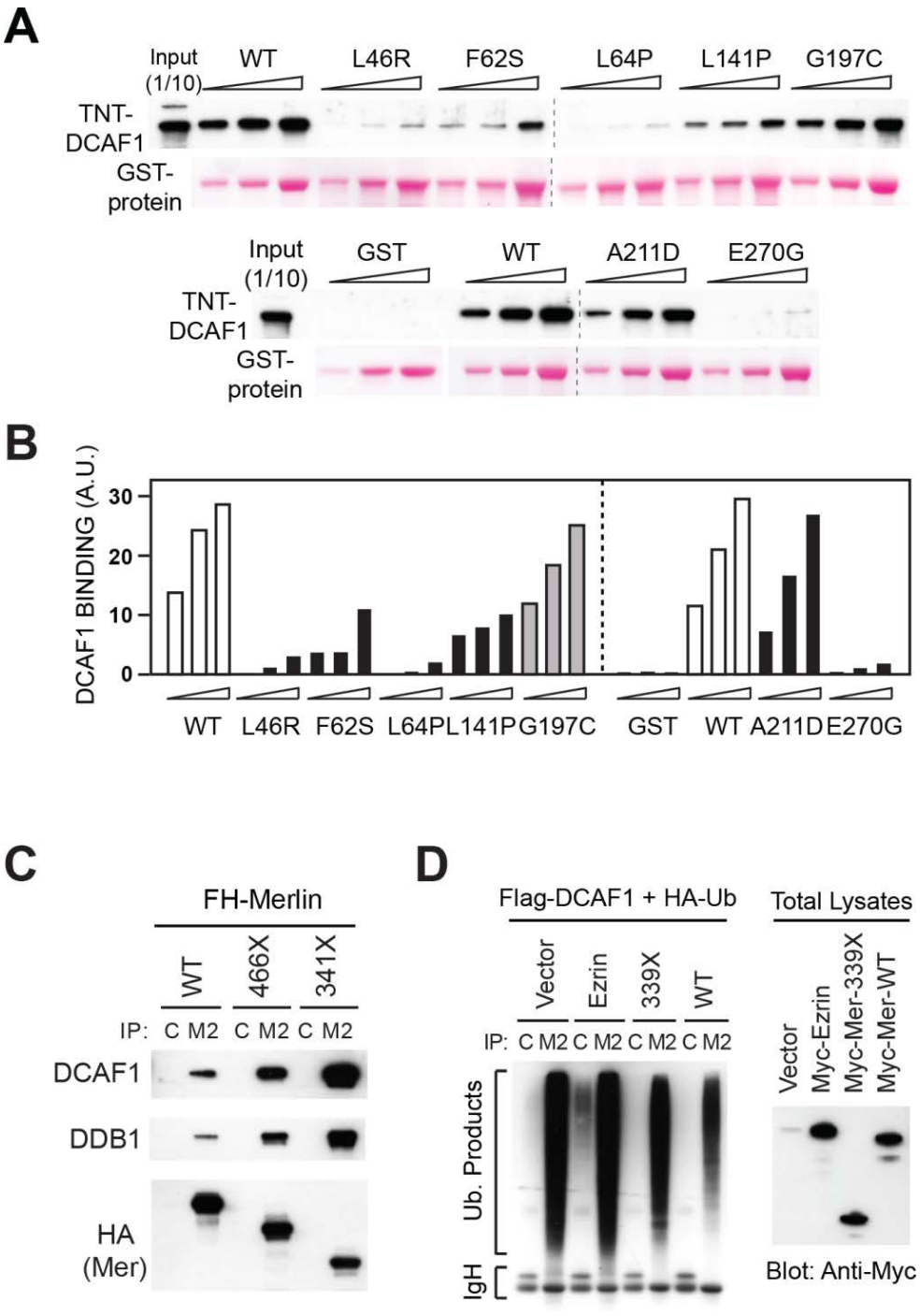
A
Input (1/10)
WT
L46R
F62S
L64P
L141P
G197C
TNT-DCAF1
GST-protein
Input (1/10)
GST
WT
A211D
E270G
TNT-DCAF1
GST-protein
B
DCAF1 BINDING (A.U.)
30
20
10
0
WT
L46R
F62S
L64P
L141P
G197C
GST
WT
A211D
E270G
C
FH-Merlin
WT
466X
341X
IP: C M2 C M2 C M2
DCAF1
DDB1
HA (Mer)
D
Flag-DCAF1 + HA-Ub
Vector
Ezrin
339X
WT
IP: C M2 C M2 C M2 C M2
Ub. Products
IgH
Total Lysates
Vector
Myc-Ezrin
Myc-Mer-339X
Myc-Mer-WT
Blot: Anti-Myc

of the interaction of Merlin with DCAF1. In contrast to the other mutations, both defective nuclear accumulation and deficient binding to DCAF1 contribute to the inability of L46R, L64P, and L141P to interact with CRL^{DCAF1} *in vivo*. Together, these experiments indicate that the six tumor-derived missense mutants that we tested do not combine with $CRL4^{DCAF1}$ *in vivo*, owing to defective accumulation in the nucleus, deficient binding to DCAF1, or a combination of the two mechanisms. These results are summarized in Table 2.1.

We speculated that mutations that introduce stop codons within Merlin's FERM domain would likely give rise to misfolded and therefore unstable protein products. However, certain nonsense mutations truncate only the carboxy terminal domain. Based on the findings by Wei Li that intramolecular associations of the FERM domain with the carboxy terminal tail promotes nuclear accumulation of Merlin (30), we speculated that deletion of Merlin's carboxy terminus would affect the ability of Merlin to maintain a closed – and presumably active – conformation. To examine if tumor-derived nonsense mutations affect the ability of Merlin to interact with or to suppress $CRL4^{DCAF1}$, I examined two prevalent truncation mutants - Merlin 466X (which lacks the C-terminal portion of α-helical domain and the carboxy terminal domain) and Merlin 341X (which retains the FERM domain but lacks both the α-helical and the carboxy terminal domain) (35). Immunoprecipitation of Flag-HA-tagged WT Merlin and its truncation mutants indicated that loss of the Merlin's carboxy terminus along with the central coiled-coil domain do not disrupt their ability to interact with $CRL4^{DCAF1}$ *in vivo* (Figure 2.5C). In fact, progressive deletion from the carboxy

Table 2.1: Patient-derived *NF2* mutations abrogate Merlin's regulation of CRL4^{DCAF1}

Patient-derived *NF2* mutations abrogate Merlin's regulation of CRL4^{DCAF1}. The indicated patient-derived missense and truncation mutants are defective in nuclear translocation, direct binding to CRL4^{DCAF1}, suppression of CRL4^{DCAF1}-mediated ubiquitylation, or a combination of these mechanisms. As a result, the NF2-derived missense mutants are unable to interact with CRL4^{DCAF1} *in vivo*, permitting the dysregulated ligase to promote tumorigenesis. NT, not tested. Data were obtained from experiments performed by Jonathan Cooper, Wei Li, and Liru You (30).

Patient-derived Merlin mutation	Biochemical defect (relative to wild-type)		
	Nuclear exclusion	Reduced In vitro DCAF1 binding	Reduced DCAF1 ligase inhibition
L46R	+	+	NT
F62S	-	+	NT
L64P	+	+	NT
L141P	+	+	NT
A211D	+	-	NT
E270G	-	+	NT
466X	NT	NT	+
341X	-	-	+

terminus resulted in augmented binding of Merlin to the ligase. Since the isolated FERM domain of Merlin accumulates in the nucleus to a larger extent than the wild type protein, whereas the C-terminal portion of Merlin including the α-helical and carboxy terminal domain remains in the cytoplasm (30), it is possible that increased nuclear accumulation facilitates the interaction of tumor-derived truncations mutants with $CRL4^{DCAF1}$. Although the isolated Merlin FERM domain binds to $CRL4^{DCAF1}$ better than WT Merlin, Liru You found that the FERM domain did not suppress $CRL4^{DCAF1}$ ligase activity *in vivo* as efficiently as wild type Merlin (Figure 2.5D), indicating that the α-helical and carboxy terminal domain contribute to Merlin's inhibitory activity. These results suggest that the tumor-derived truncation mutants of Merlin that retain the FERM domain are able to interact with $CRL4^{DCAF1}$ but fail to suppress its activity. The observation that eight distinct tumor-derived mutations impair Merlin's ability to translocate into the nucleus, to bind to DCAF1, or to inhibit $CRL4^{DCAF1}$ activity (Table 2.1) provides strong genetic evidence that Merlin suppresses tumorigenesis by inhibiting $CRL4^{DCAF1}$.

2.4: Silencing of DCAF1 suppresses the tumorigenic potential of Merlin-deficient cells

Wei Li found that DCAF1 depletion in Merlin-deficient Meso-33 mesothelioma cells and in the *Nf2*-null FC-1801 schwannoma line reduced the ability of these cells to grow in soft agar (Figure 2.6A-C) (30). The anti-mitogenic and anti-tumorigenic effect of DCAF1 depletion Merlin-deficient cells was specific

Figure 2.6: Silencing of DCAF1 suppresses the tumorigenic potential of Merlin-deficient cells

This figure was adapted from Li et al. 2010. The experiments were performed by Wei Li (**A-E**) and Lu Zhou (**F**).

(**A**) Meso-33 cells were infected with lentiviral vectors encoding two distinct shRNAs targeting DCAF1 (sh-1 and sh-2) or a control shRNA (sh-Contr.) and subjected to immunoblotting.

(**B**) FC-1801 cells treated as in (**A**). Cells infected with sh-1 were also infected with a retroviral vector encoding a shRNA-resistant version of DCAF1 or with empty vector. Lysates were immunoblotted as indicated.

(**C**) Meso-33 cells infected with the indicated lentiviral vectors were subjected to soft agar assay. The graph illustrates the total number (± SEM) of colonies present in each well after 2 weeks of culture. Representative images shown.

(**D, E**) 2 x 10^6 FC-1801 cells infected with the indicated lentiviral vectors were injected subcutaneously in nude mice. (**D**) shows the increase in volume (± SEM) over time of tumors generated by cells infected with lentiviruses encoding a control shRNA (sh-Control) or two distinct shRNAs targeting DCAF1 (sh-1 and sh-2). (**E**) shows the increase in volume (± SEM) over time of tumors generated by cells infected with sh-1 and super-infected with a retroviral vector encoding a shRNA-resistant version of DCAF1 or with empty vector. Data were obtained from the same experiment. Note the different scale of the Y axes of the two graphs.

(**F**) Primary Schwann cells from 2 normal individuals (*NF2*$^{+/+}$) and Schwannoma cells from 2 NF2 patients (*NF2*$^{-/-}$) were infected with lentiviruses encoding a shRNA targeting DCAF1 (sh-2) or a control shRNA (sh-Co.), deprived of growth factors, re-stimulated with mitogens in the presence of BrdU, and subjected to anti-BrdU staining. The graph shows the percentage (± SEM) of BrdU$^+$ cells.

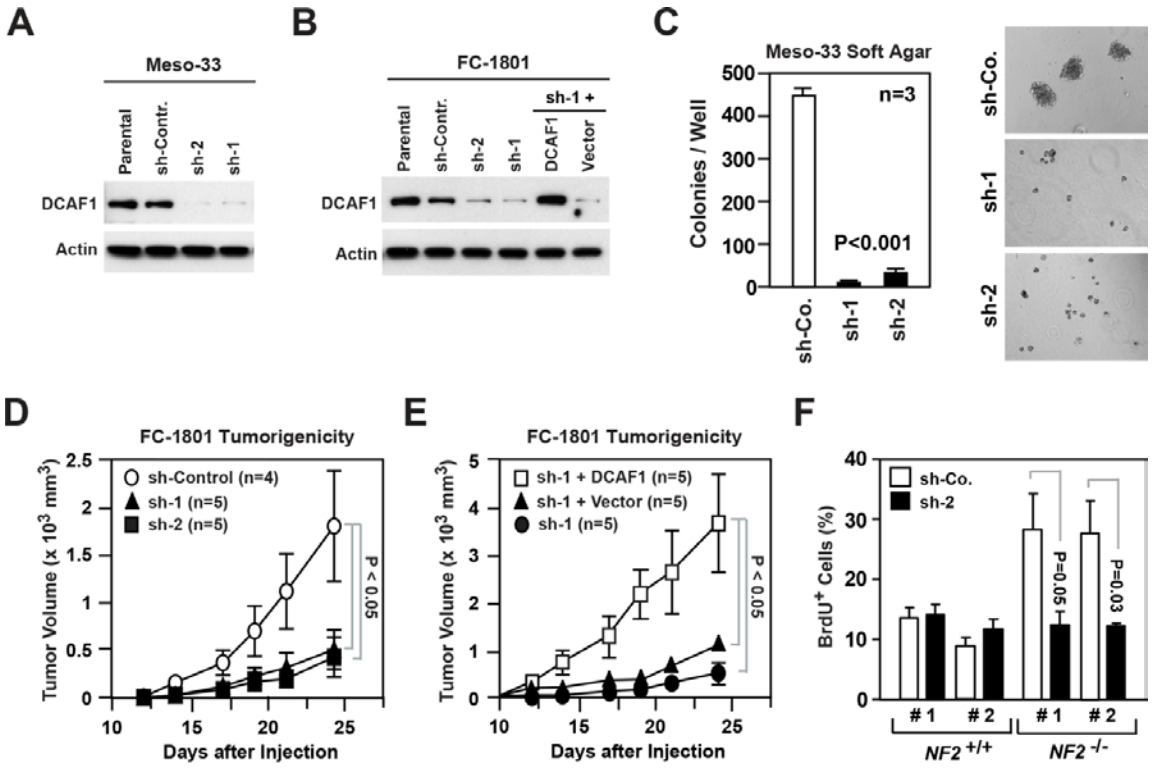
A
Meso-33
Parental
sh-Contr.
sh-2
sh-1
DCAF1
Actin
B
FC-1801
sh-1 +
Parental
sh-Contr.
sh-2
sh-1
DCAF1
Vector
DCAF1
Actin
C
Meso-33 Soft Agar
Colonies / Well
500
400
300
200
100
0
n=3
P<0.001
sh-Co.
sh-1
sh-2
sh-Co.
sh-1
sh-2
D
FC-1801 Tumorigenicity
Tumor Volume (x 10³ mm³)
sh-Control (n=4)
sh-1 (n=5)
sh-2 (n=5)
P > 0.05
Days after Injection
E
FC-1801 Tumorigenicity
Tumor Volume (x 10³ mm³)
sh-1 + DCAF1 (n=5)
sh-1 + Vector (n=5)
sh-1 (n=5)
P < 0.05
Days after Injection
F
BrdU⁺ Cells (%)
sh-Co.
sh-2
P=0.05
P=0.03
# 1
# 2
# 1
# 2
NF2 +/+
NF2 -/-

since the proliferation and soft agar growth of Ras- or Src-transformed 3T3 cells was unaffected by DCAF1 depletion (30). FC-1801 schwannoma cells express robust levels of DCAF1 and gave rise to large tumors in less than 4 weeks upon subcutaneous injection in nude mice (Figure 2.6D). Wei found that DCAF1 silencing significantly and dramatically inhibited tumor growth *in vivo*. Overexpression of a shRNA-resistant DCAF1 construct rescued the ability of DCAF1-depleted FC-1801 cells to grow as xenografts, underscoring the specificity of DCAF1 silencing (Figure 2.6E). Compellingly, the tumors with overexpressed DCAF1 grew much faster than their control counterparts (compare the Y-axes of Figures 2.6D and E), suggesting that elevated DCAF1 levels promotes tumorigenesis.

To explore the clinical relevance of our findings in the context of NF2, we collaborated with C. Oliver Hanemann and Lu Zhou at the University of Plymouth, UK. They found that silencing of DCAF1 in freshly explanted *NF2*-deficient schwannoma cells suppressed progression through G1 in response to mitogens (Figure 2.6F). Conversely, DCAF1 depletion had no effect on the proliferation of control human Schwann cells. Together, these results showed that $CRL4^{DCAF1}$ is necessary for Merlin-deficient hyperproliferation, anchorage-independent growth, and tumorigenesis.

2.5: Discussion

Prior to these studies, the underlying molecular mechanisms by which Merlin suppresses tumorigenesis had eluded NF2 research for nearly two

decades. These results revealed that dephosphorylated Merlin translocates to the nucleus where it binds to and inhibits the $CRL4^{DCAF1}$ E3 ubiquitin ligase (Figure 2.7) (30). Notably, our discovery that several tumor-derived Merlin mutants display impaired nuclear translocation, abrogated binding to $CRL4^{DCAF1}$, or attenuated CRL^{DCAF1} ligase inhibition provided compelling genetic evidence that $CRL4^{DCAF1}$ is necessary to drive tumorigenesis in Merlin-deficient tumors. Wei also found that dysregulation following Merlin deficiency shifts cells towards an oncogenic gene expression program (30). Indeed, Merlin expression and DCAF1 knockdown in Merlin-deficient cells reveal that Merlin suppresses tumorigenesis largely through DCAF1 inhibition, providing further support that Merlin regulates oncogenic gene expression through its inhibition of the $CRL4^{DCAF1}$ E3 ubiquitin ligase.

Our experiments revealed that Merlin's FERM domain binds the carboxy-terminal acidic tail of DCAF1, which is outside of the WD40 domain (30). Since the DCAF1 acidic tail is adjacent to its WD40 domain in its primary sequence, it is possible that Merlin's binding to the tail brings it in close proximity to the binding surface of the WD40 propeller. However, many possibilities exist to explain how Merlin can reduce $CRL4^{DCAF1}$ activity, which is further complicated by the multiple protein-interacting domains within DCAF1. It is possible that Merlin occludes one or more of the DCAF1 targeting domains without significant structural perturbation. In addition to - or instead of - direct competition of target recruitment, Merlin's binding may cause dramatic structural alterations, thus attenuating DCAF1 target recruitment. A study using Merlin's FERM domain and

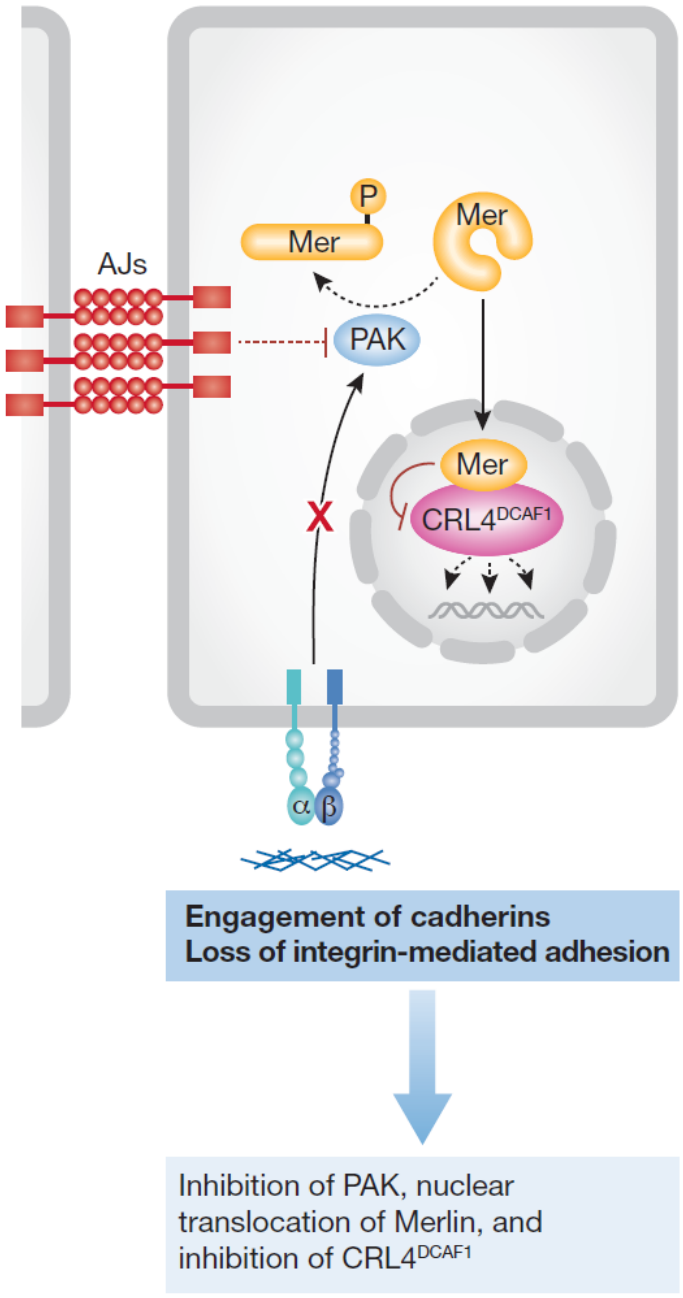

Figure 2.7: Active Merlin inhibits $CRL4^{DCAF1}$ in the nucleus.
Engagement of E-cadherin or loss of integrin-mediated adhesion leads to inactivation of PAK, promoting an accumulation of the de-phosphorylated (active) form of Merlin. Active Merlin enters the nucleus and inhibits the E3 ubiquitin ligase $CRL4^{DCAF1}$, thereby suppressing the expression of multiple pro-oncogenic genes.

an isolated FERM-binding DCAF1 region confirmed that the distal carboxy-terminal 30 residues of DCAF1 are necessary for binding to Merlin's FERM domain (128), although without full-length proteins it is difficult to interpret how Merlin's binding may affect DCAF1 function. Further biochemical studies and structural analyses will be paramount in gaining mechanistic insight into Merlin's inhibition of $CRL4^{DCAF1}$.

Our study was the first to identify a nuclear binding partner for Merlin, and further, delineated an unusual mechanism whereby an intracellular signal hijacks a cortical protein to suppress oncogenic signaling in the nucleus. These findings motivated us to identify the downstream targets of $CRL4^{DCAF1}$ to further elucidate Merlin's tumor suppressive mechanism and provide a framework for mechanism based therapies.

Chapter Three

Merlin/*NF2* loss-driven tumorigenesis is linked to $CRL4^{DCAF1}$-mediated inhibition of the Hippo pathway kinases Lats1 and 2 in the nucleus

3.1: Deregulated $CRL4^{DCAF1}$ induces activation of YAP

We previously showed that Merlin regulates several Hippo pathway target genes through inhibition of $CRL4^{DCAF1}$, raising the possibility that a Hippo pathway effector lies downstream of $CRL4^{DCAF1}$ (30). Preliminary experiments performed by Wei Li revealed that Merlin expression in *NF2*-deficient Meso-33 cells causef an increase in phosphorylation of YAP at S127, its major negative regulatory site (129). Phosphorylation of YAP at S127 causes its recruitment by 14-3-3 proteins which sequesters YAP in the cytoplasm, thereby reducing the levels of YAP in the nucleus. Subsequent expression of DCAF1 partially reversed the inhibitory phosphorylation of YAP. Expression of DCAF1-1417X, a Merlin-resistant DCAF1 mutant, almost completely counteracted Merlin's inhibition of YAP. DCAF1 knockdown similarly increased the inhibitory phosphorylation and induced YAP extrusion from the nucleus in *Nf2*-mutant FC-1801 schwannoma cells. Merlin expression and DCAF1 depletion in FC-1801 causes a significant decrease of luciferase reporter expression for TEAD, the cognate transcription factor most commonly attributed to the function of the YAP and TAZ transcriptional coactivators. These observations showed that Merlin expression or DCAF1 depletion reduce YAP activity (129). Further experiments revealed that $CRL4^{DCAF1}$ activated YAP independently of MST or Salvador, two essential

components of the Hippo kinase cascade. These results suggested that Merlin and $CRL4^{DCAF1}$ may orthogonally regulate the Hippo kinases Lats1 and 2, which functions downstream of MST and Salvador.

3.2: DCAF1 interacts with and ubiquitylates Lats1/2 *in vivo*

We examined the hypothesis that $CRL4^{DCAF1}$ inhibits Lats1 and 2 by promoting their ubiquitylation. Flag-HA-tagged DCAF1 (FH-DCAF1) associated efficiently with endogenous Lats1 and 2 (Figures 3.1A and B) but not with MST1 or 2 in 293T cells (129). To further address whether flux through the Hippo kinase cascade affects the interaction between DCAF1 and Lats, I carried out immunoprecipitations using WT FH-Lats1 and phospho-resistant (S909A/T1079A) and phospho-mimetic (S909D/T1079D) Lats1 mutants. I found that both phospho-resistant and phospho-mimetic mutants precipitated HA-DCAF1 as efficiently as WT Lats1 (Figure 3.2). I next carried out mutagenesis experiments to map the region of Lats1 that binds to DCAF1. I found that DCAF1 bound the carboxy terminal kinase domain of Lats1 (Figures 3.1C and D). I then performed *in vitro* binding assays using GST-Lats1 fusion proteins and *in vitro* translated DCAF1 fragments to determine whether these proteins directly interact. I found that the C-terminal segment of DCAF1 interacted directly with the kinase domain of Lats1 (Figures 3.3A and B). Since I could not produce recombinant Lats2 in bacteria, I was unable to verify that the C-terminal segment of DCAF1 also interacts directly with the kinase domain of Lats2. However, the homology between the kinase domains of Lats1 and 2 suggests that this is the

Figure 3.1: DCAF1 interacts with Lats1/2 *in vivo*
The experiment in (A) was performed by Wei Li.
(**A**) and (**B**) 293T cells transfected with empty vector or Flag-HA (FH)-tagged DCAF1 were immunoprecipitated with anti-Flag and immunoblotted as indicated.
(**C**) DCAF1 binds to the kinase domain of Lats1. 293T cells expressing Myc-DCAF1 in combination with Flag-HA-Lats1 or the indicated mutants were lysed in RIPA buffer. Flag immunoprecipitates (M2) and total lysates were immunoblotted as indicated. Mouse IgG agarose was used for control (C) precipitations.
(**D**) A diagram detailing the experimental results from (**B**), showing the requirement of the Lats1 kinase domain for binding DCAF1 *in vivo*.

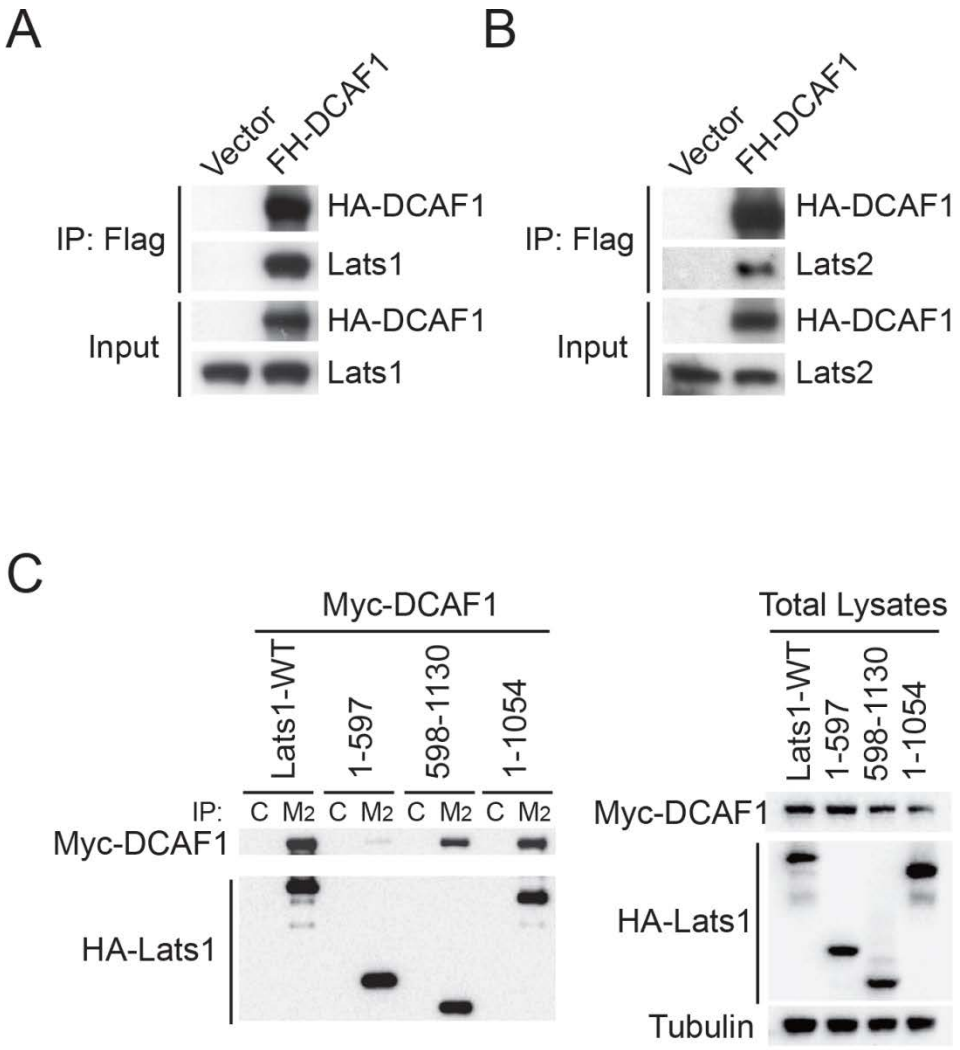
A
Vector
FH-DCAF1
IP: Flag
HA-DCAF1
Lats1
Input
HA-DCAF1
Lats1
B
Vector
FH-DCAF1
IP: Flag
HA-DCAF1
Lats2
Input
HA-DCAF1
Lats2
C
Myc-DCAF1
Lats1-WT
1-597
598-1130
1-1054
IP:
C M2 C M2 C M2 C M2
Myc-DCAF1
HA-Lats1
Total Lysates
Lats1-WT
1-597
598-1130
1-1054
Myc-DCAF1
HA-Lats1
Tubulin
D
Hydrophobic Motif
Kinase Domain
UBA
PPxY
PPxY
DCAF1 Binding
Lats1
1
1130
+
1-597
-
598-1130
+
1-1054
+

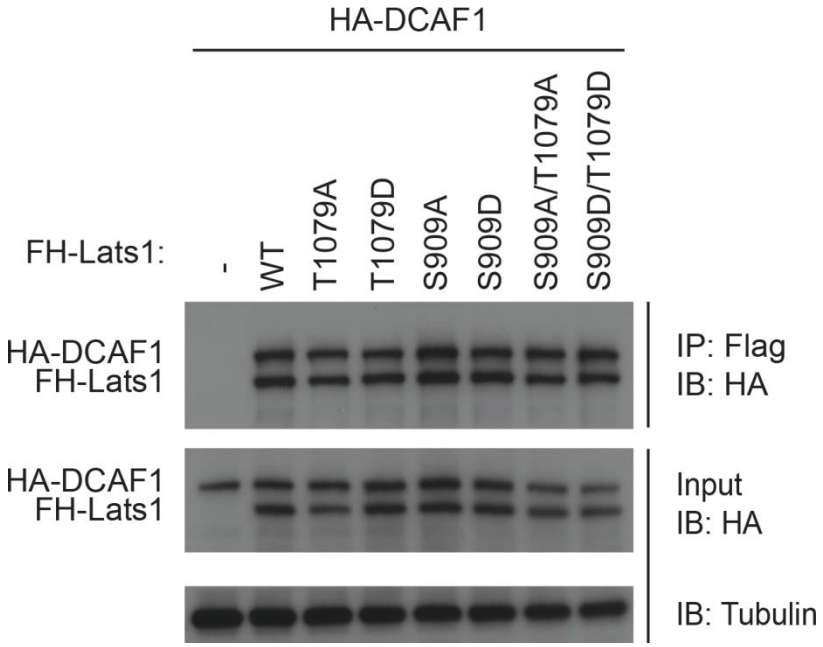

Figure 3.2: Lats1 interacts with DCAF1 independently of its phosphorylation status

Lysates and Flag immunoprecipitates from 293T cells transfected with HA-DCAF1 and WT FH-Lats1 or the indicated phosphorylation site mutants were blotted as indicated.

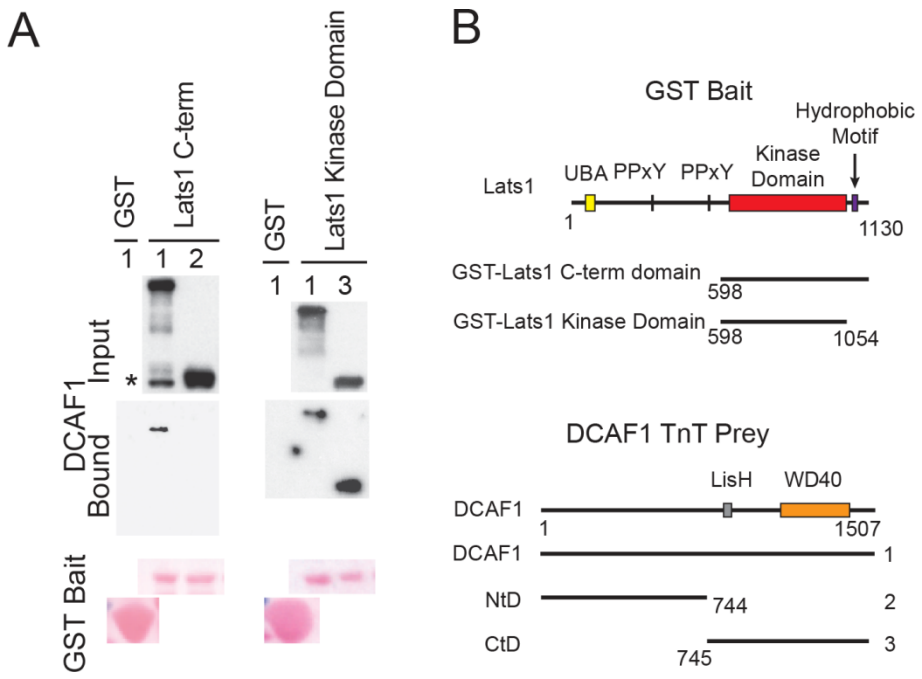

Figure 3.3: The C-terminus of DCAF1 interacts with the kinase domain of Lats1 *in vitro*

(**A**) Purified GST-Lats1-Cterm (residues 598-1130) precipitates *in vitro* transcribed and translated biotinylated (TnT) full-length DCAF1 but not the N-terminal half of DCAF1. Purified GST-Lats1-Kinase domain (residues 598-1054) precipitates full-length and C-terminal TnT-DCAF1. As a control, TnT-DCAF1 was subjected to pull down with GST. The GST-Lats1 precipitates and aliquots of TnT-DCAF1 along with respective mutants were blotted with Streptavidin-HRP.
(**B**) Diagrams showing the Lats1 and DCAF1 constructs used in (**A**).

case. Since the C-terminal fragment of DCAF1 contains the WD40 domain, which is involved in substrate recruitment (86, 130), we hypothesized that $CRL4^{DCAF1}$ recruits Lats1 and 2 in order to direct their ubiquitylation.

Wei carried out experiments revealing that Lats1 and 2 are ubiquitylated *in vivo* and that while $CRL4^{DCAF1}$ promoted Lats1 ubiquitylation *in vivo* and *in vitro*, Merlin expression largely reversed this effect (129). Moreover, Wei found that DCAF1 depletion significantly increased the half-life of Lats1 in cycloheximide-treated cells, suggesting that $CRL4^{DCAF1}$ targets Lats1 for proteasome-mediated degradation. This is consistent with the observation that Lats1 is polyubiquitylated *in vivo* (129).

3.3: Merlin inhibits $CRL4^{DCAF1}$ recruitment of Lats

Our prior studies indicated that Merlin inhibits $CRL4^{DCAF1}$ through its FERM domain to a carboxy terminal segment of DCAF1 (30). Patient-derived Merlin mutants lacking the central coiled-coil and carboxy terminal domains bind to DCAF1 but fail to suppress $CRL4^{DCAF1}$ ligase activity, suggesting these segments are also required to inhibit ligase activity. To test whether Merlin inhibits $CRL4^{DCAF1}$ by interfering with substrate recruitment, Wei tested whether Merlin expression disrupts the interaction between FH-DCAF1 and endogenous Lats1 in 293T cells. He found that co-transfection with increasing quantities of HA-Merlin led to a dose-dependent decrease in the interaction between FH-DCAF1 and endogenous Lats1 (Figure 3.4A). To determine whether Merlin may interfere with Lats1 binding, I carried out immunoprecipitations to determine whether FH-Merlin

Figure 3.4: Merlin interacts with Lats1 and disrupts $CRL4^{DCAF1}$-Lats1 binding

The experiment in (**A**) was performed by Wei Li.

(**A**) 293T cells expressing FH-DCAF1 in combination with increasing quantities of HA-Merlin were immunoprecipitated with anti-Flag and immunoblotted as indicated.

(**B**) Merlin's coiled-coil/C-terminal domain binds to the Lats1 kinase domain. 293T cells expressing HA-Lats1 in combination with Flag-HA-Merlin or the indicated mutants were lysed in RIPA buffer. Flag immunoprecipitates (M2) and total lysates were immunoblotted as indicated. Mouse IgG agarose was used for control (C) precipitations.

(**C**) Merlin binds to the kinase domain of Lats1. 293T cells expressing Myc-Merlin in combination with the indicated Flag-HA-tagged Lats1 fusion proteins were lysed in RIPA buffer. Flag immunoprecipitates (M2) and total lysates were immunoblotted as indicated. Mouse IgG agarose was used for control (C) precipitations.

(**D**) Diagram illustrates a model based on the definition of the sequence requirements for binding of DCAF1 to Lats and of Merlin to DCAF1. The WD40 domain of DCAF1, which is implicated in substrate selection, binds directly to the kinase domain of Lats (**right**). Merlin binds through its FERM domain to the C-terminal segment of DCAF1, disrupting the association of DCAF1 with Lats (**left**).

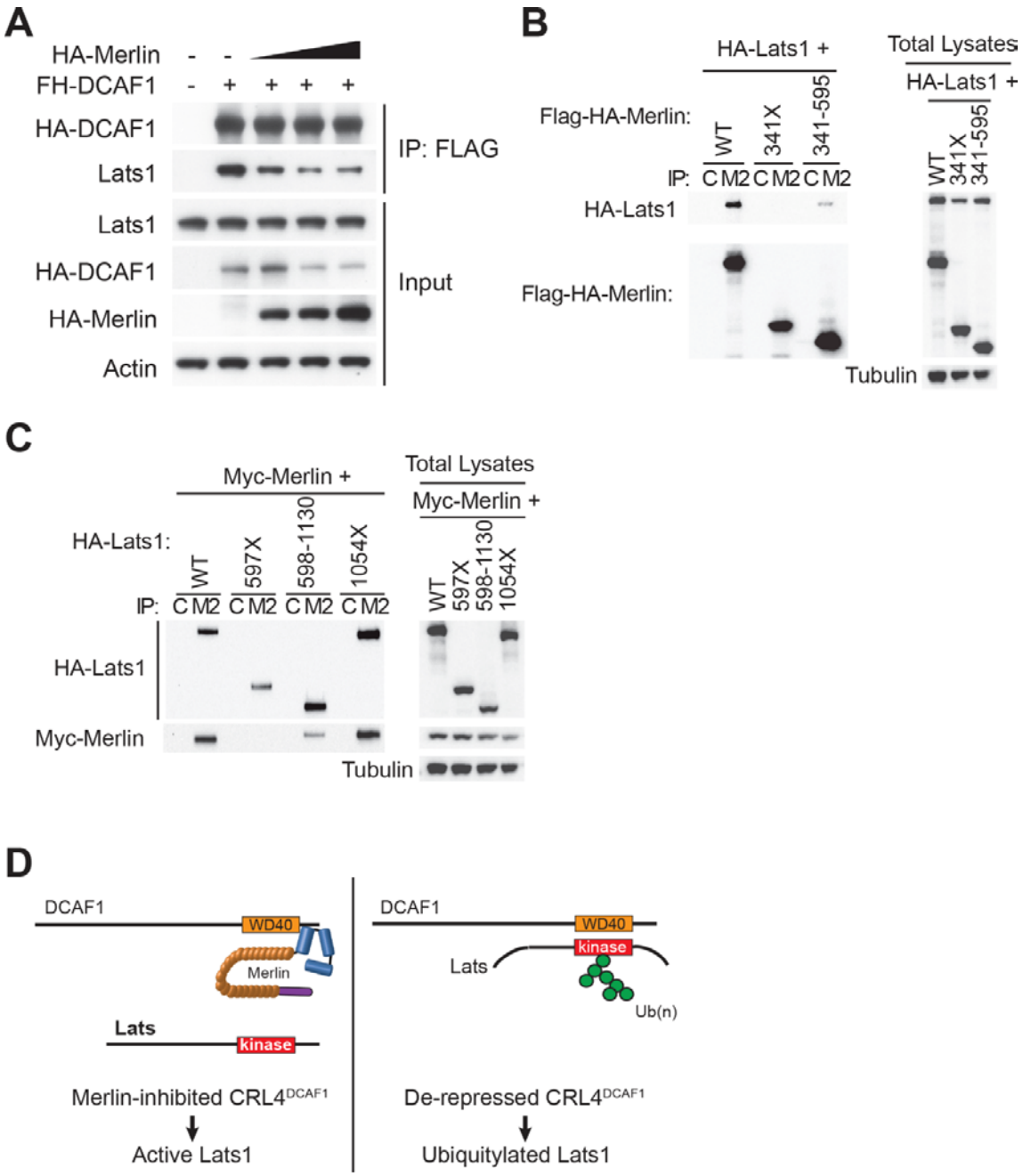
A
HA-Merlin - -
FH-DCAF1 - + + + +
HA-DCAF1
Lats1
IP: FLAG
Lats1
HA-DCAF1
HA-Merlin
Actin
Input
B
HA-Lats1 +
Total Lysates
HA-Lats1 +
Flag-HA-Merlin:
WT
341X
341-595
IP: C M2 C M2 C M2
HA-Lats1
Flag-HA-Merlin:
Tubulin
C
Myc-Merlin +
Total Lysates
Myc-Merlin +
HA-Lats1:
WT
597X
598-1130
1054X
IP: C M2 C M2 C M2 C M2
HA-Lats1
Myc-Merlin
Tubulin
D
DCAF1
WD40
Merlin
Lats
kinase
Merlin-inhibited CRL4DCAF1
Active Lats1
DCAF1
WD40
kinase
Lats
Ub(n)
De-repressed CRL4DCAF1
Ubiquitylated Lats1

and HA-Lats1 interact *in vivo*. Not only do FH-Merlin and HA-Lats1 interact *in vivo*, but Merlin's FERM domain was neither necessary nor sufficient for binding in my experiments (Figure 3.4B). It is notable, however, that loss of the FERM domain causes a decrease in HA-Lats1 binding, suggesting that residues within the FERM domain may be necessary to promote interaction between Lats1 and Merlin's coiled-coil or carboxy-terminal domains. Recent biochemical evidence suggests that Merlin's FERM domain directly interacts with the amino-termini of Lats1 and 2 (131), suggesting that Merlin's FERM domain is indeed important for Lats1 interactions. I carried out additional *in vivo* binding to determine that Merlin, like DCAF1, can bind to the kinase domain of Lats1 (Figure 3.4C). Combined, these results suggest that the coiled-coil and C-terminal domains of Merlin may occlude the binding site for Lats on the WD40 domain of DCAF1 (Figure 3.4D). Alternatively or in addition, Merlin may compete with DCAF1 for binding of the Lats kinase domain.

3.4: Nuclear Merlin promotes YAP phosphorylation and inhibits proliferation

Since $CRL4^{DCAF1}$ accumulates predominantly in the nucleus (30), Wei Li examined whether Merlin needs to enter the nucleus to inactivate YAP and to induce proliferation arrest. Using an ERT2-Merlin fusion protein, Wei found that driving Merlin to the nucleus was sufficient to induce YAP phosphorylation and to cause a two-fold decrease in progression through G1 in *NF2*-mutant Meso-33 cells (129). To determine whether Merlin's nuclear localization is necessary to

induce YAP phosphorylation and reduce cell proliferation, Wei used mutation analysis to identify a four-residue mutant - Merlin Δ24-27 or Merlin 24-27A - which is completely defective in nuclear translocation. In contrast to WT Merlin, the nuclear localization defective mutants were highly defective in their ability to suppress proliferation, anchorage independent growth, or to induce YAP phosphorylation in Meso-33 cells (129). These mutants were still able to interact with the tight-junction associated protein Angiomotin, an established Merlin-binding protein, suggesting that the deficiencies of these mutants are not due to gross folding defects. Combined, Wei's experiments showed that Merlin needs to enter the nucleus to inactivate YAP and to suppress cell proliferation.

3.5: $CRL4^{DCAF1}$ inhibits Lats in the nucleus

The core Hippo pathway components are generally considered to function at the cell cortex or in the cytosol (116). Lats1 and 2 were assumed to function in these compartments based on immunofluorescence experiments on cells overexpressing tagged forms of these proteins or subcellular fractionation experiments excluding nuclear fractions (132-134). Since active $CRL4^{DCAF1}$ exerts its pro-oncogenic function in the nucleus (30) and ubiquitylates Lats1 and 2, we hypothesized that Lats1 and 2 also localize in the nucleus. Wei carried out fractionation and immunofluorescence experiments revealing that a majority of Lats1 and 2 are localized in the nucleus in untransformed Met5a mesothelial cell. Interestingly, following precipitation of endogenous Lats1 from cytosolic/crude membrane or nuclear fractions, Wei found that active Lats1 resides largely in the

nuclear fraction (129). This observation was corroborated using human liver epithelial cells and primary mouse fetal liver progenitor cells. Interestingly, these results suggest that MST or an unknown upstream kinase translocates into the nucleus to phosphorylate and activate Lats.

Although Lats1 and 2 appear to localize predominantly in the nucleus in both sparse and confluent cells, Wei also observed that Lats1 localizes at the cell cortex in normal, but not *NF2*-mutant cells (129). Following this observation, Wei hypothesized that Merlin expression modifies the subcellular localization of Lats1 in *NF2*-mutant cells. Indeed, transiently transfected WT Merlin localized predominantly at lamellipodia and membrane ruffles in Meso-33 cells and enhanced the recruitment of endogenous Lats1 to these compartments. Lats1 interacts with Merlin *in vivo* (Figures 3.4B and C), in agreement with the recently proposed hypothesis that Merlin recruits Lats to the plasma membrane to promote its activation (132) and recent structural data showing that Merlin's FERM domain interacts directly with an amino-terminal region on Lats1 and 2 (131).

3.6: Merlin does not suppress tumorigenesis from the cell cortex

Based on our findings, I investigated the functional relevance of Merlin's interaction with the Lats kinases at the cell cortex. I tested four patient-derived missense mutants, which fail to accumulate in the nucleus (L46R, L64P, L141P, and A211D), and one that enters into the nucleus but does not bind to DCAF1 (E270G) (30). In addition, I examined the two synthetic nuclear-defective

mutants, Merlin 24-27A and Merlin Δ24-27. Co-immunoprecipitation analysis indicated that recombinant wild type Merlin combines with endogenous Lats1 much less efficiently than with $CRL4^{DCAF1}$ in an extraction buffer containing 0.5% Triton-X100 but no ionic detergent (Figures 3.5A and B). In addition, whereas all nuclear-defective and patient-derived mutants of Merlin failed to associate with DCAF1 in this assay, none of them exhibited reduced ability to interact with Lats1 (Figures 3.5A and B). Similar results were obtained by using RIPA buffer containing 0.1% SDS (Figure 3.5C), although we note that this buffer may unfold the FERM domain of Merlin exposing hydrophobic segments (73). In agreement with these results, none of the patient-derived mutants exhibited reduced ability to recruit Lats1 to lamellipodia and membrane ruffles upon transient overexpression in Meso-33 cells (129). In contrast, they all failed to induce phosphorylation of YAP at Ser 127. These findings support the conclusion that Merlin suppresses tumorigenesis by inhibiting $CRL4^{DCAF1}$, thereby stabilizing activated Lats in the nucleus, rather than by recruiting Lats to the plasma membrane.

3.7: $CRL4^{DCAF1}$-mediated inhibition of Lats and deregulated YAP signaling sustain the oncogenic properties of Merlin-deficient tumor cells

Wei used genetic epistasis experiments to test the hypothesis that $CRL4^{DCAF1}$ promotes tumorigenesis by inhibiting Lats1 and 2. Merlin-deficient tumor cells, including Meso-33 human mesothelioma and FC-1801 mouse schwannoma undergo a significant growth arrest upon DCAF1 depletion (30).

Figure 3.5: Merlin does not suppress tumorigenesis from the cell cortex
(**A**) 293T cells were transfected with empty vector (HA Ctrl) or Flag-HA-tagged Merlin (wild type or its mutants) and were lysed 24 hours later in a buffer containing 0.5% Triton X-100 without ionic detergent. Flag immunoprecipitates were washed using the same buffer. Flag immunoprecipitates and input were immunoblotted as indicated.
(**B**) Fold enrichment of immunoprecipitated DCAF1 and Lats1 was estimated by densitometry of blots in (**A**), where enrichment is expressed as the total density of the immunoprecipitated bands normalized to their respective inputs.
(**C**) As in (**A**) except using a more stringent buffer. RIPA buffer containing 0.1% SDS was used for cell lysis and immunoprecipitation.

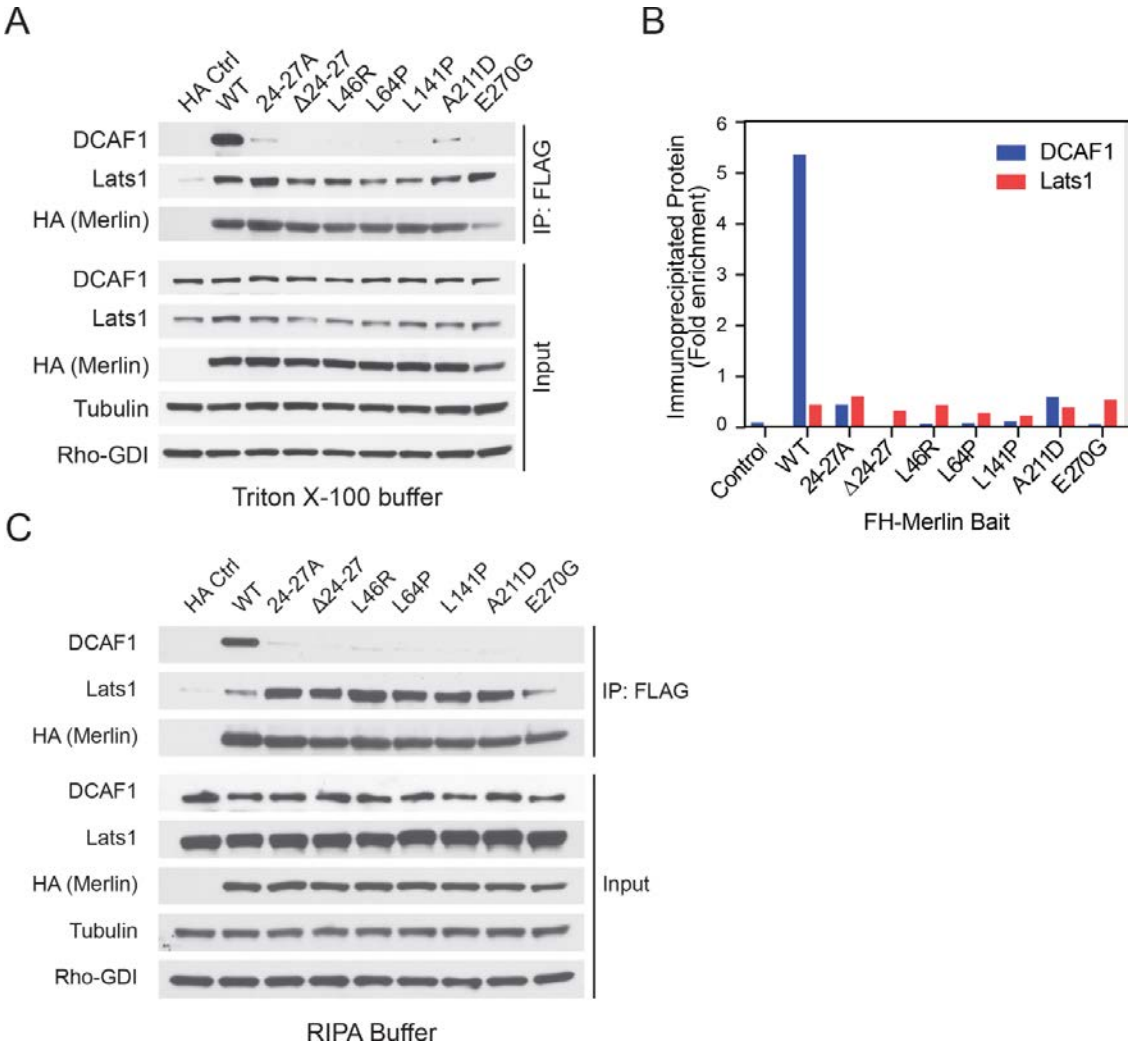
A
HA Ctrl
WT
24-27A
Δ24-27
L46R
L64P
L141P
A211D
E270G
DCAF1
Lats1
HA (Merlin)
IP: FLAG
DCAF1
Lats1
HA (Merlin)
Tubulin
Rho-GDI
Input
Triton X-100 buffer
B
Immunoprecipitated Protein
(Fold enrichment)
DCAF1
Lats1
Control
WT
24-27A
Δ24-27
L46R
L64P
L141P
A211D
E270G
FH-Merlin Bait
C
HA Ctrl
WT
24-27A
Δ24-27
L46R
L64P
L141P
A211D
E270G
DCAF1
Lats1
HA (Merlin)
IP: FLAG
DCAF1
Lats1
HA (Merlin)
Tubulin
Rho-GDI
Input
RIPA Buffer

Expression of WT Yap or YAP-5SA – a phospho-resistant and constitutively active YAP mutant – rescued the ability of DCAF1-depleted Meso-33 and FC-1801 cells to proliferate (129). Moreover, YAP-5SA expression completely reversed the anti-tumorigenic effect of DCAF1 depletion in FC-1801 xenografts. Similarly, simultaneous knockdown of Lats1 and 2 rescued the ability of DCAF1-depleted Merlin-deficient tumors to proliferate, grow independent of anchorage, and xenograft in nude mice. Together, these findings provided mechanistic evidence that dysregulated $CRL4^{DCAF1}$ promotes tumorigenesis in Merlin-deficient cells by inactivating Lats1 and 2, thereby activating YAP (Figure 3.6).

3.8: $CRL4^{DCAF1}$ controls YAP/TAZ-dependent gene expression in NF2 mutant tumors

Following our delineation of the mechanism by which DCAF1 promotes oncogenic signaling through activation of YAP in Merlin-deficient cells, we set out to explore the clinical relevance of our observations. I examined a panel of 11 human malignant mesothelioma cell lines, seven of which carried inactivating mutations at the *NF2* locus. Immunoblotting revealed that the *NF2* mutant lines exhibited severely diminished levels of Lats1, but not Lats2, as compared to *NF2* wild type lines (Figures 3.7A and 3.7B, left). In addition, all except one of the *NF2* mutant cell lines displayed decreased phosphorylation of YAP, and 4 out of 7 lines displayed increased expression of the YAP target gene *CTGF* (Figures 3.7A and 3.7B, right). These results are consistent with the conclusion that $CRL4^{DCAF1}$

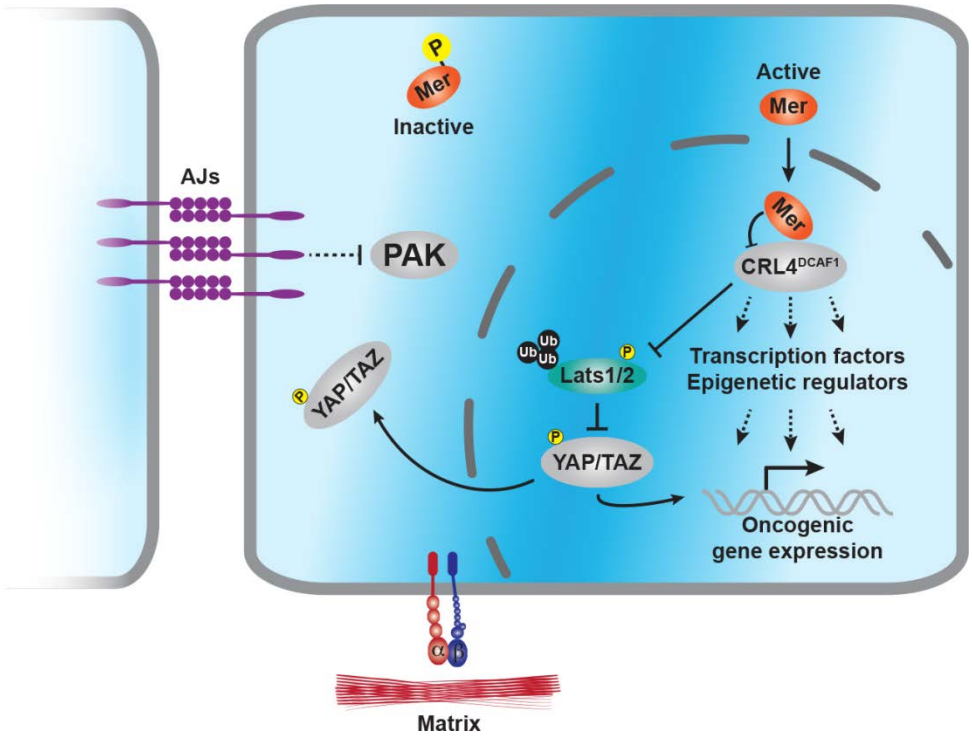

Figure 3.6: Merlin suppresses YAP/TAZ activity and oncogenic gene expression by inhibiting CRL4^{DCAF1} in the nucleus

Merlin's regulation of CRL4^{DCAF1} likely impinges on multiple downstream epigenetic mechanisms and blocks oncogenic gene expression. In contact inhibited cells, active Merlin translocates to the nucleus where it binds to and inhibits the CRL4^{DCAF1} E3 Ubiquitin ligase. Active or dysregulated CRL4^{DCAF1} induces an oncogenic gene expression program by promoting downstream Hippo pathway targets via inhibition of the Lats1 and 2 kinases and through modulation of epigenetic modifiers and transcription factors.

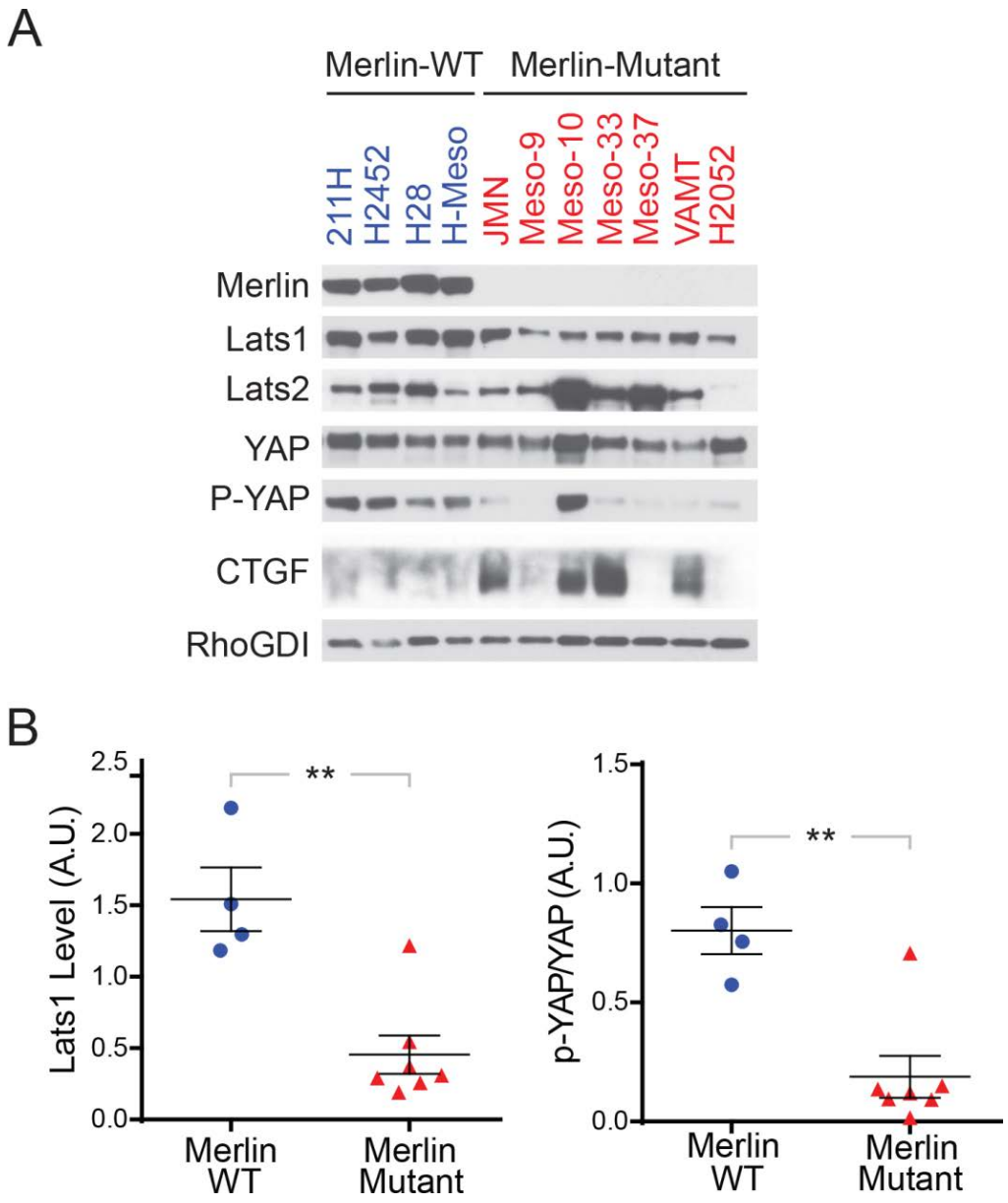

Figure 3.7: CRL4^{DCAF1} controls YAP/TAZ-dependent gene expression in *NF2* mutant tumors

(**A**) A panel of human mesothelioma cell lines, including Merlin-wild-type (WT) and Merlin-mutant, were cultured under the same condition. Lysates were immunoblotted as indicated.

(**B**) Densitometry of Lats1 (**left**) and p-YAP/YAP (**right**) signals from blots in (A) was performed and plotted.**P<0.01.

promotes activation of YAP in malignant mesothelioma at least in part by increasing degradation of Lats1.

Wei next examined whether loss of *NF2* induces YAP-dependent oncogenic gene expression in mesothelioma patient samples by generating a gene expression signature that reflects $CRL4^{DCAF1}$-dependent YAP activity. He established the gene expression signature by comparing the expression profile of Meso-33 cells depleted of DCAF1 or YAP/TAZ. Single knockdown of YAP or TAZ did not elicit a profound change in gene expression, consistent with the finding that only simultaneous YAP and TAZ depletion causes a proliferation arrest in Meso-33 to the same extent as DCAF1 loss (129). Expectedly, simultaneous YAP/TAZ depletion causes a significant decline in gene expression, of which almost 40% were similarly regulated by DCAF1. These results revealed that $CRL4^{DCAF1}$ controls a large fraction of the YAP/TAZ gene expression program in *NF2*-mutant cells. Wei used the genes that were similarly regulated by YAP/TAZ and DCAF1 depletion as a signature to perform unsupervised hierarchical clustering of the gene expression profiles from 53 human mesotheliomas. 39 of these mesotheliomas harbored a mutation or genomic loss at the *NF2* locus and, by and large, had a largely distinct gene expression program that segregated them from the *NF2*-positive mesotheliomas. Gene set enrichment analysis revealed that $CRL4^{DCAF1}$-activated genes were highly enriched in *NF2*-mutant mesotheliomas compared with the remaining mesotheliomas. Importantly, among those DCAF1-activated genes, those that were also regulated by YAP and TAZ

were even more enriched. These data showed that $CRL4^{DCAF1}$ controls YAP/TAZ-dependent gene expression in *NF2*-mutant mesotheliomas (129).

To examine the clinical relevance of our findings in NF2 tumors, we collaborated with Lu Zhou and C. Oliver Hanemann at the Plymouth University, UK, to analyze freshly explanted human schwannoma cells. Our prior studies showed that re-expression of Merlin or silencing of DCAF1 suppresses the proliferation of these cells (30). Re-expression of Merlin or DCAF1 depletion induced YAP phosphorylation to a similar extend in these cells, suggesting that $CRL4^{DCAF1}$ also controls oncogenic YAP/TAZ signaling in patient-derived *NF2*-deficient schwannomas. Wei next collaborated with Matthias A. Karajannis and Matija Snuderl at NYU Langone Medical Center to examine Yap activation in 40 human meningioma and vestibular schwannoma samples classified by *NF2* mutational status. Wei found that the inhibitory S127 phosphorylation of YAP was significantly lower in the *NF2*-mutant tumors as assessed by western blotting. Staining of formalin-fixed meningiomas revealed strong nuclear YAP expression in 73% of *NF2*-mutant samples. Overall, there was a strong positive correlation between nuclear YAP staining and weak/absent cytoplasmic phospho-YAP staining in tumors with low Merlin expression. Combined, these clinical findings support the hypothesis that $CRL4^{DCAF1}$ inhibits Lats and thereby activates YAP in *NF2*-mutant tumors.

3.9: Discussion

Drosophila genetics experiments provided strong evidence that Merlin functions with Ex to activate Hippo signaling (25). However, two recent landmark studies revealed separate, non-linear mechanisms by which Merlin promotes Hippo signaling. DJ Pan's group found that Merlin could directly bind to Wts/Lats in both *Drosophila* and mammals, recruiting these proteins to the plasma membrane to be phosphorylated by active Mst1/2 (Figure 3.8A) (132). This study further used genetic experiments in mammalian cells to show that Merlin promotes downstream Hippo signaling independently of Mst1/2, revealing Merlin's direct biochemical role in regulating the Hippo pathway. However, our findings showed that dysregulated $CRL4^{DCAF1}$ promotes YAP function and TEAD-dependent transcription by ubiquitylating and inhibiting Lats1/2 in the nucleus (Fig. 3.8B) (129). Genetic experiments and analysis of Merlin mutations revealed that $CRL4^{DCAF1}$-mediated inhibition of Lats1/2 sustains the tumorigenicity of Merlin-deficient cells. Compellingly, analysis of clinical samples strongly suggested that this YAP- and TAZ-promoting circuit of the Hippo pathway functions in Merlin-deficient malignancies. Furthermore, our experiments revealed that tumor-derived Merlin mutants are invariably defective in binding to $CRL4^{DCAF1}$ yet retain Lats1 binding, providing genetic evidence that Merlin's interaction with Lats1 at the plasma membrane is not sufficient to suppress tumorigenesis. Merlin's recruitment of Lats1 at the plasma membrane is an important and evolutionarily conserved non-canonical Hippo pathway mechanism. However, it appears that Merlin's suppression of the $CRL4^{DCAF1}$ E3 ubiquitin ligase is a paramount tumor

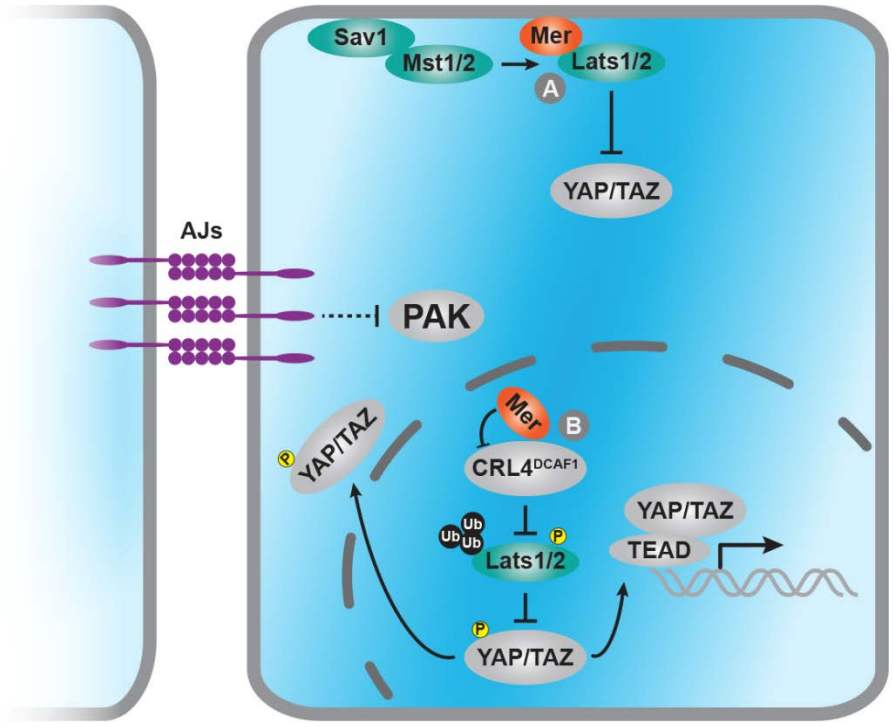

Figure 3.8: Cortical and nuclear models of Merlin's regulation of Hippo signaling

(**A**) At the plasma membrane, Merlin recruits the Lats kinases and coordinates their activation by Mst1, driving phosphorylation and inhibition of YAP/TAZ.

(**B**) Dephosphorylated Merlin translocates to the nucleus and inhibits $CRL4^{DCAF1}$, preventing this E3 ligase from ubiquitinating and inhibiting Lats1/2. These core Hippo pathway components, activated by an upstream kinase, phosphorylate and inactivate YAP/TAZ.

suppressive clamp embedded in the human Hippo pathway. *In vivo* insight into the contribution of both of these mechanisms in mammals will be an essential step in validating their significance in the context of normal function and tumorigenesis. These findings further emphasize the lack of conservation between the linear model for Hippo activation in *Drosophila* and the multifarious regulation of YAP and TAZ in mammals. Combined, insights over the past five years have shown that Merlin regulates the Hippo pathway at multiple levels, yet these signals seem to invariably converge to regulate YAP and TAZ activation (116). It will be important to determine the spatio-temporal hierarchy of Merlin's effects on Hippo signaling and the importance of these pathways in pathogenically relevant tissues, which may unmask the most significant druggable targets for Merlin-deficient malignancies.

Chapter Four

In vivo mouse modeling of CRL4^{DCAF1} function in Merlin-deficient Tumorigenesis

4.1: Introduction

Nf2 knockout mice succumb in utero, whereas heterozygous *Nf2* mutant mice develop multiple malignancies, especially if an allele of p53 is simultaneously inactivated. The tumors arising in *Nf2* mutant mice include hepatocellular carcinomas and osteosarcomas among others, but not schwannomas or meningiomas, which are the hallmark tumors of NF2 patients (135). This finding illustrates the differences in kinetics of loss of heterozygosity (LOH) between humans and mice, but also points to Merlin's broad tumor suppressor function. Conditional biallelic inactivation of *Nf2* in Schwann cells leads to Schwann cell hyperplasia and schwannoma formation (136), mimicking human neurofibromatosis type 2, which results from LOH at the *NF2* locus (35). Furthermore, biallelic inactivation of *Nf2* in arachnoidal cells leads to the formation of meningiomas, which have significant histological similarity to the corresponding human tumors (137). In a similar fashion, *Nf2*$^{+/-}$ mice have increased sensitivity to the carcinogenic effect of inhaled asbestos (138) and conditional deletion of *Nf2* in mesothelial cells cooperates with loss of Ink4a/Arf and p53 to drive malignant mesothelioma (139). Conditional biallelic loss of *Nf2* in the liver was recently shown to result in hepatomegaly and formation of malignant tumors (140, 141). Liver-specific *Nf2* deletion causes expansion of a

progenitor population able to differentiate at least partially along the ductal lineage (142) and more recent evidence suggests the cells arise from de-differentiation of hepatocytes into a bipotential state (143). The complete penetrance observed in this model indicates that Merlin is a potent regulator of liver size and tumor suppression, and future studies using this model may provide great insight into Merlin's normal biological function and role in tumor suppression.

We previously found that DCAF1 is necessary for the growth of *Nf2*$^{-/-}$ Schwann cells injected in the rear flanks of nude mice (30). These preliminary results entreated investigation of the hypothesis that Merlin suppresses tumorigenesis *in vivo* through inhibition of CRL4^{DCAF1} using pathogenically relevant mouse models. I elected to use Merlin-deficient liver tumorigenesis models due to the pathogenic relevance in the mouse, where 10% of *Nf2*$^{+/-}$ mice develop liver tumors (135). I also set out to develop a genetically tractable model for Merlin-deficient malignant pleural mesothelioma, a disease which has a poor prognosis and few *in vivo* models to dissect its underlying genetics.

4.2: Development of a *Dcaf1* conditional allele

To determine the *in vivo* role of CRL4^{DCAF1} in Merlin-deficient tumorigenesis, I developed a targeting strategy to conditionally delete *Dcaf1* exon 14 (Figure 4.1). Deletion of this exon, the largest in *Dcaf1*, truncates more than half of the coding region. In the unlikely event that this allele encodes a stable protein, it would lack its entire WD40 domain and a conserved helix-loop-

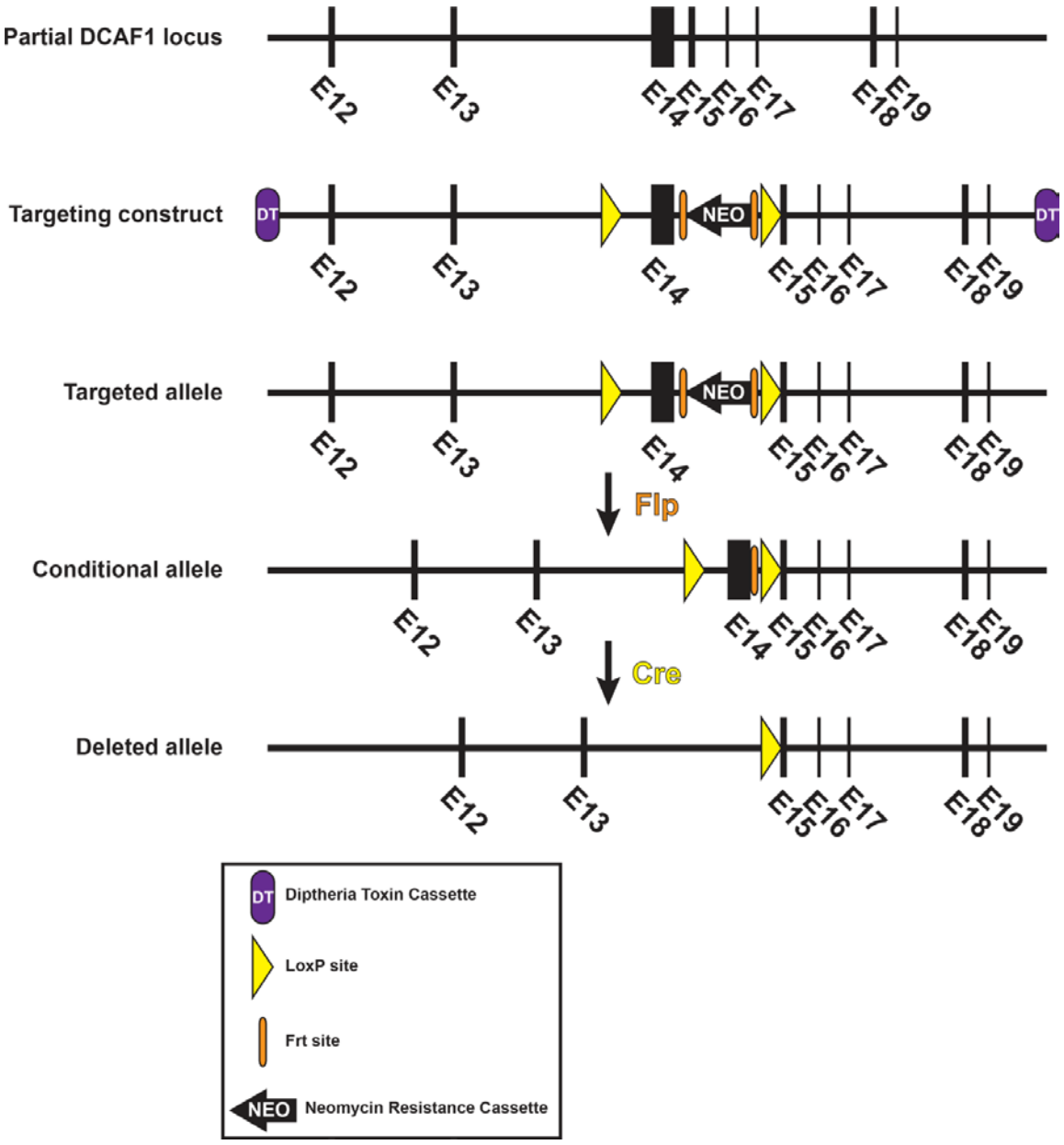

Figure 4.1: Schematic of *Dcaf1* targeting
A targeting construct designed for the conditional deletion of *Dcaf1* exon 14 is shown below its targeted endogenous locus. Flp recombinase-mediated excision of the Neo cassette was carried out to establish founder *Dcaf1* conditional mice. Cre-mediated recombination of the conditional allele deletes exon 14 and causes an early stop codon in exon 15, terminating the transcript before the WD40 domain of DCAF1.

helix which is necessary for interaction with DDB1 (144). Abolishing DDB1 interaction would prevent DCAF1 from functioning within the $CRL4^{DCAF1}$ ligase. I collaborated with the Rockefeller University Gene Targeting Resource Center which carried out the initial gene targeting steps in mouse embryonic stem cells (ESCs) and helped me design a Southern blotting strategy to identify positively targeted clones. *Dcaf1* targeting resulted in ~5% positive clones based on the first round of Southern blotting (Figure 4.2A). These initial positive clones were subjected to a second round of Southern blotting to further assess proper integration of the targeting construct at the *Dcaf1* locus. Blastocyst injections of targeted ES cells by the MSKCC Mouse Genetics Core yielded several highly chimeric mice which were bred with wild-type mice to obtain founders carrying the $Dcaf1^{Flox}$ allele (Figure 4.2B). These mice were then crossed with Flp-expressing mice to excise the Neomycin cassette, thereby precluding any potential issues with hypomorphic function of the targeted allele which can arise due to defects in splicing. I developed a genotyping strategy with Peter Romanienko of the MSKCC Colony Management Group to differentiate between mice carrying the wild-type or targeted *Dcaf1* allele (Figure 4.2C). To determine whether this conditional *Dcaf1* allele directed Cre-mediated recombination at the *Dcaf1* locus and subsequent ablation of DCAF1 protein, I isolated mouse embryonic fibroblasts (MEFs) from $Dcaf1^{F/F}$ mice. I infected these MEFs with control GFP-expressing lentivirus or Cre-expressing lentivirus. Immunoblotting DCAF1 confirmed complete loss of DCAF1 expression (Figure 4.2D).

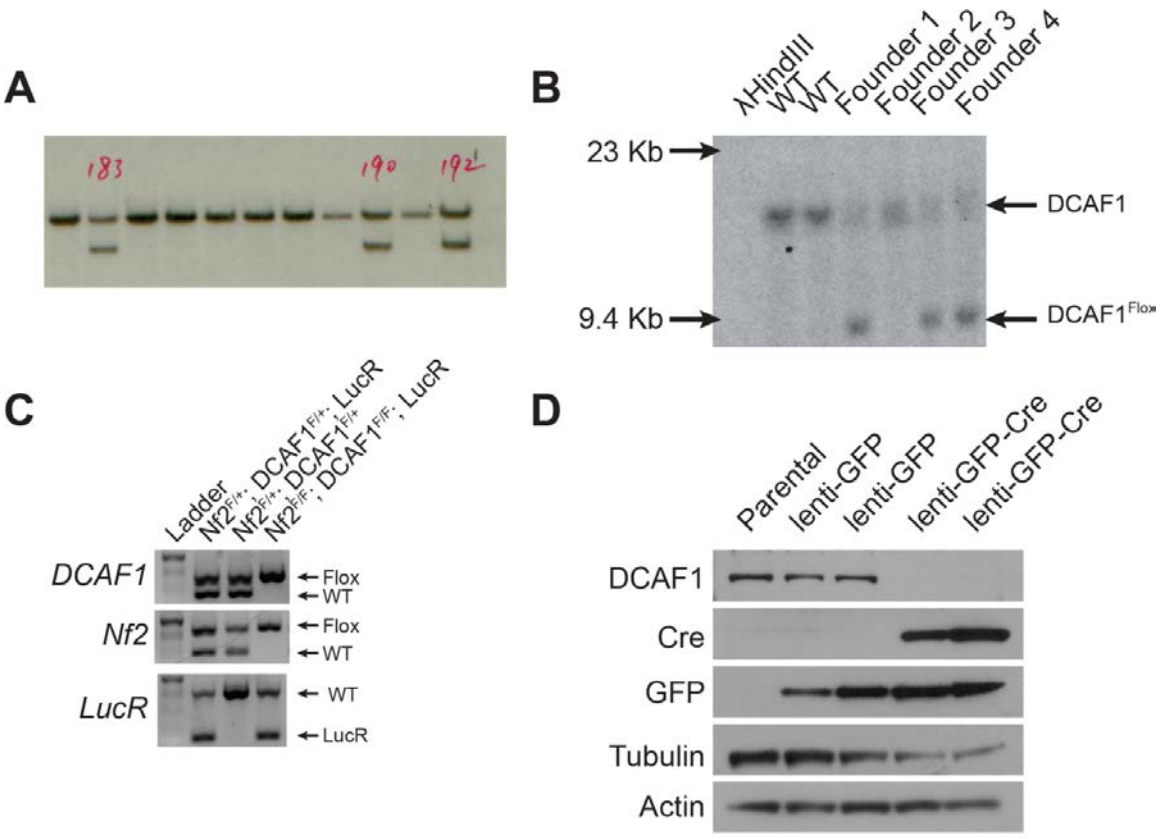

Figure 4.2: Confirmation of *Dcaf1* targeting

(**A**) Southern blot analysis using a probe specific to the *Dcaf1* locus shows three representative positive clones obtained from targeting in mouse ES cells.

(**B**) Southern blot analysis using a probe specific to the *Dcaf11* locus reveal the presence of the targeted allele in $Dcaf1^{F/+}$ founders (top) and a probe specific to the Neomycin cassette reveals single integration of the targeting construct in these mice (bottom).

(**C**) Following removal of the Neomycin resistance cassette by breeding of *DCAF1* mice with *Flp* mice, conditional *Dcaf1* mice were bred to conditional *Nf2* mice and *LSL-Luciferase* (*LucR*) reporter mice to obtain $Nf2^{F/F}$;$Dcaf1^{F/F}$;*LucR* mice. A representative genotyping gel is shown to illustrate amplicons corresponding to the endogenous and targeted alleles of each gene.

(**D**) $Dcaf1^{F/F}$ mouse embryonic fibroblasts infected with control lentivirus expressing GFP or lentivirus expressing GFP and Cre were lysed and immunoblotted as indicated.

4.3: *Dcaf1* is necessary for Merlin-deficient tumorigenesis in a non-germline genetically engineered mouse model

To rapidly determine whether DCAF1 is necessary for the development or maintenance of Merlin-deficient tumors, I elected to use an orthotopic liver transplant model initially developed by Scott Lowe and colleagues (145). This model has proved to be effective in rapidly screening for tumor suppressors and oncogenes (146-148) and testing mechanism-based hypotheses of oncogene function in liver tumorigenesis (149). I isolated E13.5-14.5 bipotential fetal liver progenitor cells (LPCs) from $Nf2^{Flox/Flox}$ and $Nf2^{Flox/Flox}$;$Dcaf1^{Flox/Flox}$ fetal livers and immortalized them with Cre, c-Myc, and a shRNA targeting p53. c-Myc expression and p53 depletion are necessary for LPC immortalization but not sufficient for tumorigenesis (147). I grew these cells, along with identically immortalized $Apc^{Flox/Flox}$ LPCs, in soft agar to assess their anchorage independent growth (Figure 4.3A). Surprisingly, $Apc^{-/-}$ LPCs displayed only modest growth in soft agar, despite APC functioning as a potent tumor suppressor in the mouse liver (147). $Nf2^{-/-}$ LPCs grew readily in soft agar, consistent with Merlin's role as a tumor suppressor in the mouse (24, 135, 140). Importantly, *Dcaf1* loss significantly reduced the ability of immortalized LPCs to grow in soft agar (Figure 4.3B), suggesting that $CRL4^{DCAF1}$ is necessary to sustain oncogenic signaling in Merlin-deficient tumors. Although inactivation of *Dcaf1* in freshly isolated and non-immortalized LPCs reduced the expression of CTGF, it did not increase the stability of Lats1 or the activation of YAP in both control and $Nf2^{-/-}$ non-immortalized LPCs (Figure 4.3C). These results suggest

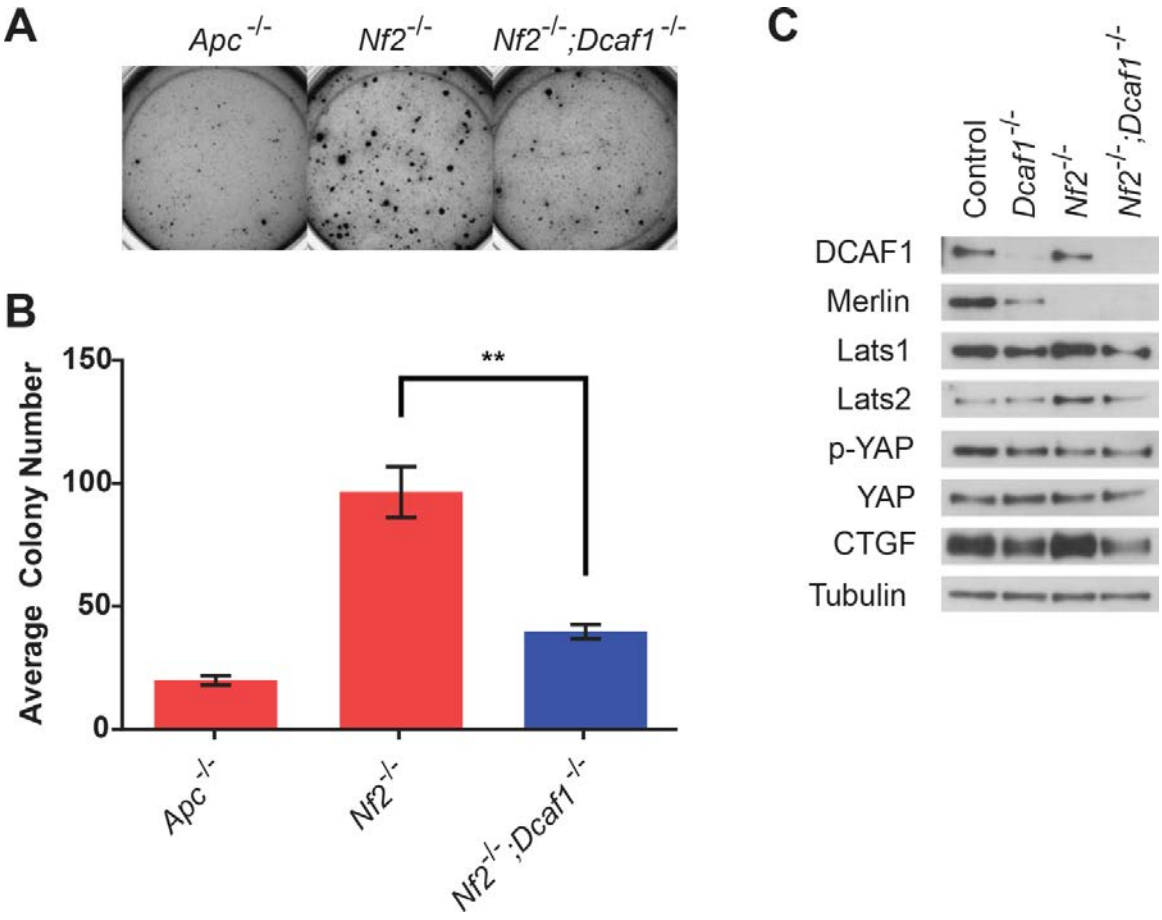

Figure 4.3: *Dcaf1* is necessary for the transformation of *Nf2*-deleted liver progenitor cells

(**A**) Fetal liver progenitor cells (LPCs) isolated from $Nf2^{Flox/Flox}$, $Nf2^{Flox/Flox}$;$Dcaf1^{Flox/Flox}$, or $Apc^{Flox/Flox}$ mice were transduced with Lenti-shp53-Cre and MSCV-Myc. These cells were seeded in soft agar and allowed to grow into colonies as shown.

(**B**) The graph indicates the number of colonies in each well. Error bars indicate ±SEM (n=3, **p<0.01).

(**C**) LPCs isolated from $Dcaf1^{Flox/Flox}$, $Nf2^{Flox/Flox}$, or $Nf2^{Flox/Flox}$;$Dcaf1^{Flox/Flox}$ mice were infected with Lenti-Cre. As a control, $Dcaf1^{Flox/Flox}$ LPCs were infected with Lenti-TdTomato. Total lysates from these cells were immunoblotted as indicated.

that $CRL4^{DCAF1}$ can sustain oncogenic signaling of Merlin-deficient liver cells through ubiquitylation of targets independently of Lats1 and 2. These results also raise the possibility that $CRL4^{DCAF1}$ induces expression of canonical Hippo target genes independently of flux through the Hippo pathway.

I subsequently isolated LPCs from $Nf2^{Flox/Flox}$ and compound $Nf2^{Flox/Flox}$;$Dcaf1^{Flox/Flox}$ mice also carrying a Cre-inducible Luciferase allele (*LucR*) and immortalized them using the method already described. Upon orthotopic subcapsular liver injection in nude mice, $Nf2^{-/-}$;*LucR* LPCs yielded large tumors within one month (Figure 4.4A). Strikingly, simultaneous loss of *Nf2* and *Dcaf1* completely abolished the ability of these cells to grow as tumors (Figures 4.4A-C), providing genetic evidence that $CRL4^{DCAF1}$ is necessary for the oncogenicity of *Nf2* mutant liver cells. Notably, although the $Nf2^{-/-}$;$Dcaf1^{-/-}$;*LucR* LPCs did not proliferate or form tumors, bioluminescent imaging confirmed that they were still alive after one month, suggesting they may have undergone cellular senescence or quiescence.

4.4: *Dcaf1* deletion exacerbates hepatomegaly and liver tumorigenesis associated with conditional *Nf2* loss

Following the results from the non-germline genetically liver tumorigenesis model, I set out to determine whether $CRL4^{DCAF1}$ is necessary for Merlin-deficient tumorigenesis in a spontaneous genetically engineered mouse model. To recombine conditional alleles in the liver, I used the Albumin-Cre (*Alb-Cre*) allele which directs Cre-mediated recombination in hepatocytes (150). *Alb-Cre* drives

Figure 4.4: *Dcaf1* is necessary for the orthotopic growth of *Nf2*$^{-/-}$ fetal liver progenitors tumors

(**A**) *Nf2*$^{F/F}$*;LucR* and *Nf2*$^{F/F}$*;Dcaf1*$^{F/F}$*;LucR* LPCs were infected with shp53-Cre lentivirus and c-Myc retrovirus and implanted below the liver capsule of nude mice. Cell growth was monitored using bioluminescent imaging. Large tumor growth was evident in the *Nf2*$^{-/-}$ LPC-injected livers within 30 days. At lower thresholds, *Dcaf1*$^{-/-}$ LPCs were detectable throughout the experiment. A representative pair of mice is shown (n=5).

(**B**) The average photon flux for an identically sized region of interest from the mice from the experiment in (**A**) was tracked over the course of 28 days. Error bars are ±SEM (n=5).

(**C**) A whisker plot of average photon flux, as measured in (**B**), for each mouse 28 days post-injection of LPCs. Error bars are ±SEM (n=5). Representative gross liver images are shown beneath respective groups.

A

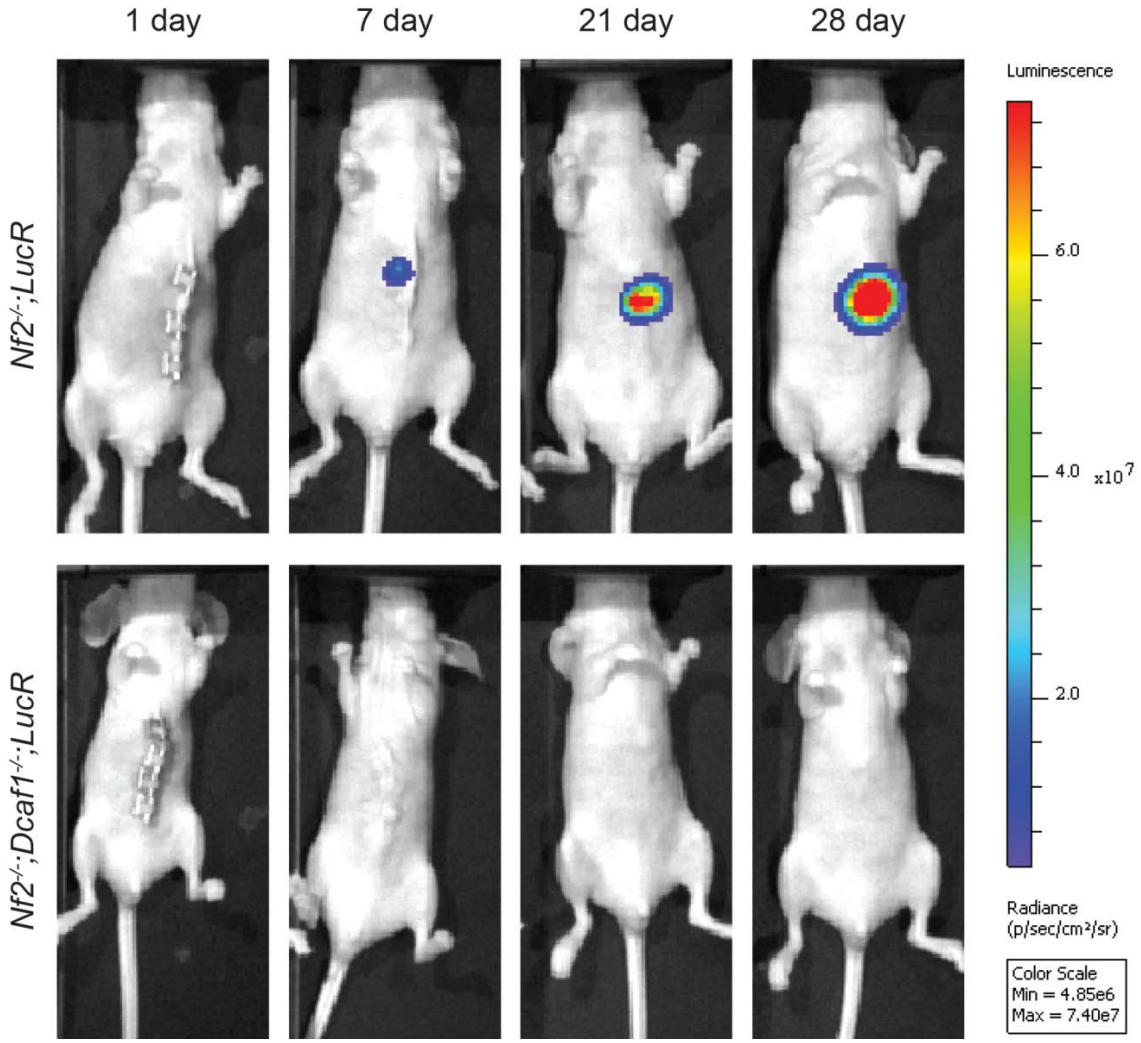
1 day
7 day
21 day
28 day
Nf2-/-;LucR
Nf2-/-;Dcaf1-/-;LucR
Luminescence
6.0
4.0
x10 7
2.0
Radiance
(p/sec/cm²/sr)
Color Scale
Min = 4.85e6
Max = 7.40e7

Figure 4.4 (continued)

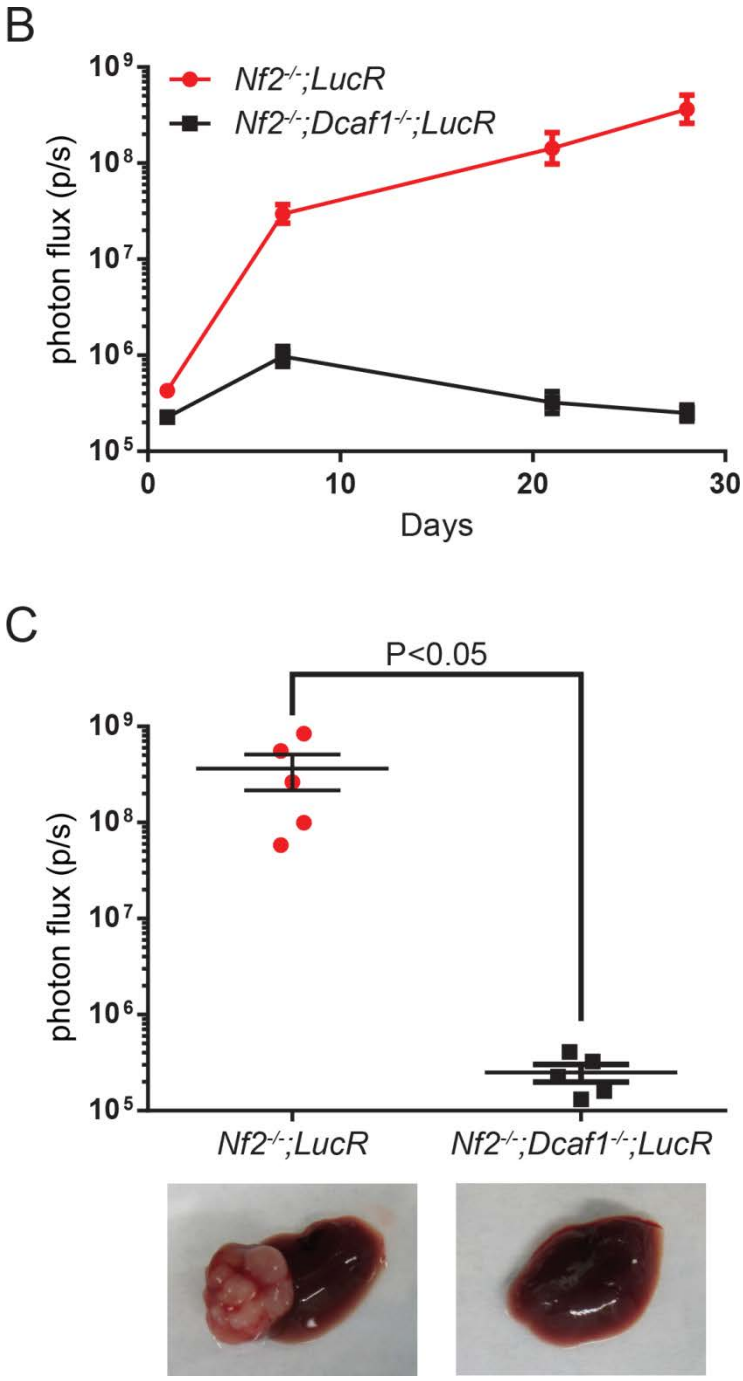

Cre expression parsimoniously in the fetal and neonatal liver, which is primarily a hematopoietic organ sparsely populated by hepatocytes. During late embryonic and early neonatal development, hematopoietic functions move to the bone marrow and the liver becomes increasingly hepatic in morphology and function. Within the first several postnatal weeks, the majority of the liver parenchyma is replaced by hepatocytes expressing Albumin, which in turn drive Cre expression in *Alb-Cre* mice (151).

I bred *Nf2$^{F/F}$;Alb-Cre*, *Dcaf1$^{F/F}$;Alb-Cre*, and *Nf2$^{F/F}$;Dcaf1$^{F/F}$;Alb-Cre* mice and analyzed cohorts at 3, 6, 9, and 12 months to assess liver size and tumorigenesis. Consistent with the studies performed by the Pan and McClatchey groups, *Nf2* deletion in the liver led to early expansion of Sox9^{+} bile duct cells or bipotential hepatobiliary progenitors (Figure 4.5) (24, 140). The liver weight to body weight ratio for normal mice is approximately 5% throughout adult life. *Nf2* deletion in the liver caused a subtle increase in this ratio at 9 months and a more dramatic change at 12 months with livers reaching up to 25% of the total body mass (Figure 4.6). In agreement with prior observations (24, 140), the bipotential hepatobiliary progenitors and bile duct cells in the *Nf2$^{F/F}$;Alb-Cre* livers arise in the within or immediately adjacent to the portal area (Figure 4.7). Importantly, loss of *Dcaf1* did not counter the liver overgrowth phenotype elicited by *Nf2* loss. Contrary to my predictions, loss of both *Dcaf1* alleles in this context led to exacerbated hepatomegaly within 3 months (Figure 4.6). These changes were accompanied by increased Sox9^{+} bipotential hepatobiliary progenitors and bile duct cells (Figures 4.8). It was also recently reported that the Hippo pathway

Figure 4.5: Expansion of Sox9^{+} bipotential hepatobiliary progenitors and bile duct cells in *Nf2*- and *Nf2/Dcaf1*-depleted livers at 3 months

Serial paraffin sections from mice of the indicated genotypes were stained with Hematoxylin and Eosin (H&E) or immunostained for Sox9, a marker of bipotential hepatobiliary cells and bile duct cells in the liver. Mice were all three months of age at time of sacrifice. Representative images are shown at 5x magnification.

H&E
Sox9
WT Nf2F/F
Nf2F/F;Dcaf1+/+;Alb-Cre
Nf2F/F;Dcaf1F/+;Alb-Cre
Nf2F/F;Dcaf1F/F;Alb-Cre

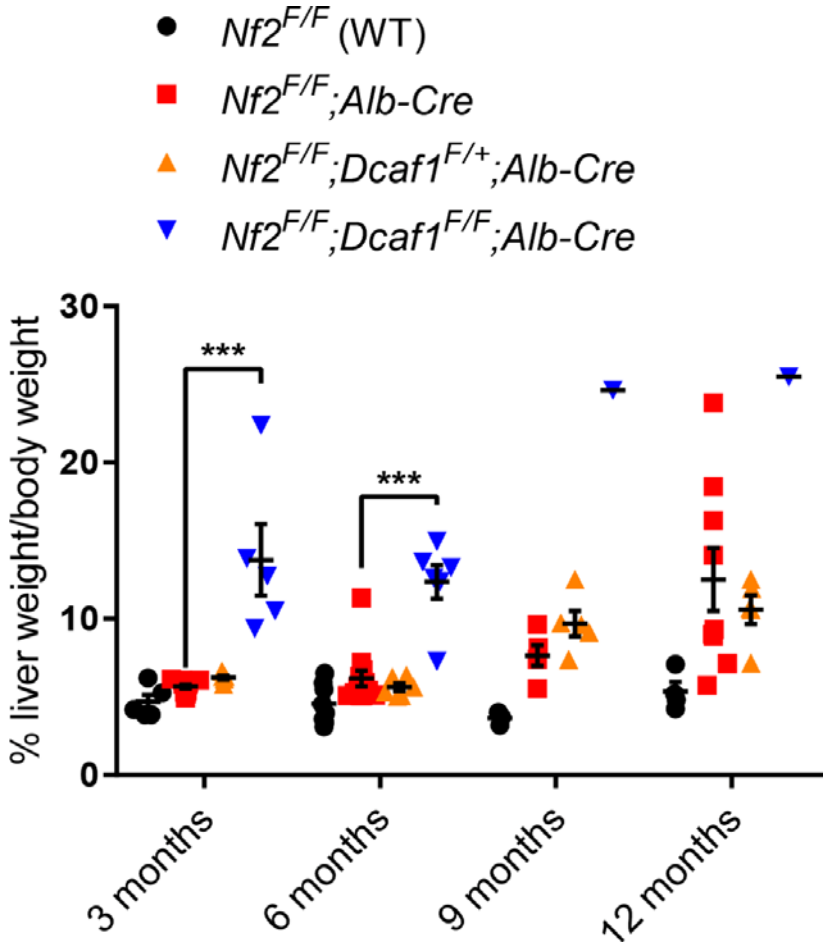

Figure 4.6: *Nf2* loss and simultaneous *Nf2/Dcaf1* loss causes hepatomegaly
Graph shows the distribution of liver weight/body weight ratios for mice of the indicated genotypes at 3, 6, 9, and 12 months. Error bars indicate ±SEM (***p<0.0001).

Figure 4.7: Expansion of Sox9^{+} bipotential hepatobiliary progenitors and CK19^{+} bile duct cells *Nf2* -depleted livers at 3 months

Gross livers and serial paraffin sections from mice of the indicated genotypes at 3 months were imaged. Paraffin sections were stained with H&E and immunostained for Sox9, Cytokeratin 19 (CK19; a bile duct epithelial cell marker), DCAF1, and YAP. In the Sox9 staining of WT liver, the black arrowhead indicates a normal bile duct with Sox9^{+} cells. Orange arrowheads indicate weakly positive Sox9^{+} hybrid periportal hepatocytes. CK19 staining shows differentiated bile duct epithelial cells. Representative microscopy images at 20x magnification are shown.

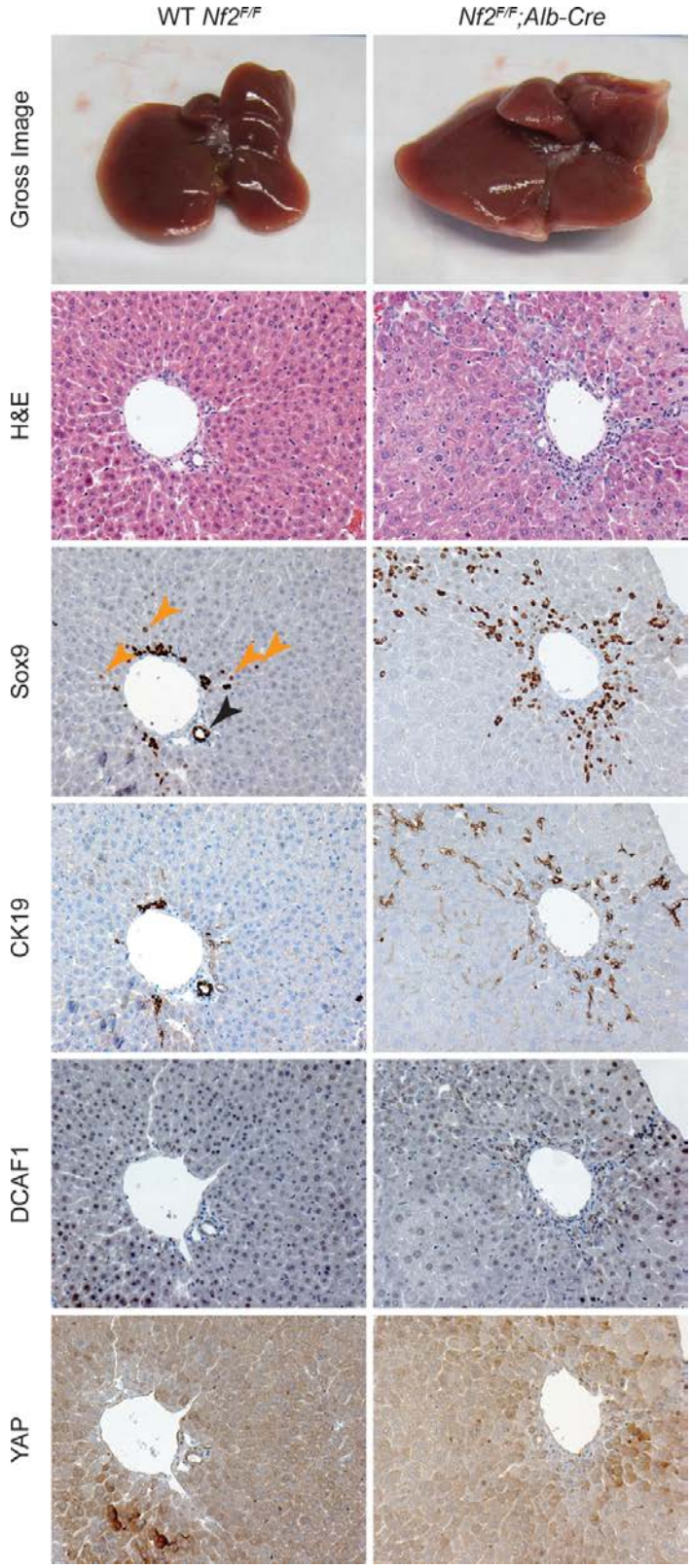
WT Nf2F/F
Nf2F/F;Alb-Cre
Gross Image
H&E
Sox9
CK19
DCAF1
YAP

Figure 4.8: *Dcaf1* deletion exacerbates the expansion of bipotential hepatobiliary progenitors and bile duct cells elicited by *Nf2* deletion in the liver

Gross livers and serial paraffin sections from mice of the indicated genotypes at 3 months were imaged. Paraffin sections were stained with H&E and immunostained for Sox9, Cytokeratin 19 (CK19; a bile duct epithelial cell marker), DCAF1, and YAP. In the DCAF1 staining of *Nf2/Dcaf1* double knockout liver, the black arrowhead indicate positive nuclear DCAF1 staining and therefore cells that escaped recombination of the *Dcaf1* conditional allele. In the YAP immunostainings, the orange arrowheads show cells with strongly positive nuclear signal.

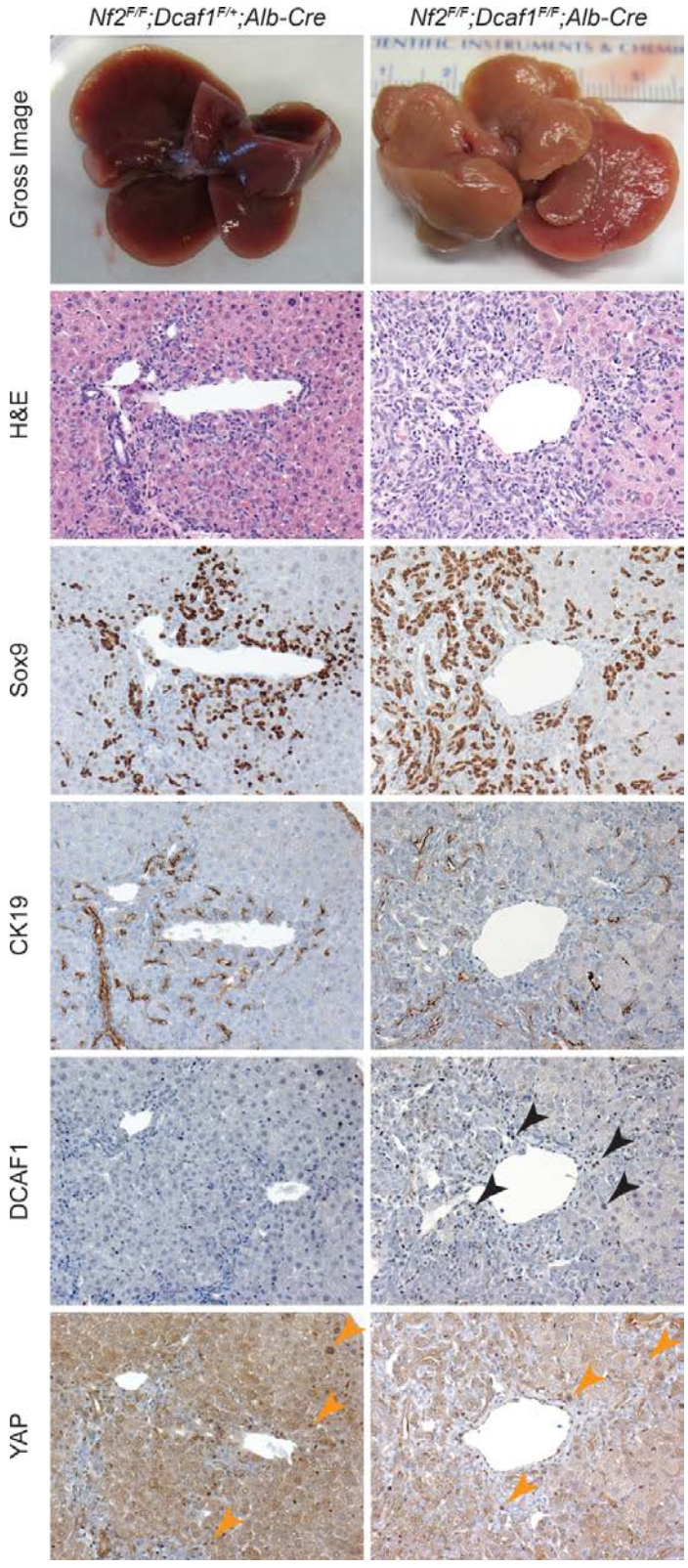
Nf2F/F;Dcaf1F/+;Alb-Cre
Nf2F/F;Dcaf1F/F;Alb-Cre
Gross Image
H&E
Sox9
CK19
DCAF1
YAP

influences portal area zonation and profoundly affects the gene expression program in hepatocytes (152). Since Merlin regulates YAP activation in the liver (24, 132), *Nf2* could abrogate normal liver zonation and induce hepatocyte de-differentiation and/or hyperproliferation. Despite the previously observed decrease in S127 phosphorylated YAP and increase in nuclear YAP in *Nf2*-deficient livers (24, 132), I did not observe a noticeable increase in YAP nuclear localization in *Nf2*-deficient livers as assessed by immunohistochemistry (Figure 4.7).

$Nf2^{F/F}$;$Dcaf1^{F/F}$;Alb-Cre mice were obtained at expected Mendelian ratios, however many did not survive into adulthood due to impaired liver function. Deletion of both *Nf2* and *Dcaf1* causes much of the liver parenchyma to be replaced by bile duct cells or bipotential hepatobiliary progenitors (Figure 4.8), I speculated that the synthetic functions of these livers are low since I observed early mortality in a notable fraction of these animals. The vast majority of the *$Nf2^{F/F}$;$Dcaf1^{F/F}$;Alb-Cre* mice died within one year, presumably due to impaired liver function and the presence of multifocal malignant tumors (Figure 4.9D). It was not uncommon for these mice to display profuse ascites (Figure 4.9E) or, less frequently, hemorrhagic ascites. In contrast, the majority of *$Nf2^{F/F}$;Alb-Cre* mice lived for more than 12 months without ascites, despite the presence of tumors (Figure 4.9B). Loss of even one *Dcaf1* allele exacerbated hepatomegaly and tumorigenesis (Figure 4.9C), although not to the same extent as the double knockout. These results suggested that *Dcaf1* loss not only increases the expansion of abnormal parenchyma, but increases malignant tumor burden. Loss

Figure 4.9: *Dcaf1* deletion does not reduce hepatomegaly or tumorigenesis induced by *Nf2* deletion in the liver

(**A**) – (**D**) Representative livers from the mice of the indicated genotypes are shown. The livers were taken from mice 12 months of age, with the exception of (**D**), which was taken from a mouse at 10 months. Black arrowheads indicate tumor nodules.

(**E**) An image taken of the mouse from (**F**) prior to liver extraction. The peritoneal cavity was filled with ascites.

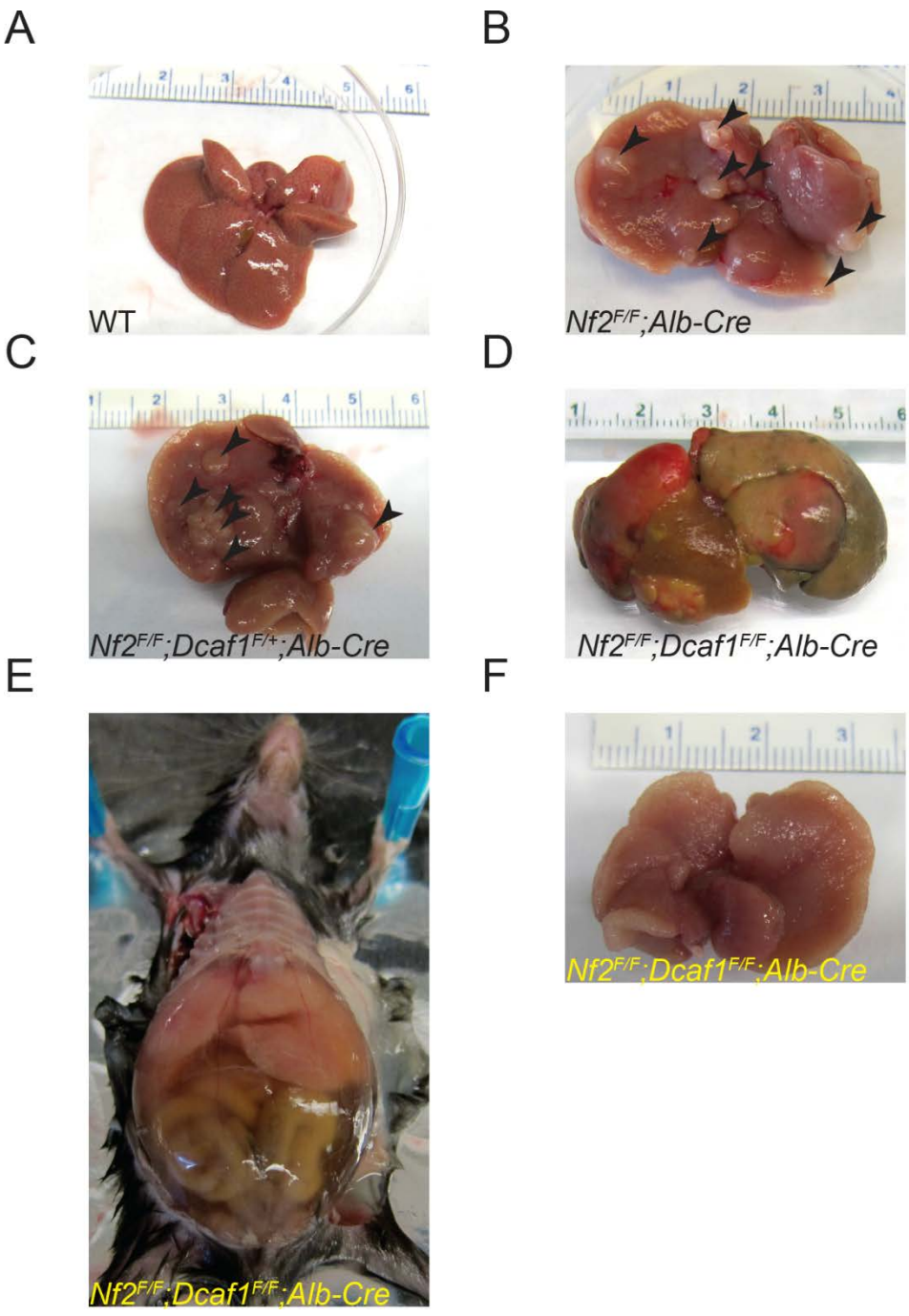
A
B
WT
Nf2F/F;Alb-Cre
C
D
Nf2F/F;Dcaf1F/+;Alb-Cre
Nf2F/F;Dcaf1F/F;Alb-Cre
E
F
Nf2F/F;Dcaf1F/F;Alb-Cre
Nf2F/F;Dcaf1F/F;Alb-Cre

of *Nf2* and either one or both *Dcaf1* alleles led to an increase in cells with nuclear YAP (Figure 4.8), particularly in areas of abnormal parenchyma and tumorigenesis. Combined, these results suggest that *Dcaf1* loss is not sufficient to mitigate oncogenic gene expression in *Nf2*-deficient liver tumorigenesis.

Interestingly, *Dcaf1* loss alone is not sufficient to overtly affect normal liver development. The liver from a 6-month *Dcaf1$^{F/F}$;Alb-Cre* mouse is histologically unremarkable, an observation which was confirmed by Dr. Julie White, a comparative pathologist for the Laboratory of Comparative Pathology and the Genetically Engineered Mouse Phenotyping Service at Sloan Kettering Institute (Figures 4.10A-C). *Dcaf1* deletion did not noticeably affect bile duct morphology (Figure 4.10E) nor YAP expression or localization as compared to wild type livers (compare Figures 4.10E and F with Figure 4.7). However, I noted an increase in the number of Sox9^{+} periportal hepatocytes in the *Dcaf1* knockout liver which lacked CK19 expression, confirming that they were not of a bile duct lineage (Figures 4.10D and E). Notably, there was a dramatic increase in Sox9^{+} hepatocytes adjacent to nearly all discernible portal triads (Figures 4.10G and H). These Sox9^{+} periportal hepatocytes could be an expanded population of hybrid periportal hepatocytes, which can give rise to hepatocytes and bile duct epithelial cells (153). This raises the possibility that exacerbated proliferation of bile duct epithelial cells and bipotential hepatobiliary progenitors in *Nf2$^{F/F}$;Dcaf1$^{F/+}$;Alb-Cre* and *Nf2$^{F/F}$;Dcaf1$^{F/F}$;Alb-Cre* mice may be due to the expansion of the hybrid periportal hepatocyte niche resulting from *Dcaf1* loss.

Figure 4.10: *Dcaf1* deletion in the liver does not overtly affect organ morphology but induces the expansion of a periportal Sox9^{+} hepatocyte niche

(**A**) Image of a 6 month *Dcaf1$^{F/F}$;Alb-Cre* liver.

(**B**)-(**F**) Serial sections of the liver in (**A**) were stained with H&E (**B**) or immunostained for DCAF1 (**C**), Sox9 (**D**), CK19 (**E**), and YAP (**F**). Representative images were taken at 20x magnification.

(**G**) and (**H**) Serial sections of the liver in (**A**) were immunostained for Sox9 (**G**) or CK19 (**H**). Black arrowheads indicate bile duct epithelia. Orange arrowheads indicate some of the myriad Sox9^{+} periportal hepatocytes. These cells are not of a bile duct epithelial lineage as they lack CK19 expression. Representative images were taken at 10x magnification.

A

B

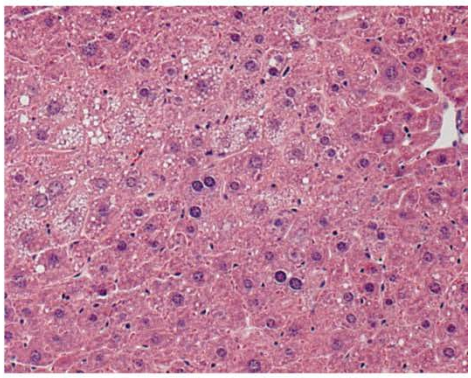

C

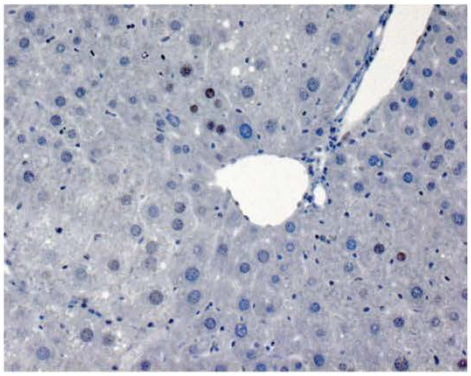

D

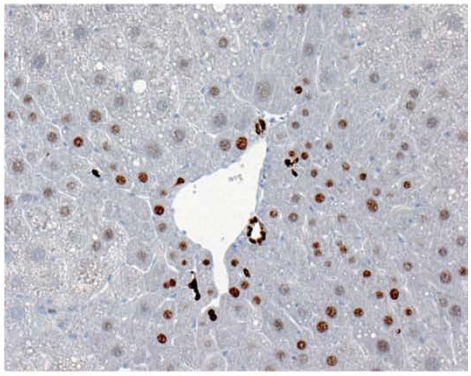

E

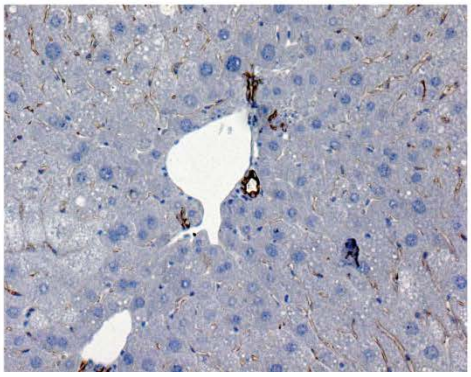

F

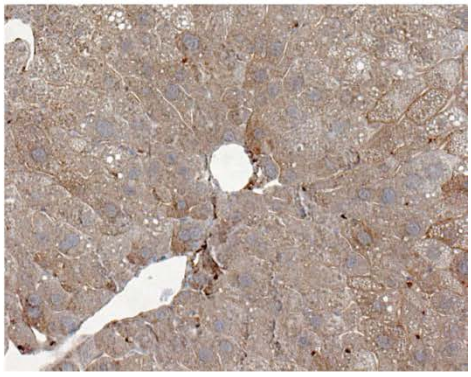

Figure 4.10 (continued)

G

Sox9

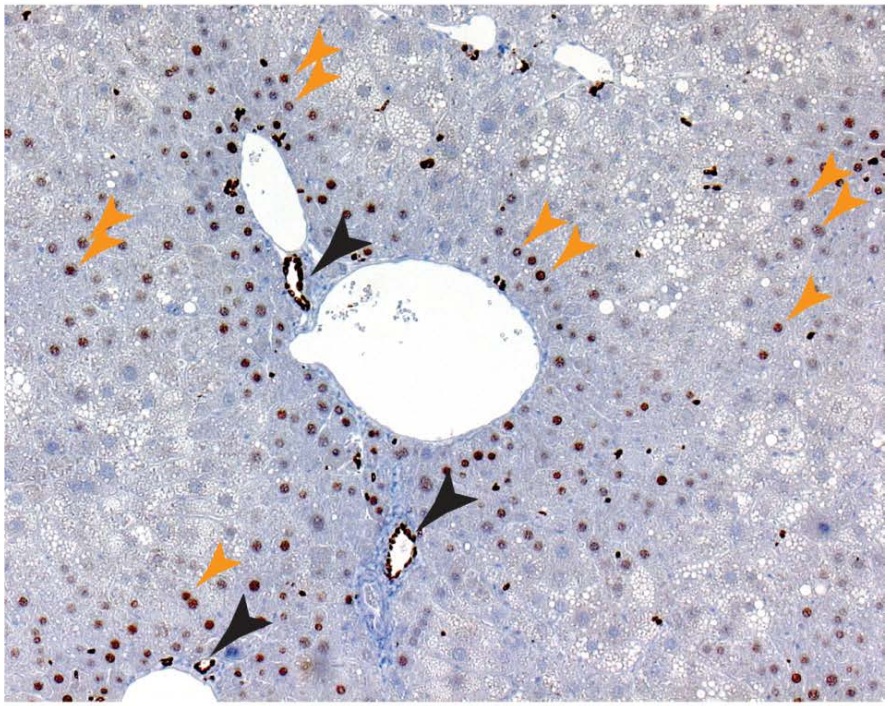

H

CK19

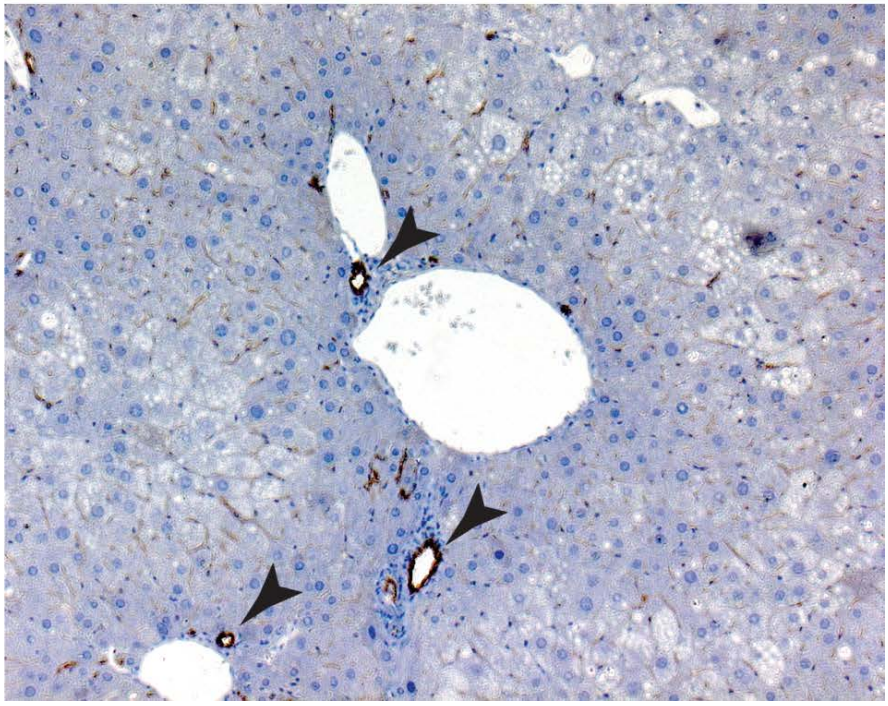

4.5: Development of a mouse model to dissect genetics of malignant pleural mesothelioma

The development of targeted therapies for malignant pleural mesothelioma (MPM) has been hampered by the apparent lack of actionable targets along the signaling pathways that are activated in this disease. Although about 75% of MPM carry mutations at the *NF2* locus (Figure 4.11), the mechanism by which Merlin suppresses tumorigenesis in this tissue has remained, until recently, obscure. Studies in our lab revealed that loss of Merlin/*NF2* drives the development and maintenance of MPM by activating the pro-oncogenic E3 ubiquitin ligase $CRL4^{DCAF1}$, which in turn inhibits the Hippo pathway tumor suppressors Lats1 and 2 (30, 154). In light of our previous results and to further address the hypothesis that dysregulation of DCAF1 drives oncogenesis in Merlin-deficient mesothelioma, I set out to develop a Merlin-deficient malignant pleural mesothelioma *in vivo*.

Prior studies indicated that inactivation of *Nf2* in combination with loss of *Tp53* is sufficient to initiate the development of mesotheliomas bearing striking resemblance to human malignant mesotheliomas (139). These studies relied on injection of Adenoviral Cre into the pleural cavity of $Nf2^{Flox/Flox};Tp53^{Flox/Flox}$ mice. To establish a model of *Nf2*-deficient mesothelioma requiring fewer conditional alleles, I developed a lentivirus simultaneously encoding Cre and a miR30-based short hairpin targeting p53 (Figure 4.12A) (155). Injection of Lenti-shp53-Cre virus into the pleural cavity of a TdTomato reporter mouse revealed viral Cre-mediated recombination of a *LSL-TdTomato* reporter on the visceral pleura

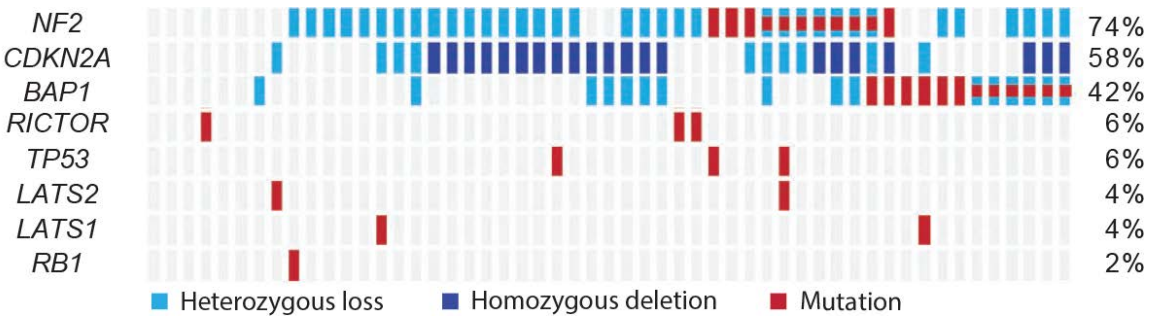

Figure 4.11: Integrated gene map showing loss of common tumor suppressors among 53 mesothelioma patients
Adapted from Bott et al., 2011 (9).

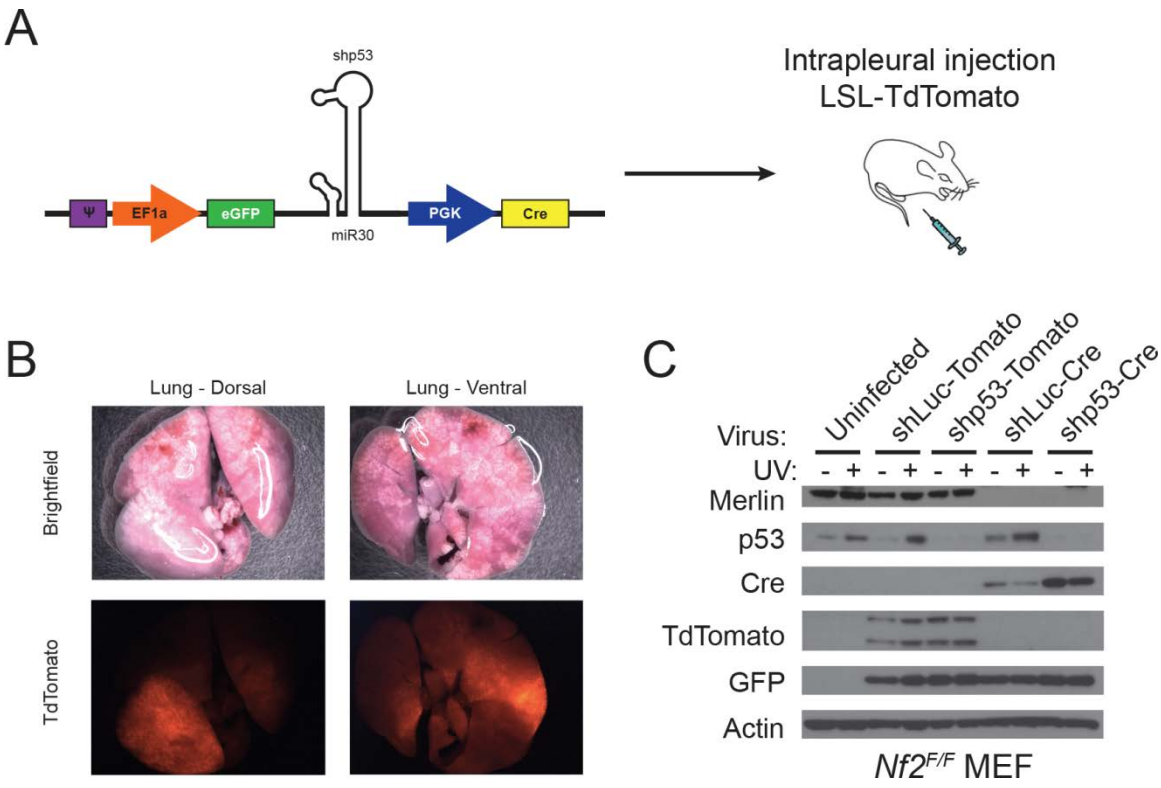

Figure 4.12: Intrapleural injection of Lenti-shp53-Cre induces efficient loss of conditional alleles and knockdown of p53

(**A**) A schematic of the Lenti-shp53-Cre viral vector. A short EF1a promoter drives expression of enhanced GFP and a miR30-based shRNA targeting p53. The PGK promoter drives expression of Cre.

(**B**) Fluorescent dissecting microscopy was performed on lungs after intrapleural injection of Lenti-shp53-Cre in a *LSL-TdTomato* reporter mouse.

(**D**) Lysates of $Nf2^{F/F}$ MEFs infected with the indicated lentiviruses were immunoblotted as indicated.

(Figure 4.12B). Lenti-shp53-Cre induced efficient knockdown of endogenous p53 in *Nf2*$^{F/F}$ mouse embryonic fibroblasts (MEFs), even when p53 is upregulated following UV irradiation (Figure 4.12C). The virus also efficiently recombined the conditional *Nf2* allele. Notably, injection of Lenti-shp53-Cre into the pleural cavity of *Nf2*$^{Flox/Flox}$*;LucR* mouse resulted in the formation of thoracic neoplasia within four weeks following injection (Figure 4.13A). However, despite efficient *in vitro* knockdown of p53 and recombination of the conditional *Nf2* allele, malignant tumors never developed in this model. Some of the injected mice developed what appeared to be tumor nodules as assessed by bioluminescent imaging, however their growth arrested within two months following injection of the virus (Figure 4.13A). When I analyzed a set of animals which showed the highest signals, I observed a significant increase in the neoplasia size of *Nf2*$^{F/F}$*;LucR* versus *Nf2*$^{F/F}$*;DCAF1*$^{F/F}$*;LucR* mice (Figure 4.13B). However, I emphasize that these were cherry-picked animals and some of the injected *Nf2*$^{F/F}$*;LucR* animals showed little bioluminescent signal. Upon necropsy, I was not able to find any discernible tumor tissue in the virus-injected *Nf2*$^{F/F}$*;LucR* which yielded the highest neoplasia signal.

Based on these preliminary results, I speculated that more efficient knockdown of additional cooperating tumor suppressors may induce malignant pleural mesothelioma in this model. I used a tandem miRNA backbone to increase the knockdown efficiency of the shRNAs and include knockdown of the CDK inhibitor p16 and the p53 activator ARF, the protein products of *Cdkn2a*, one of the most frequently mutated genes in MPM (Figure 4.11).

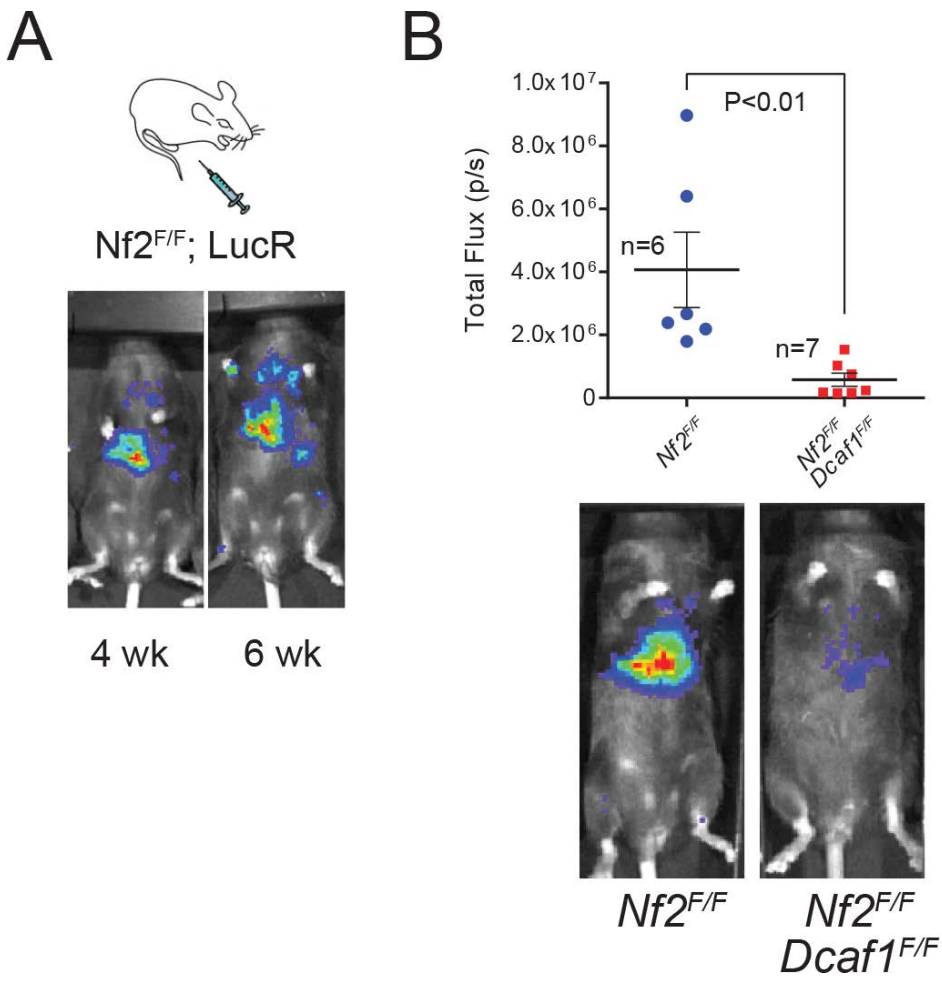

Figure 4.13: Injection of Lenti-shp53-Cre virus in *Nf2* conditional mice does not induce malignant tumorigenesis

(**A**) Injection of Lenti-shp53-Cre virus into the pleural cavity of *Nf2$^{F/F}$;LucR* mice induce the growth of neoplasia within one month but growth arrested within two months.

(**B**) The bioluminescent signal-bearing neoplastic tissue from *Nf2$^{F/F}$;LucR* mice injected with Lenti-shp53-Cre was significantly higher than that of *Nf2$^{F/F}$;Dcaf1$^{F/F}$;LucR* animals. Graph shows bioluminescent intensity and pictures are representative images at 6 weeks.

Conditional deletion of the *Cdkn2a* locus, like *Trp53*, cooperates with *Nf2* deletion to induce tumorigenesis in germline conditional MPM models (139). I designed a new lentivirus encoding an enhanced miR30 backbone, called miR-E, which is more efficiently processed by the Drosha enzyme (156). I also designed this vector with a tandem miR-E cassette that directs multiplex expression of two shRNAs, one targeting p53 and another targeting both products of the *Cdkn2a* gene – p16-Ink4a and p19-ARF (Figure 4.14A). This virus was able to efficiently knockdown p16, p19, and p53 in MEFs (Figure 4.14B). Cre expression from the viral construct also recombined conditional alleles. However, despite these excellent *in vitro* results, this virus also failed to induce malignant tumorigenesis.

I speculated that either incomplete knockdown or silencing of the miR30-based shRNA was preventing sufficient depletion of the cooperating tumor suppressors in this model. To address this pitfall, I elected to use viral-mediated somatic genome engineering with multiplex CRISPR/Cas9 to permanently mutate cooperating tumor suppressors in Merlin-deficient MPM. The Ventura lab has recently used a multiplex Adenoviral CRISPR/Cas9 system to drive tumorigenesis in a lung cancer model with 100% penetrance (157). Following a similar strategy, we will induce MPM by injecting into the pleural cavity of adult *Nf2*$^{F/F}$*;LucR* mice a dual-Adenovirus system including Adeno-Cre - to recombine the conditional *Nf2* and LucR alleles - and a second Adenovirus - to inactivate *Cdkn2a* (Ink4a/ARF) using the CRISPR/Cas9 system. Tumor onset and expansion will be monitored using bioluminescent imaging. Adenovirus efficiently

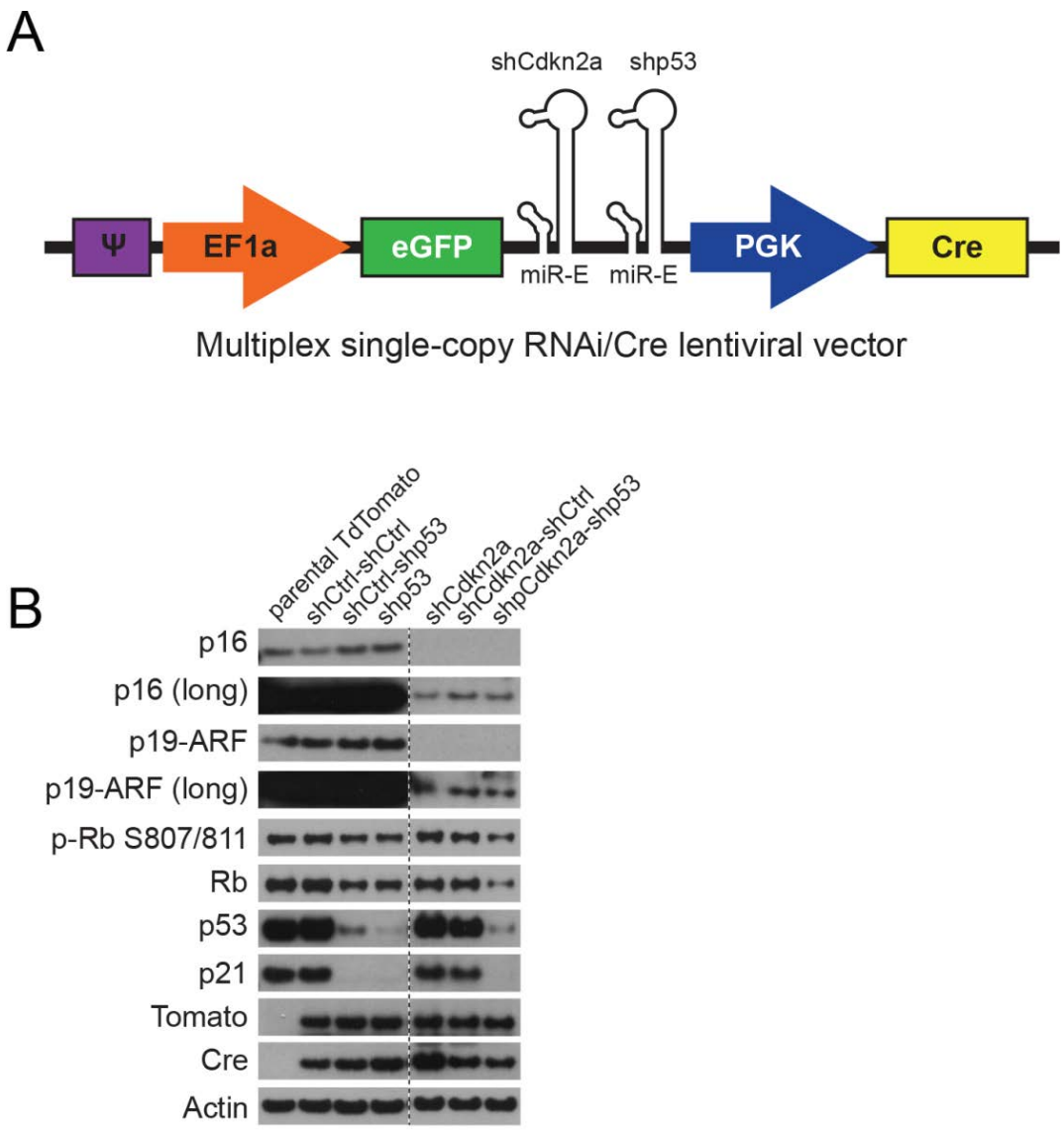

Figure 4.14: *In vitro* application of multiplex single-copy RNAi vector for simultaneous gene knockdown and Cre-mediated recombination
(**A**) Schematic of a lentiviral vector encoding GFP, Cre, and tandem miR-E cassettes targeting Cdkn2a and p53.
(**B**) Lysates of *LSL-TdTomato* reporter MEFs infected with the indicated lentiviruses were immunoblotted as indicated. Multiplex RNAi-mediated knockdown of both Cdkn2a and p53 is efficient, and corresponding downstream pathways are concomitantly downregulated.

infects the pleural mesothelium of mice (139), and the transient expression of the CRISPR/Cas9 system precludes undesired off-target effects resulting from extended CRISPR/Cas9-sgRNA expression. Intrapleural administration of Adeno-Cre and a multiplex CRISPR/Cas9-sgRNA Adenovirus into conditional *Nf2;LucR* mice can yield inactivation of six alleles or more while avoiding the long and inefficient breeding strategy required for germline genetically engineered mouse models.

I obtained a multiplex CRISPR/Cas9-sgRNA shuttle vector from the Ventura lab and cloned into it guide RNAs targeting the *Cdkn2a* and *Trp53* loci (Figure 4.15A). I also replaced the Cas9 cDNA with Cre in order to drive recombination of conditional alleles and to uncouple the guide RNAs from Cas9 as an additional safety precaution. I transfected this sg*Trp53*/sg*Cdkn2a*-Cre vector into Cas9-expressing *LSL-TdTomato* MEFs where I observed Cre-induced TdTomato expression in the transfected cells. I carried out a mismatch-sensitive endonuclease assay to detect indels within the target loci. This assay confirmed that the vector directs Cas9-mediated endonuclease activity and indel formation at the *Trp53* and *Cdkn2a* loci (Figure 4.15B). Western blotting of these cells lysed one week post-transfection revealed only modest knockdown of endogenous p53, p16, and p19 (Figure 4.15C). After ten more days, I saw a positive selection for the TdTomato^{+} transfected cells. This observation coincided with positive selection of cells in which p53 and p16/p19 expression were abolished (Figure 4.15C). These *in vitro* results confirmed the efficacy of this construct in mediating simultaneous excision of conditional alleles and somatic

Figure 4.15: Development of a multiplex CRISPR/Cas9 system for somatic mutation of Cdk2na and *Trp53*
(**A**) Schematic of control (a) and tumor suppressor-targeting (b and c) vectors driving simultaneous expression of Cre recombinase.
(**B**) gDNA extracted from Cas9-expressing MEFs transfected with the vectors in (**A**) were subjected to a mismatch-sensitive endonuclease assay revealing indels in the *Trp53* and *Cdkn2a* loci as indicated by cleaved amplicons.
(**C**) MEFs from (**B**) were lysed after 7 or 17 days post-transfection and immunoblotted as indicated.
(**D**) Proposed *in vivo* application of multiplex CRISPR/Cas9 system in conditional animals to dissect MPM genetics.

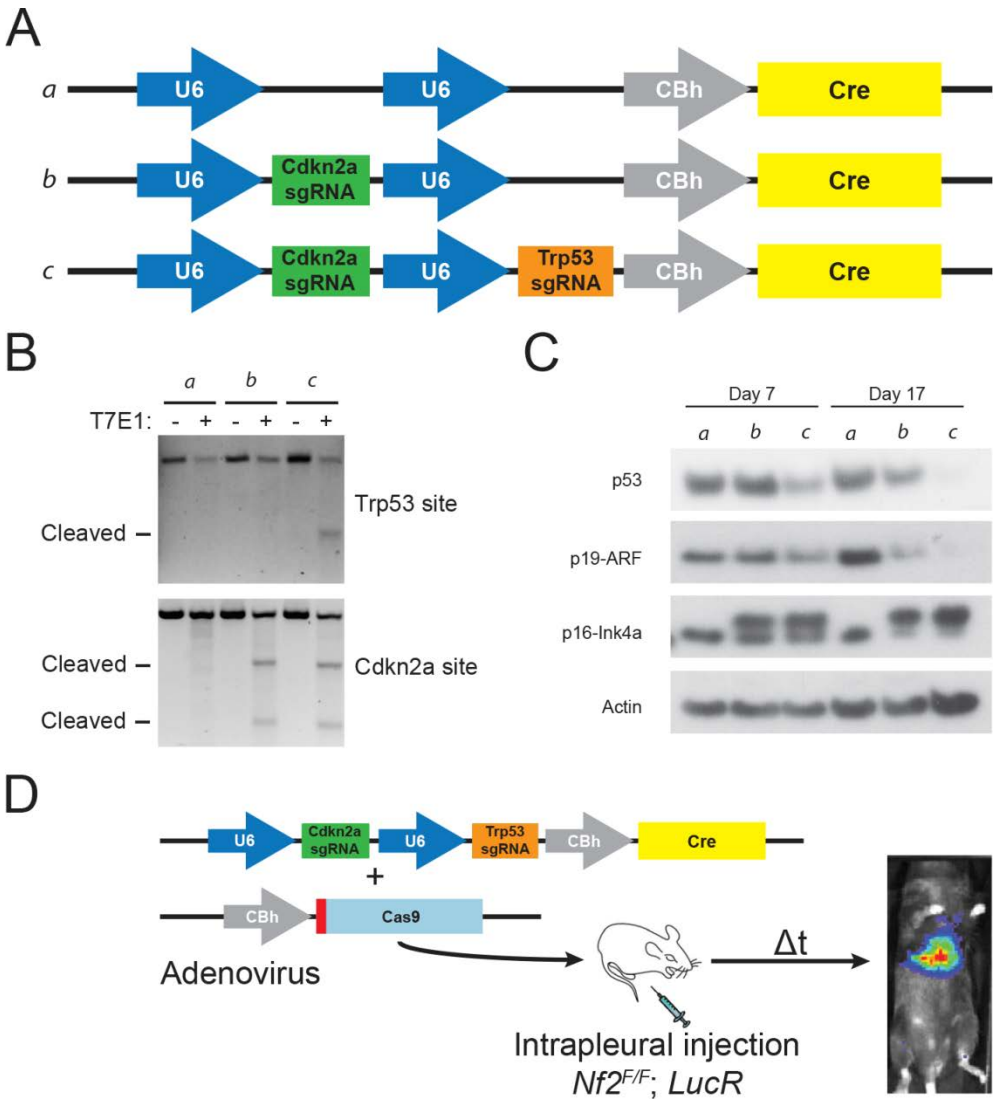
A
a
U6
U6
CBh
Cre
b
U6
Cdkn2a sgRNA
U6
CBh
Cre
c
U6
Cdkn2a sgRNA
U6
Trp53 sgRNA
CBh
Cre
B
a
b
c
T7E1: - + - + - +
Cleaved
Trp53 site
Cleaved
Cleaved
Cdkn2a site
C
Day 7
Day 17
a
b
c
a
b
c
p53
p19-ARF
p16-Ink4a
Actin
D
U6
Cdkn2a sgRNA
U6
Trp53 sgRNA
CBh
Cre
+
CBh
Cas9
Adenovirus
Δt
Intrapleural injection
Nf2F/F; LucR

alterations in cooperating tumor suppressors. Viraquest produced high titer sg*Trp53*/sg*Cdkn2a*-Cre adenovirus along with a control sgEmpty-sgEmpty-Cre adenovirus for *in vivo* application. I now plan to inject these viruses, along with Cas9-expressing adenovirus, into the pleural cavity of *Nf2*$^{F/F}$*;LucR* mice to induce Merlin-deficient MPM (Figure 4.15D).

4.6: Discussion

4.6.1: *Nf2*-deficient liver tumorigenesis models

My preliminary genetic experiments revealed that *Dcaf1* is necessary to sustain tumorigenicity of *Nf2*-deficient bipotential fetal liver progenitor cells (LPCs). Western blotting suggested that DCAF1 does not regulate Hippo signaling in LPCs as it does in other Merlin-deficient cells including schwannoma and mesothelioma (154). These results implied that CRL4^{DCAF1} sustains oncogenic signaling in LPCs through a mechanism independent of Lats1 and 2 inhibition. Our previous findings revealed that DCAF1 promotes oncogenic gene expression through alternative pathways in addition to YAP and TAZ (154). These findings are consistent with the notion that CRL4^{DCAF1} has multiple ubiquitylation targets which may be differentially expressed and whose signaling mechanisms vary between cells.

I subsequently assessed the requirement of DCAF1 in Merlin-deficient tumorigenesis in the adult mouse liver using *Alb-Cre* to drive recombination of the *Nf2* and *Dcaf1* conditional alleles in hepatocytes. At first glance, these

experiments yielded overtly negative results as I observed a dramatic increase in hepatomegaly and tumorigenesis of compound *Nf2/Dcaf1*-deficient livers versus those with *Nf2* loss alone. However, there are two factors that could explain how *Dcaf1* loss exacerbates *Nf2*-deficient phenotypes in the liver. Firstly, DCAF1 immunohistochemistry on compound *Nf2/Dcaf1* knockout livers suggested the presence of cells escaping *Dcaf1* recombination (Figure 4.8). Interestingly, DCAF1 has been implicated as functioning in mammalian cell competition (103, 158). Notably, when DCAF1 was depleted, these cells underwent apoptosis and were extruded from the cell culture layer when they were surrounded by normal cells but not other DCAF1-depleted cells. If DCAF1 is also functioning in cell competition in the liver, it is plausible that those cells escaping recombination expand and outgrow. If these cells escaped recombination due to low expression of Albumin, such as in a periportal bipotential progenitor or a transient amplifying cell that lacks full hepatocytes or bile duce epithelial characteristics, then perhaps they are able to out-compete their neighboring cells and grow without restraint, resulting in hyperplasia arising from a bipotential progenitor or bile duct epithelial niche. I observed areas of $DCAF1^{+}$ cells scattered throughout compound *Nf2/Dcaf1* knockout livers and within their tumors, however the majority of the tumors appeared *Dcaf1*-negative. It may be possible that the “winner” $DCAF1^{+}$ cells are initially required to establish a hyperproliferative niche which then loses DCAF1 expression following differentiation into (or through) an Albumin-expressing phase.

A second factor which could explain how *Dcaf1* loss exacerbates *Nf2*-deficient hepatomegaly and liver tumorigenesis lies in the expansion of a bipotential hepatobiliary progenitor niche. While loss of *Dcaf1* alone did not affect normal liver function nor did it affect normal liver pathology, there was a notable expansion of $Sox9^+$ periportal hepatocytes. Consistent with recent findings, the normal mouse liver has low-expressing periportal $Sox9^+$ cells which are negative for the bile duct marker Cytokeratin-19 (Figure 4.7) (153). These cells morphologically resemble hepatocytes yet they express Sox9, indicative of a bipotential progenitor phenotype. Yimlamai et al. recently found that loss of *Nf2* in hepatocytes leads to dedifferentiation into hepatobiliary progenitors - or what they refer to as atypical ductal cells - using lineage tracing models (143). Most recently, however, findings by Font-Burgada et al. revealed hybrid periportal hepatocytes can generate both ductal cells and hepatocytes, and moreover, can repopulate the damaged liver to a greater extent than normal hepatocytes or bipotential oval cells (153). These findings raise the intriguing possibility that *Nf2* loss in hybrid periportal hepatocytes give rise to the $Sox9^+$ atypical ductal cells in this model. The $Sox9^+$ periportal hepatocytes I observed in the *Dcaf1*-depleted liver may very well be an enlarged bipotential hepatobiliary progenitor niche. The expansion of this niche, which may be a target of Merlin-deficient hyperplasia and tumorigenesis, could then exacerbate the *Nf2*-deficient phenotype in the liver. Consistent with this hypothesis, the highly disorganized *Nf2/Dcaf1* knockout livers are heavily populated by $Sox9^+$ duct-like structures, of which only a fraction are $CK19^+$ (Figure 4.8). This suggests that these cells are bipotential progenitors

not arising from a bile duct lineage. To address this hypothesis, I will need to definitively differentiate these populations with additional markers.

Speculation aside, the origin of bipotential hepatobiliary cells and/or bile duct epithelial hyperplasia following *Nf2* and *Nf2/Dcaf1* loss is an outstanding question that is part of a broader issue in the field of liver development, regeneration, and tumorigenesis. The stem cell niche of the liver - a normally quiescent organ which has very little parenchymal cell turnover - has been a subject of intense research and contention in the past decade. Acute liver injury induces hepatocyte proliferation which can reconstitute a 70% loss in liver mass in a matter of weeks (159). When hepatocyte proliferation is blocked, however, the origin of those cells which regenerate the liver parenchyma remains elusive. Within this enigma may lie the origin of *Nf2* and *Nf2/Dcaf1*-deficient tumorigenesis in the mouse liver, and thereby an explanation of the exacerbated phenotypes resulting from *Nf2* and *Dcaf1* deletion in the liver. However, it is important to note that *Nf2* loss-driven tumorigenesis in the liver is more pathogenically relevant in the mouse. Whereas NF2 patients do not suffer to any significant extent from liver tumors, mice with only one functional *Nf2* allele suffer from a wide array of malignant tumors - including those arising in the liver – due to differences in the kinetics of loss of heterozygosity (135). This major difference favors the use of a more clinically relevant model to study *NF2*/Merlin loss-driven tumorigenesis.

4.6.2: *Nf2*-deficient malignant pleural mesothelioma models

A recent personal communication with Anton Berns corroborated my *in vivo* findings showing lentiviral shRNA-mediated knockdown of cooperating tumor suppressors to drive Merlin-deficient MPM is ineffective. His lab tried to use an almost identical approach with lentiviral-mediated knockdown of cooperating tumor suppressors to induce MPM in mice but found this technique to be insufficient to drive tumorigenesis. He assured me that the small fraction of p53 remaining in the infected cells following shRNA-mediated knockdown is sufficient to arrest growth in this model. This correspondence with Anton Berns reinforced my decision to develop an analogous model using CRISPR/Cas9-mediated somatic alterations. Due to the permanent deletion of the targeted alleles and positive selection of *Cdkn2a*- and *Trp53*-mutated cells induced by sg*Trp53*/sg*Cdkn2a*-Cre *in vitro*, I am optimistic that adenovirus expressing this construct will induce MPM upon intrapleural injection in conditional *Nf2* mice. Once I am able to reliably and quickly induce MPM using this virus in $Nf2^{F/F}$;*LucR* mice, I will determine whether $CRL4^{DCAF1}$ is necessary for Merlin-deficient tumorigenesis by injecting the same virus into $Nf2^{F/F}$;$Dcaf1^{F/F}$;*LucR* mice. Analysis of the resulting MPM tumors will also reveal whether YAP/TAZ is activated and ensuing oncogenic signaling is upregulated in this model, as it is in human Merlin-deficient MPM (154). This *in vivo* MPM model, if successful, could provide compelling pre-clinical rationale for DCAF1 inhibition in Merlin-deficient MPM. Furthermore, it can serve as a pre-clinical model to test the efficacy of

targeted therapies in preventing the initiation and progression of a genetically-defined MPM.

I am developing an analogous lentiviral strategy to mediate multiplex somatic deletions of cooperating tumor suppressors using recently published methods (160). This system will allow for a flexible somatic deletion of tumor suppressors which can be used to rapidly model patient-derived mutations and test mechanistic-based hypotheses. One hypothesis that I'd like to address using this model is whether mutations in Lats1 and 2 in combination with cooperating tumor suppressors (i.e. *Cdkn2a* and *Trp53*) are sufficient to drive MPM. This hypothesis arises from the observation that Lats1 and 2 are mutated in MPM (9, 161, 162), which is notable since members of the core Hippo kinase cascade are not significantly mutated in human cancer (27). Combined, mutations in *LATS1*/2 and *NF2* may comprise a very high proportion of human MPM with dysregulated Hippo signaling. Testing these hypotheses *in vivo* has been hampered by the difficulty of multi-allele germline mouse genetics, a hurdle for which a virus mediating multiplex somatic genome alterations is well suited. Exploring the underlying genetics and oncogenic signaling pathways activated in these MPM models could provide a platform to derive and test the mechanistic-based therapies which are required to treat this fatal cancer.

Chapter Five

Mechanism-based pharmocological targeting of *NF2*-mutant malignancies

5.1: Introduction

Merlin has emerged as a major effector of contact inhibition and adhesion signaling, and is encoded by the *NF2* tumor suppressor which becomes inactivated in the familial cancer syndrome Neurofibromatosis type 2 (NF2). Loss of Merlin function contributes to the development of sporadic meningiomas, ependymomas, and schwannomas, which are also the hallmark tumors arising in NF2 patients. Merlin is frequently lost in malignant pleural mesothelioma (MPM) and to a lesser extent in other solid tumors, implicating *NF2* as a broadly functioning tumor suppressor (163-165). The last decade has seen notable strides towards elucidating the intracellular signaling underlying Merlin's tumor suppressive functions. Since its discovery in 1993, we have learned that Merlin is a multifunctional protein which shuttles between the cell cortex and the nucleus in a manner reminiscent but antithetic to that of the cell adhesion and signaling component β-catenin (30, 164, 165). At the cell cortex, Merlin interacts with the scaffold and signaling protein Angiomotin to suppress mitogenic signaling through Rac, thereby inhibiting PAK (29). Merlin also regulates mitogenic signaling by suppressing mTORC1 in mesothelial and meningeal cells (18, 19). Interestingly, inactivation of *NF2* confers sensitivity to rapalogs in bladder cancer and Cetuximab-resistant lung cancer, suggesting that mTORC1 signaling broadly sustains oncogenic signaling in Merlin-deficient cells (166, 167).

Recently, we discovered that the de-phosphorylated conformer of Merlin accumulates in the nucleus and suppresses tumorigenesis by inhibiting the Cullin E3 ubiquitin ligase $CRL4^{DCAF1}$ (30). Depletion of DCAF1, the substrate recognition component of the ligase, blocked the hyperproliferation caused by inactivation of Merlin. Importantly, tumor-derived mutations invariably disrupted Merlin's ability to enter into the nucleus, to interact with $CRL4^{DCAF1}$, or to inhibit its ligase activity. Finally, depletion of DCAF1 inhibited the hyperproliferation of Schwannoma cells isolated from NF2 patients and suppressed the oncogenic potential of Merlin-deficient Schwannoma and mesothelioma cell lines (30). Intriguingly, the oncogenic program of gene expression controlled by $CRL4^{DCAF1}$ included TEAD target genes, suggesting that Merlin controls Hippo signaling by inhibiting $CRL4^{DCAF1}$. Following up on this hypothesis, we found that de-repressed $CRL4^{DCAF1}$ targets Lats1 and 2 for ubiquitylation and inhibition in the nucleus and thus activates YAP-driven transcription and oncogenesis. Analysis of clinical samples indicated that this oncogenic pathway is consistently activated in human *NF2* mutant mesotheliomas, Schwannomas, and meningiomas (129).

There are few treatment options for NF2 patients and standard chemotherapies for MPM are ineffective. In this chapter, I set out to establish a mechanism-based therapy for Merlin-deficient MPM, a rare but almost universally fatal cancer. Multimodal therapy including surgery and chemotherapy extends patient survival by only a few months from the median survival of 1.5 years (168). Mechanism-based inhibition of the oncogenic signaling pathways underlying *NF2*-deficient tumorigenesis would be of particular value in fast-growing and

aggressive cancers such as MPM. During this study, I found that inhibition of $CRL4^{DCAF1}$ using MLN4924 - a NEDD8 Activating Enzyme (NAE) inhibitor - sensitizes cells to traditional chemotherapy and additional mechanism-based therapies. By inhibiting $CRL4^{DCAF1}$-mediated oncogenic signaling in combination with standard chemotherapy and mechanism-based therapies, we are able to significantly reduce the growth of *NF2*-deficient tumors.

5.2: DCAF1 depletion reduces the growth of Merlin-deficient malignant pleural mesothelioma cells

Based on our previous observation that DCAF1 depletion reduces the tumorigenic potential of Merlin-deficient tumors (30), I set out to test whether acute loss of DCAF1 reduces the growth of Merlin-deficient MPM cell lines. siRNA-mediated depletion of DCAF1 reduced the proliferation of Meso-33, a Merlin-deficient MPM line (Figures 5.1A and B). VAMT, another Merlin-deficient line, displayed higher dependency on DCAF1 for proliferation (Figure 5.1A). Since DCAF1 depletion elicited a notable reduction in proliferation within four days, I speculated that a therapeutic regimen of DCAF1 depletion in Merlin-deficient tumors would induce a similar proliferation arrest. Tetracycline-inducible knockdown of DCAF1 using two independent shRNAs (Figure 5.1C) consistently reduced proliferation of Merlin-deficient MPM cells which largely correlated with the extent of DCAF1 depletion (Figures 5.1C and D). In light of the anti-proliferative effects of DCAF1 depletion in these models, I hypothesized that

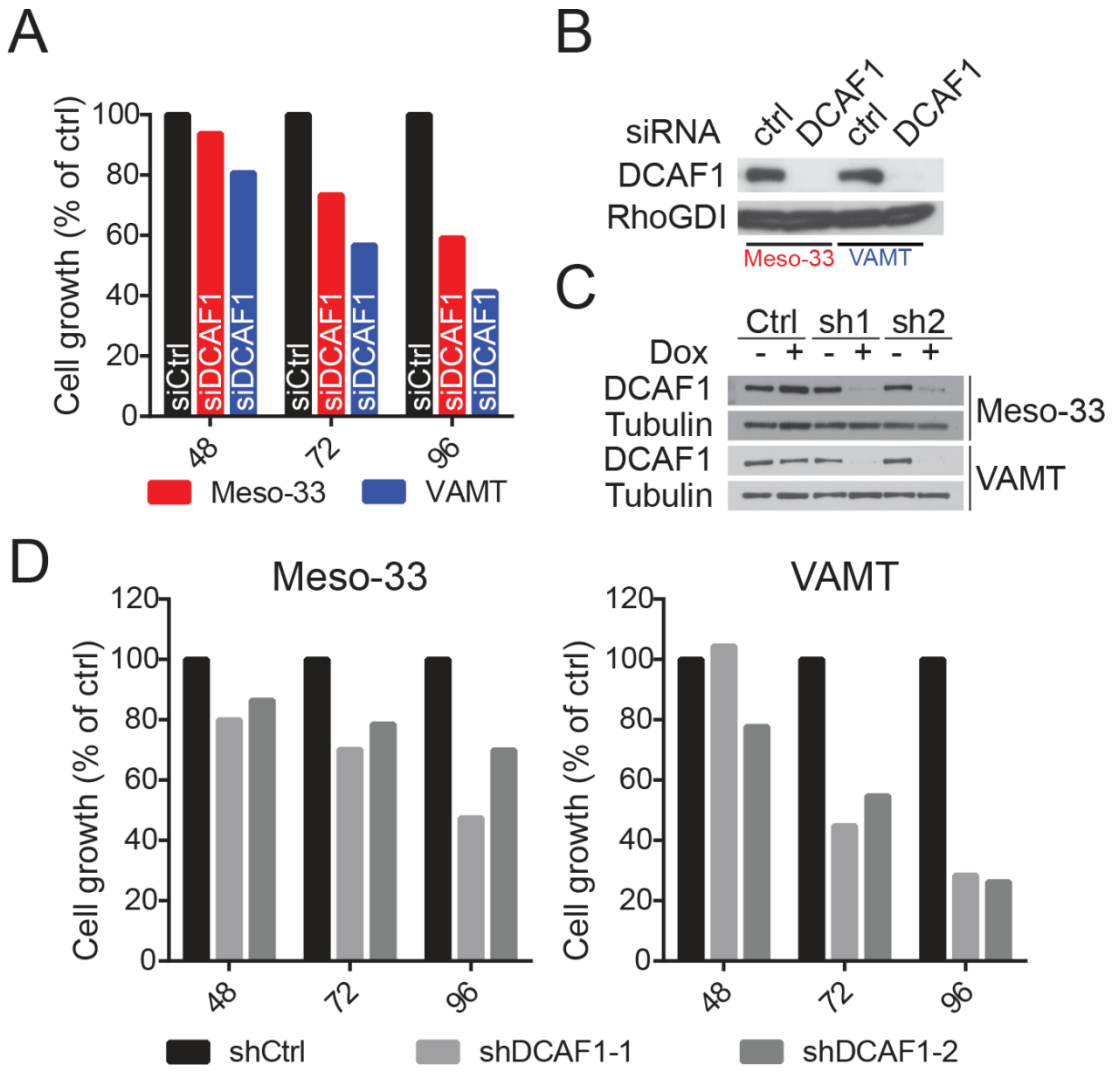

Figure 5.1: Acute DCAF1 depletion reduces the growth of Merlin-deficient MPM cells

(**A**) Merlin deficient Meso-33 and VAMT cells were transfected with control siRNA or a DCAF1 siRNA SMARTpool and subjected to MTT cell proliferation assay for three days beginning at 48 hours post-transfection. Average values for three technical replicates were normalized to cells treated with a control siRNA.

(**B**) Western blotting indicating efficient knockdown of DCAF1 from the same batch of cells in (**A**) 72 hours post-transfection. Cell lysates were immunoblotted as indicated.

(**C**) Meso-33 and VAMT cell lines stably expressing TripZ vectors mediating doxycycline-inducible expression of control or DCAF1 shRNAs were treated ± doxycycline for 72 hours. Lysates were imunoblotted as indicated.

(**D**) Meso-33 (**left**) and VAMT (**right**) cells from (**C**) were subjected to MTT proliferation assay for the indicated times following doxycycline administration. Average values for three technical replicates were normalized to that of control shRNA-treated cells.

pharmacological inhibition of $CRL4^{DCAF1}$ would likewise counteract oncogenic signaling and hyperproliferation in Merlin-deficient MPM.

5.3: *NF2*-mutant mesothelioma is sensitive to MLN4924-mediated $CRL4^{DCAF1}$ inhibition

MLN4924 is a first-in-class inhibitor of NAE, blocking conjugation of NEDD8 to target proteins (169). Cullin E3 ligases, including $CRL4^{DCAF1}$, are the best-characterized targets of neddylation. Neddylation of the cullin subunit at a conserved lysine residue promotes a conformational shift that fully activates ubiquitin ligase conjugating activity (91, 170, 171). While several factors influence the activity of E3 ligases, including the abundance of adaptor modules, many E3 ligases display decreased ubiquitylation of target proteins upon NEDD8 depletion via MLN4924 treatment (172). To address whether I could acutely block dysregulated $CRL4^{DCAF1}$ by inhibiting NEDD8 activation, I first confirmed that the fraction of Cul4 associated with DCAF1 is de-neddylated by MLN4924 (Figure 5.2A). To assess whether neddylation is necessary for the ubiquitin conjugating activity of $CRL4^{DCAF1}$, I carried out an *in vivo* ubiquitylation assay by transfecting cells with Flag-HA-tagged DCAF1 (FH-DCAF1) and Myc-tagged ubiquitin. Following precipitation of DCAF1, I observed a MLN4924-induced dose-dependent decrease in the precipitation of lower weight ubiquitylated species (Figure 5.2B). I speculate that the higher molecular weight species which are not regulated by MLN4924 are likely auto-ubiquitylated DCAF1, whose conjugation may not depend on the conformational shift induced by neddylation of Cul4.

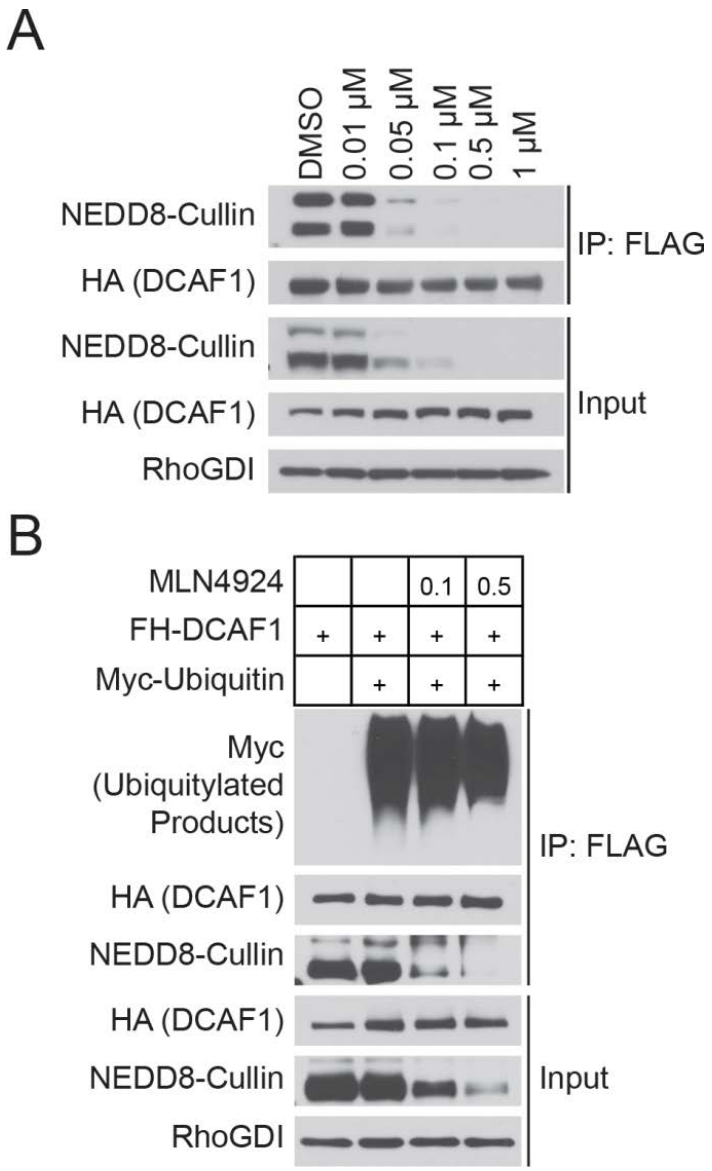

Figure 5.2: MLN4924 reduces the pool of active CRL4^{DCAF1}
(**A**) 293T cells transfected with Flag-HA-tagged DCAF1 (FH-DCAF1) were treated with the indicated concentrations of MLN4924 for 4 hours and then lysed in RIPA buffer. Input and FLAG immunoprecipitates were immunoblotted as indicated.
(**B**) COS-7 cells were transfected with FH-DCAF1 and Myc-Ubiquitin as indicated and then treated with MLN4924 at the indicated concentrations for 4 hours. FLAG immunoprecipitates and input were immunoblotted as indicated.

These *in vitro* findings along with the well-characterized anti-tumorigenic activities of MLN4924 encouraged me to assess the preclinical efficacy of NAE inhibition in Merlin-deficient MPM as a method to inhibit dysregulated $CRL4^{DCAF1}$. MLN4924 was particularly effective in inhibiting the growth of the rapidly proliferating Merlin-deficient MPM lines JMN, Meso-33, VAMT, H2052, and Meso-37. The slowest growing lines, Meso-9 and Meso-10, were presumably less susceptible to the anti-mitogenic effects of MLN4924 due to their longer cell cycle. The half-maximal growth inhibition (GI_{50}) of the faster-growing Merlin-deficient lines ranged from 0.24 to 0.56 μM with an average of 0.42 μM (Figures 5.3A and C), whereas the Merlin-positive MPM lines 211H, H-Meso, H2452, and H28 had GI_{50} values spanning 0.13 to 1.11 μM with an average GI_{50} of 0.54 μM (Figures 5.3B and D). Notably, the immortalized but untransformed mesothelial cell lines Met5a and LP9 were particularly resistant to MLN4924 (Figure 5.3B), suggesting that MPM is more sensitive to the anti-proliferative effects of MLN4924 versus normal tissue.

5.4: MLN4924 suppresses oncogenic signaling in Merlin-deficient cells

In Meso-33 and VAMT cells, MLN4924 reduces Cullin neddylation within two hours followed by a subtle but noticeable increase in phosphorylation of YAP at its inhibitory phosphorylation site Serine 127 (Figure 5.4A). In VAMT, this leads to a notable decline in the expression of Cyr61, an established YAP transcriptional target. Extended MLN4924 administration halted cell-cycle progression as assessed by reduced Rb phosphorylation in Meso-33 and

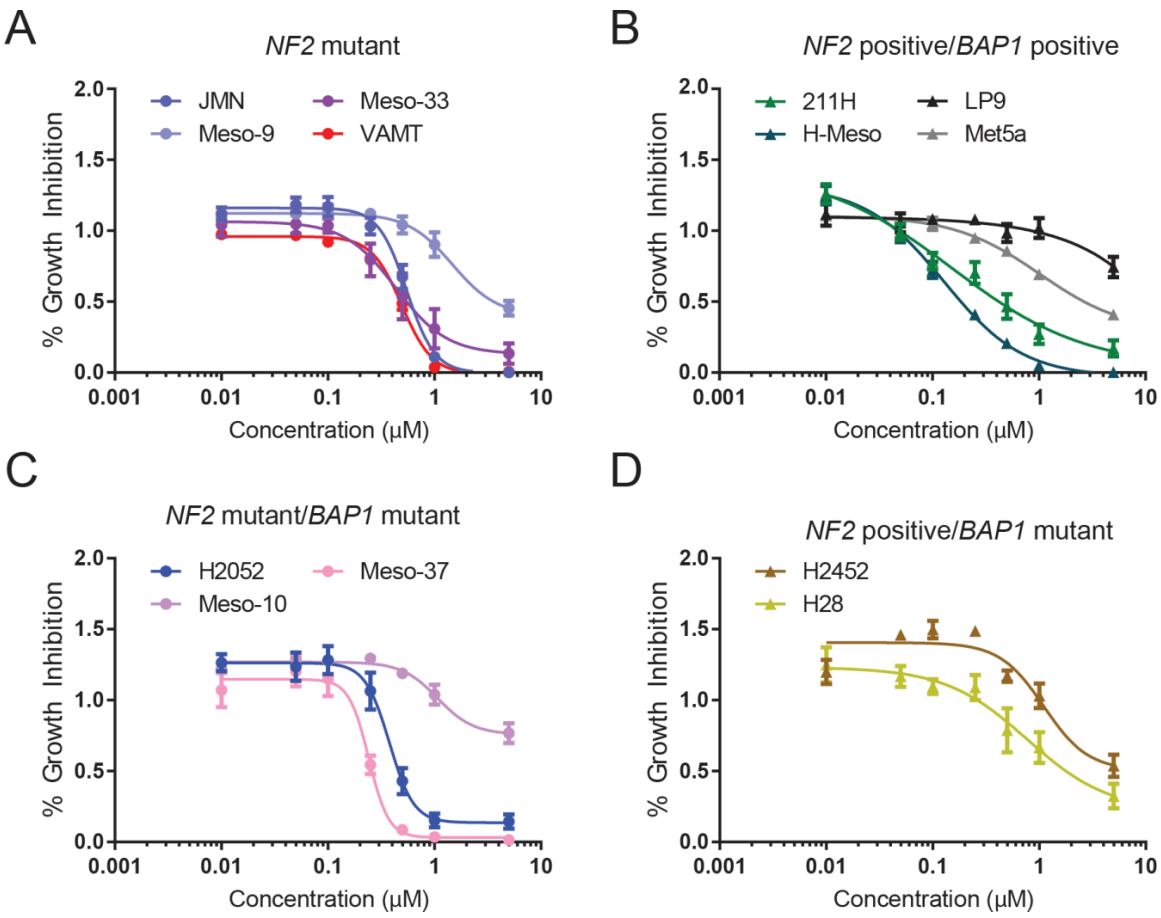

Figure 5.3: Merlin-deficient MPM lines are particularly sensitive to CRL4^{DCAF1}

(**A**) Merlin deficient MPM lines were treated with increasing doses of MLN4924 and subjected to MTT growth proliferation assay after 72 hours of treatment. Proliferation of MLN4924-treated cells was normalized to respective DMSO-treated controls. Error bars are ±SEM (n=3).

(**B**) *NF2*-positive/*BAP1*-positive MPM lines (211H and H-Meso) or immortalized mesothelial lines (Met5A and LP9) were treated as in (**A**). The immortalized but untransformed mesothelial lines are particularly resistant to MLN4924.

(**C**) MPM lines carrying both *NF2* and *BAP1* mutations were treated as in (**A**). The slow growing Meso-10 line is particularly resistant to MLN4924.

(**D**) MPM lines with mutated *BAP1* which express Merlin were treated as in (**A**). These lines have GI_{50} values exceeding 1μM.

Figure 5.4: MLN4924 suppresses oncogenic signaling and promotes cell cycle arrest in Merlin-deficient MPM cells
(**A**) and (**B**) Lysates from Meso-33 and VAMT treated with 0.5μM MLN4924 for the indicated times were immunoblotted as indicated.
(**C**) *In vivo* Lats1 ubiquitylation assay. 293T cells were transfected as indicated. 24 hours following transfection, cells were treated with the proteasome inhibitor MG132 for 4 hours to accumulate ubiquitylated proteins. Cells were also treated with the indicated μM concentration of MLN4924 for 4 hours prior to lysis in a denaturing buffer. Input and nickel precipitates were immunoblotted as indicated.

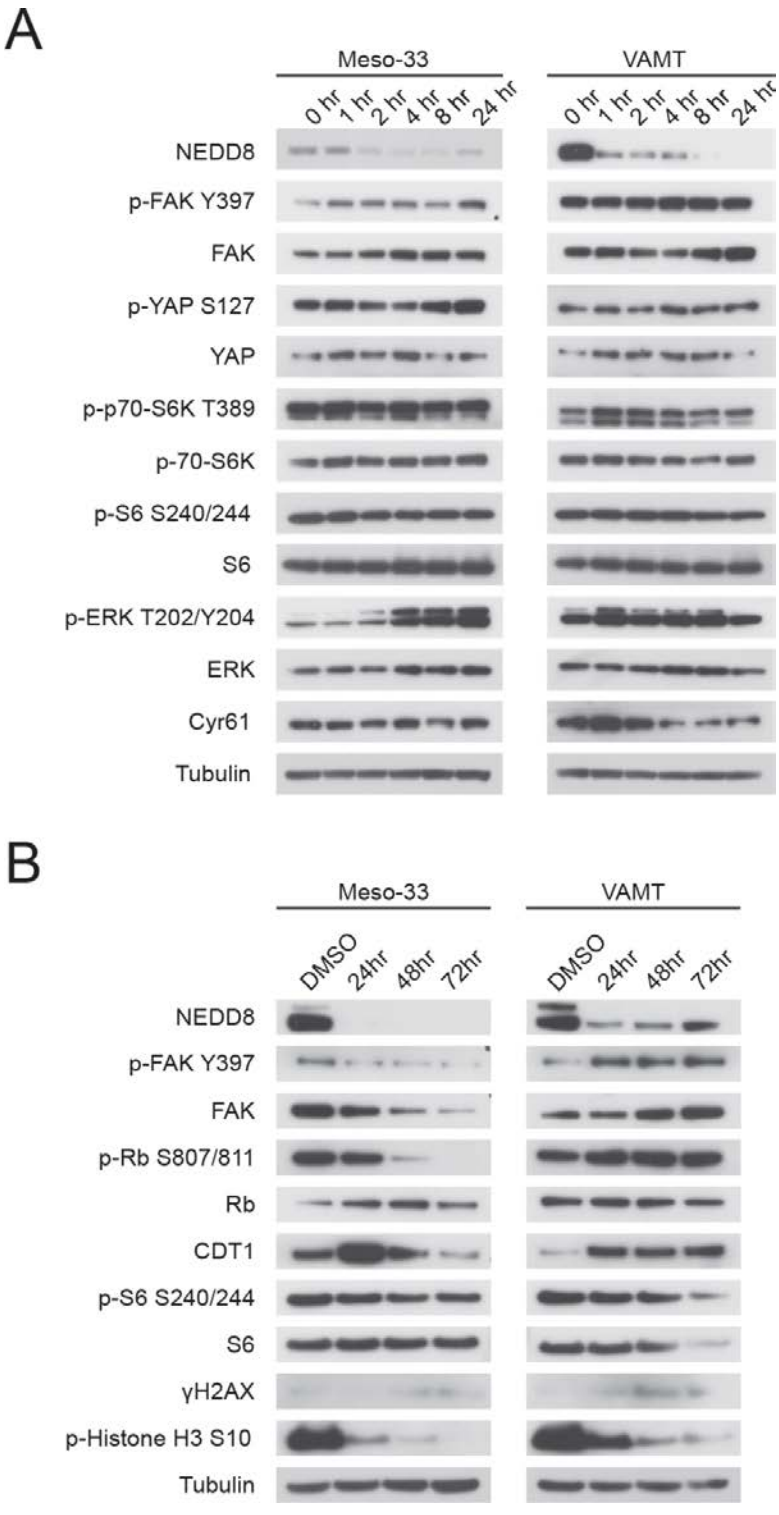
A
Meso-33
VAMT
0 hr
1 hr
2 hr
4 hr
8 hr
24 hr
NEDD8
p-FAK Y397
FAK
p-YAP S127
YAP
p-p70-S6K T389
p-70-S6K
p-S6 S240/244
S6
p-ERK T202/Y204
ERK
Cyr61
Tubulin
B
Meso-33
VAMT
DMSO
24hr
48hr
72hr
NEDD8
p-FAK Y397
FAK
p-Rb S807/811
Rb
CDT1
p-S6 S240/244
S6
γH2AX
p-Histone H3 S10
Tubulin

Figure 5.4 (continued)

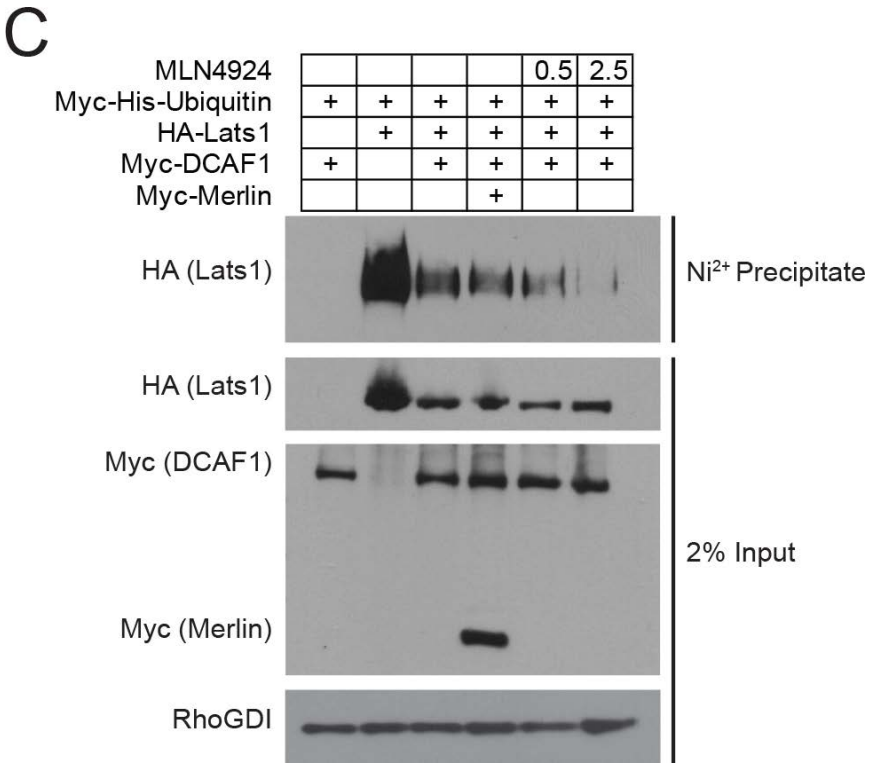

reduced Histone H3 phosphorylation in both cell lines (Figure 5.4B). MLN4924 did not consistently inhibit other oncogenic pathways in Merlin-deficient tumors including that of FAK, ERK, or mTORC (Figures 5.4A and B). These results suggested that NAE inhibition in Merlin-deficient MPM cells may reduce pro-tumorigenic YAP signaling. I conducted a ubiquitylation assay to determine whether MLN4924 blocks the ability of $CRL4^{DCAF1}$ to ubiquitylate and inhibit the Hippo pathway kinase Lats1. While Merlin expression only marginally reduced ubiquitylation of Lats1, MLN4924 administration caused a dose-dependent decrease in Lats1 ubiquitylation (Figure 5.4C). These data suggest that MLN4924 blocks inhibitory ubiquitylation of Lats1, thereby promoting inhibitory phosphorylation of oncogenic YAP. Since dysregulation of YAP-dependent transcription contributes heavily to the oncogenicity of *NF2*-mutant cells (129), the ability of MLN4924 to inhibit $CRL4^{DCAF1}$-mediated ubiquitylation of Lats may represent a critical anti-tumorigenic effect.

5.5: MLN4924 cooperates with chemotherapy to significantly delay Merlin-deficient MPM tumorigenesis

The pro-apoptotic effects of MLN4924 have been largely attributed to the stabilization of the replication licensing factor CDT1, thereby inducing DNA re-replication and contributing to DNA damage and apoptosis (173, 174). Notably, CUL4A and CUL4B are strongly linked to the DNA damage response. Blocking CRL4 ligase activity disrupts nucleotide excision repair (NER) mediated by $CRL4^{DDB2}$ and $CRL4^{CSA}$, which function in global genome NER and transcription

coupled NER, respectively. Recently it was discovered that MLN4924 blocks Ku-mediated DSB repair (175). Consistently, several studies have characterized cooperation between MLN4924 and DNA cross-linking agents (173, 176-179). I set out to determine whether MLN4924 synergizes with cisplatin - a platinum-containing DNA cross-linking drug which is used in combination with the folate antimetabolite pemetrexed as first-line chemotherapy for MPM. Treatment of Merlin-deficient cells with MLN4924, cisplatin, or both resulted in DNA damage as shown by Chk1 and Histone H2AX phosphorylation (Figure 5.5A). While cisplatin induced CDT1 degradation to halt the cell cycle as a result of DNA damage, MLN4924 stabilized CDT1 even in the presence of cisplatin. While MLN4924 and cisplatin caused a comparable level of apoptosis in Merlin-deficient MPM, the combination of the two compounds led to a synergistic increase in apoptosis (Figure 5.5B). To assess the efficacy of MLN4924 and first-line chemotherapy *in vivo*, I assessed the anti-tumorigenic activity of these compounds in two Merlin-deficient MPM xenograft models – VAMT and Meso-10. Single agent MLN4924 therapy yielded a statistically significant delay in growth (Figures 5.6A and B). In both models, first-line chemotherapeutics cisplatin and pemetrexed modestly outperformed MLN4924. Combination therapy with MLN4924, cisplatin, and pemetrexed yielded the most effective growth delay, consistent with the synergistic apoptosis induced by MLN4924 and cisplatin *in vitro* (Figures 5.5A and B and Figures 5.6A and B). It is worth noting that Meso-10 was highly resistant to MLN4924 *in vitro* as compared to the other Merlin-deficient cell lines which were faster growing in cell culture (Figures 5.3A and C).

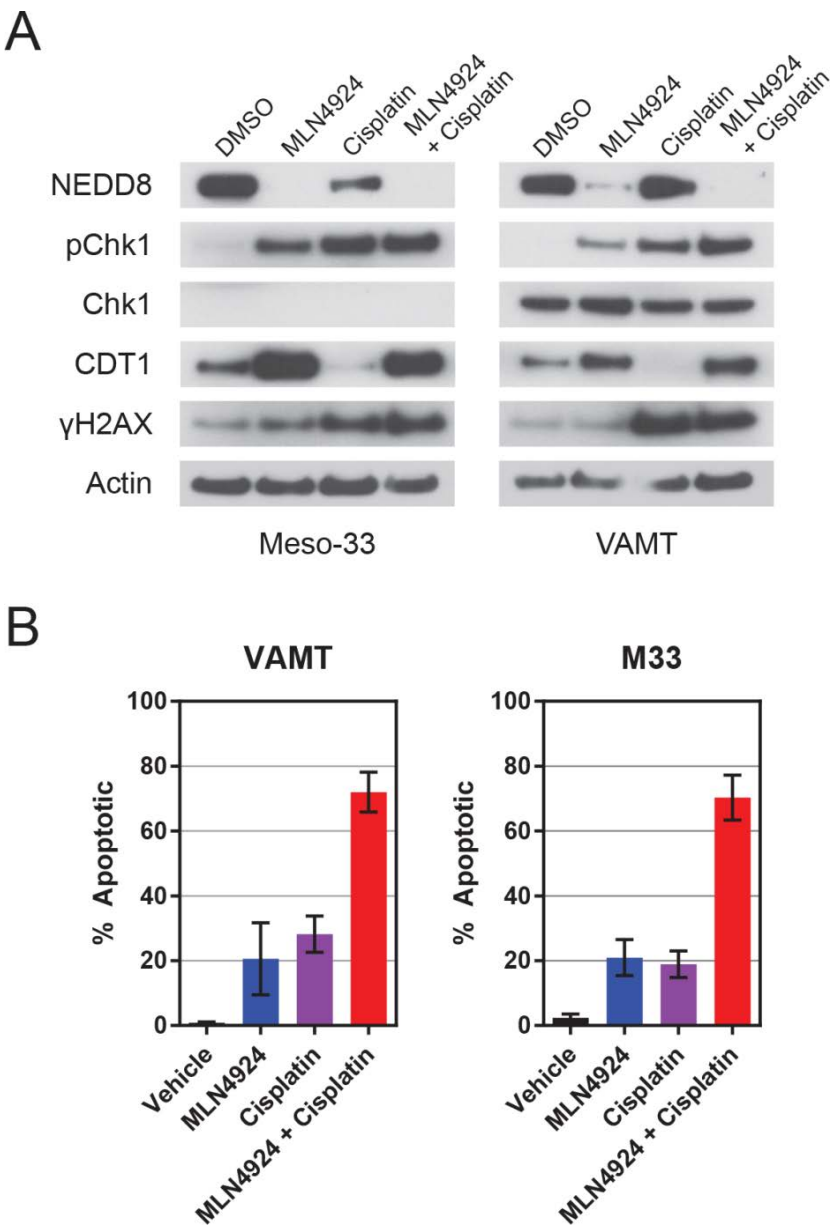

Figure 5.5: NAE inhibition cooperates with traditional MPM chemotherapy
(**A**) Meso-33 and VAMT were treated with vehicle or the indicated drugs at their respective GI_{50} concentrations for 24 hours. Cell lysates were immunoblotted as indicated.
(**B**) Meso-33 and VAMT cells were treated with vehicle or the indicated drugs at twice their respective GI_{50} concentrations for 72 hours and then subjected to an Annexin-5/PI apoptosis assay. Error bars indicate ±SEM (VAMT, n=3; Meso-33, n=2).

Figure 5.6: Pathogenic mutations disrupt the ability of Merlin to bind to DCAF1 or to inhibit CRL4^{DCAF1}

(**A**) 15 x 10^6 VAMT cells were injected bilaterally in the rear flanks of NSG mice. After xenografts exceeded 100mm^3, mice were treated with vehicle or the indicated drugs. All cisplatin treatments were 3 mg/kg (intraperitoneally, once every 7 days), pemetrexed treatments 100 mg/kg (intraperitoneally, once daily, 5 days on, 2 days off), and MLN4924 treatments 90 mg/kg (subcutaneously, twice per day, three times per week M-W-F). A 7-day holiday was provided between chemotherapy regimens while the MLN4924 was administered continuously. Data are means ± SEM (n≥12). ***$P < 0.001$, unpaired T-test.

(**B**) 8 x 10^6 Meso-10 cells were injected bilaterally in the rear flanks of NSG mice which were then treated as in (**A**). Data are means ± SEM (n≥12). ***$P < 0.001$, unpaired T-test.

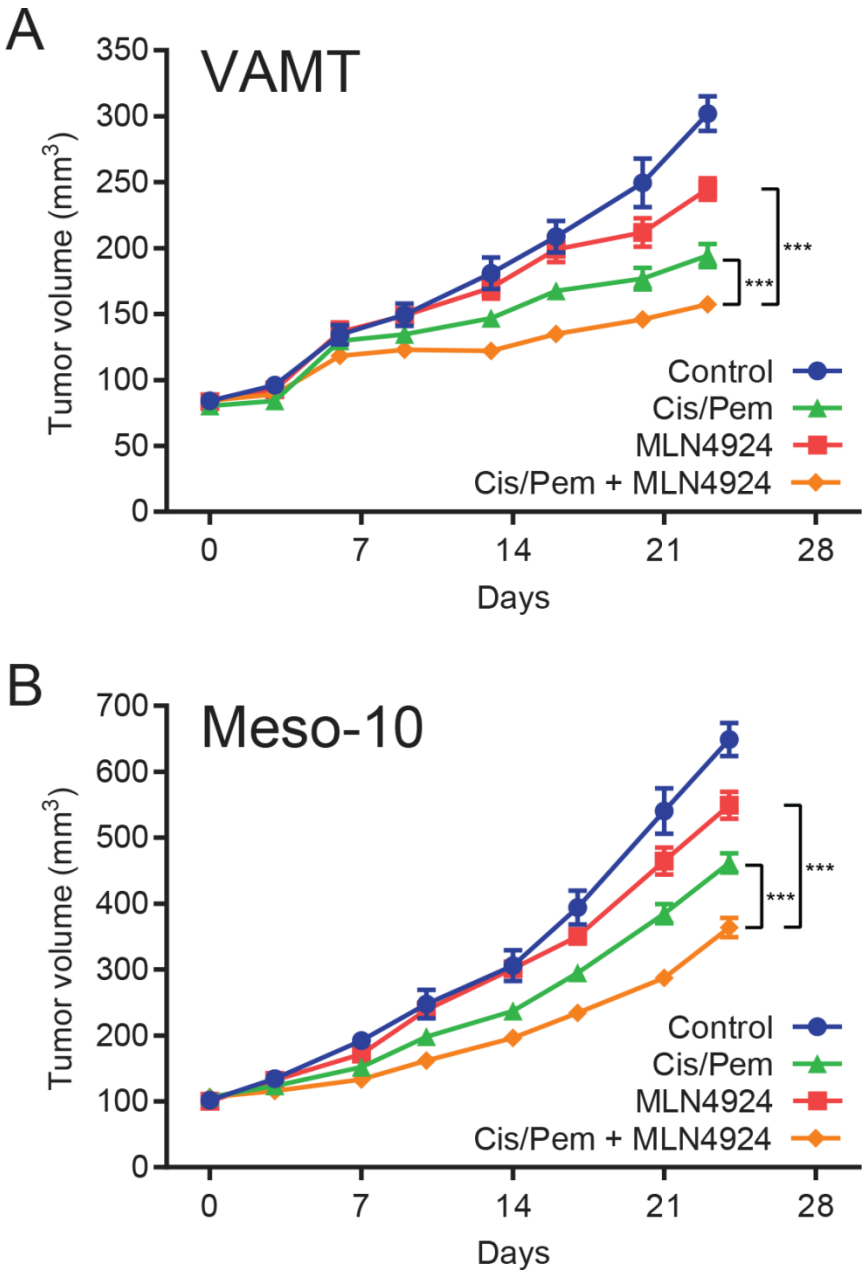
A
VAMT
Tumor volume (mm3)
350
300
250
200
150
100
50
0
0
7
14
21
28
Days
***
***
Control
Cis/Pem
MLN4924
Cis/Pem + MLN4924
B
Meso-10
Tumor volume (mm3)
700
600
500
400
300
200
100
0
0
7
14
21
28
Days
***
***
Control
Cis/Pem
MLN4924
Cis/Pem + MLN4924

However, Meso-10 grew nearly twice as fast as VAMT *in vivo*, despite it being one of the fastest-growing Merlin-deficient MPM lines in culture (compare Y-axes in Figures 5.6A and B).

5.6: NAE inhibition coupled with mechanism-based therapeutics cooperate to delay Merlin-deficient MPM

Our *in vitro* and *in vivo* efficacy studies revealed that MLN4924 administration does not inhibit mTORC1 signaling in Merlin-deficient MPM (Figures 5.4A and B). These results suggest that DCAF1 promotes oncogenic signaling independently of flux through the mTORC1-PI3K signaling axis. Interestingly, Merlin-deficient MPM lines are significantly more sensitive to the cytostatic effect of Rapamycin than Merlin-positive lines (19). We rationalized that inhibition of DCAF1 and mTORC/PI3K signaling would inhibit two prominent signaling pathways sustaining MPM tumorigenesis. A serious drawback of Rapamycin or Rapalog use in cancer is that these compounds release mTORC1-mediated negative feedback loops that function to restrain AKT-TOR signaling, leading to hyperactivation of both AKT and ERK in MPM lines (19, 180-184). Rapamycin blocks activation of S6K but releases feedback inhibition of IGF-1 by phosphorylating IRS-1 (183) whereas ERK is likely activated through loss of mTORC1-mediated phosphorylation and stabilization of GRB10 (184). GDC-0980, a dual mTOR/PI3K inhibitor, blocks mTORC1 signaling without activating feedback by simultaneously inhibiting PI3K (185). We confirmed that GDC-0980

blocks mTORC1 signaling without activating Akt or ERK in several Merlin-deficient MPM lines including Meso-33 (Figure 5.7A, Inset). Single agent therapy with GDC-0980 in VAMT xenografts yielded marginally higher, albeit statistically insignificant, efficacy relative to MLN4924 alone (Figure 5.7A). Since MLN4924 does not inhibit mTORC1 signaling, I speculated that combination therapy with MLN4924 and GDC-0980 would inhibit two of the major signaling pathways sustaining MPM proliferation. Indeed, simultaneous GDC-0980 and MLN4924 treatment resulted in tumor stasis (Figure 5.7A) which exceeded the efficacy of either single agent alone, standard first-line chemotherapy and combination therapy with MLN4924 (Figures 5.5C and D).

I collaborated with the Charles Rudin lab and the Antitumor Assessment Core at MSKCC to obtain two MPM patient-derived xenografts (PDXs). Western blotting revealed that Ru19, a rapidly growing epithelioid PDX, completely lacked Merlin expression (Figure 5.7B, Inset). Ru19 retained expression of BAP1, a deubiquitinase which is frequently lost or mutated in MPM (9, 186) and other cancers (187, 188). In contrast, I found that the slow-growing Ru13 PDX expresses Merlin but is BAP1-deficient. I elected to use Ru19 as a preclinical Merlin-deficient MPM PDX model based on its mutational status. Ru19 grew sizable tumors within two weeks following subcutaneous injection in NSG mice (Figure 5.7B). Single agent MLN4924 and GDC-0980 induced significant tumor delay ($P<0.01$ and $P<0.001$, respectively). Notably, combined MLN4924 and GDC-0980 treatment induced tumor stasis ($P<0.001$) (Figure 5.7B). Combined,

Figure 5.7: MLN4924 combined with mTORC1/PI3K inhibition induces MPM tumor stasis

The western blot in (**A, Inset**) was performed by Kamalika Moulick.

(**A**) 8-10 x 10^6 VAMT cells were injected bilaterally in the rear flanks of NSG mice. After xenografts exceeded 100mm^3, mice were treated with vehicle or the indicated drugs. MLN4924 treatments were 120 mg/kg (subcutaneously, twice per day, three times per week M-W-F). GDC-0980 treatments were 5 mg/kg (oral, once per day, five times per week). Data are means ± SEM (n=10). ****P* < 0.001, unpaired T-test. (**Inset**) Lysates from Meso-33 cells treated with increasing concentrations of GDC-0980 were immunoblotted as indicated.

(**B**) Serially transplanted Ru19 tumors were injected unilaterally in the rear flanks of NSG mice. After tumors exceeded 100mm^3, mice were treated as in (**A**). Data are means ± SEM (n=7). **P* < 0.05, unpaired T-test. (**Inset**) Lysates from Ru13 and Ru19 PDXs were immunoblotted as indicated.

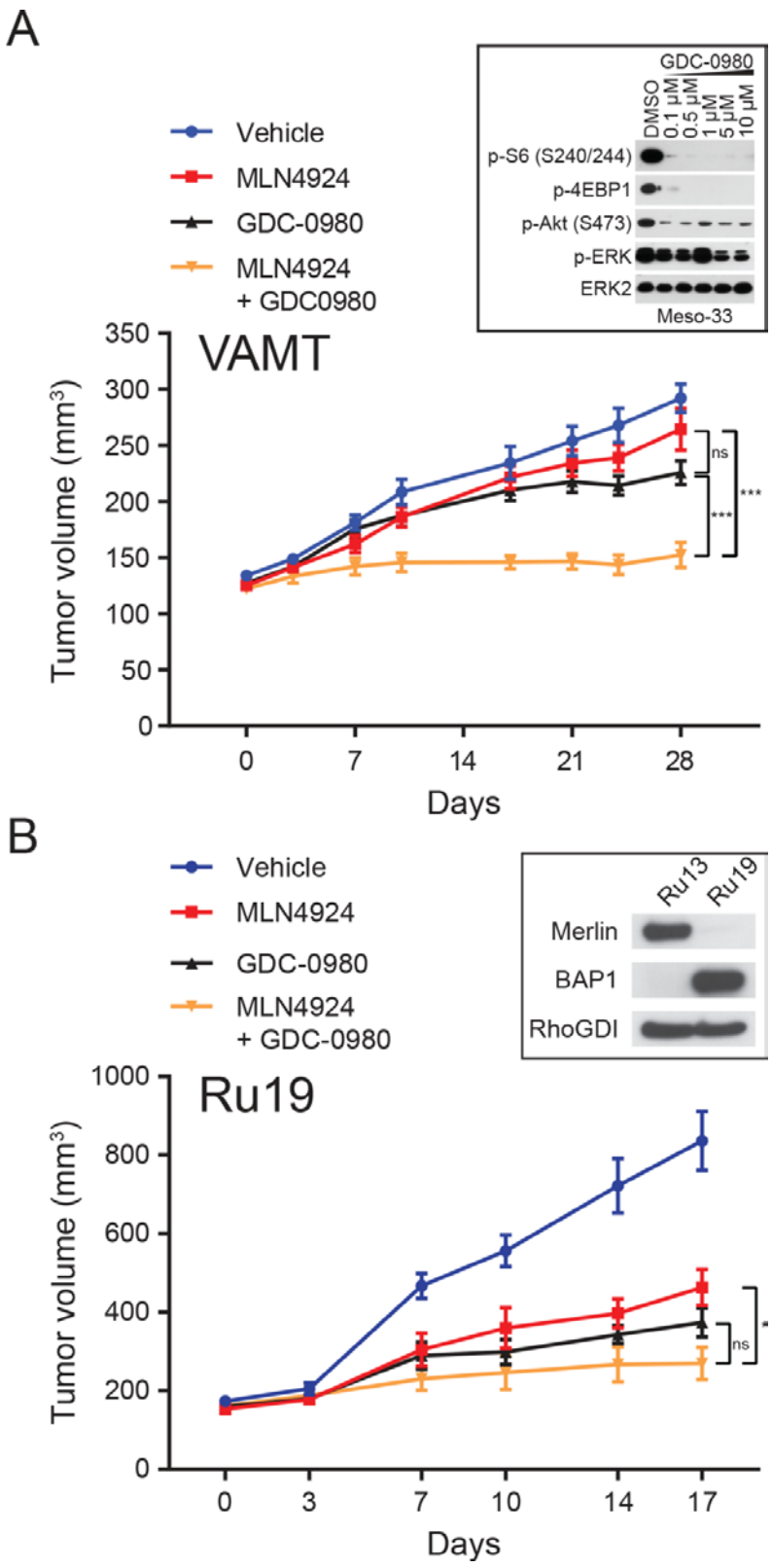
A
Vehicle
MLN4924
GDC-0980
MLN4924
+ GDC0980
GDC-0980
DMSO
0.1 μM
0.5 μM
1 μM
5 μM
10 μM
p-S6 (S240/244)
p-4EBP1
p-Akt (S473)
p-ERK
ERK2
Meso-33
VAMT
Tumor volume (mm3)
350
300
250
200
150
100
50
0
0
7
14
21
28
Days
ns
***
***
B
Vehicle
MLN4924
GDC-0980
MLN4924
+ GDC-0980
Ru13
Ru19
Merlin
BAP1
RhoGDI
Ru19
Tumor volume (mm3)
1000
800
600
400
200
0
0
3
7
10
14
17
Days
ns

these data suggest that dual inhibition of $CRL4^{DCAF1}$ and mTORC1/PI3K abrogates two of the key oncogenic signaling pathways in Merlin-deficient MPM.

5.7: Discussion

As personal cancer care progresses, it has become clear that some tumors are less amenable to targeted therapy than others. These difficult tumors lack the overexpression/amplification of well-known oncogenes such as EGFR, and instead appear to rely upon poorly characterized signaling pathways resulting from deregulation of specific tumor suppressors. Malignant pleural mesothelioma (MPM) seems to be predominantly driven by loss of tumor suppressors including *NF2*, *BAP1*, and *CDKN2A*. Targeted personalized care for patients affected with MPM is therefore likely to stem from dissection of the oncogenic signaling ensuing secondarily to tumor suppressor loss. In Merlin-deficient MPM, we found that dysregulated $CRL4^{DCAF1}$ promotes oncogenic signaling through its inhibition of the Lats1 and 2 kinases, thereby activating YAP and TAZ (129). In this study, I found that inhibition of NAE using MLN4924 reduces $CRL4^{DCAF1}$ activity. Neddylation is required to fully activate the Cullin backbone of the $CRL4^{DCAF1}$ E3 ubiquitin ligase, and disrupting this post-translational modification reduces its ubiquitin conjugating activity and specifically reduces ubiquitylation of Lats1 *in vivo*. Retaining active Lats1 and 2 thereby inhibits YAP/TAZ and ensuing oncogenic signaling. MLN4924 also broadly affects CRL ligases and therefore regulates other signaling pathways (172). Indeed, MLN4924 induces DNA re-replication and apoptosis through inhibition of

$CRL4^{CDT2}$ and inhibits multiple DNA damage repair pathways (144, 173-175, 189). NAE inhibition using MLN4924 provides a targeted therapy by inhibiting $CRL4^{DCAF1}$ but also elicits a broad chemotherapeutic effect by simultaneously inducing DNA damage and abrogating its repair.

A notable observation that arose from the xenograft experiments was that Meso-10 is more susceptible to MLN4924 *in vivo*, whereas it is relatively resistant to the compound *in vitro*. This finding could be attributed to the rapid *in vivo* growth of Meso-10, where it grows at a similar rate or likely accelerated rate relative to VAMT - an MPM line that proliferates rapidly in culture. This finding may point to *in vivo* chemotherapeutic or mechanistic-based effects of MLN4924 that are otherwise lacking in cell culture. The oncogenic pathways necessary for cell proliferation and survival *in vivo* may be more sensitive to NAE inhibition than those necessary for *in vitro* proliferation, supporting the need for pathogenically relevant tumorigenesis models.

Our lab previously found that Merlin suppresses MPM tumorigenesis by regulating mTORC1 (19). mTORC1 was shown to drive proliferation in canonical NF2 tumors including meningioma and schwannoma (18), suggesting that dysregulated mTORC1 signaling broadly promotes Merlin-deficient tumorigenesis. Dual mTOR/PI3K inhibition significantly reduces Merlin-deficient MPM tumorigenesis. Combining mTOR/PI3K blockade with MLN4924 – which blocks dysregulated $CRL4^{DCAF1}$ – abrogates two of the driving oncogenic pathways in Merlin-deficient MPM. When combined, MLN4924 and GDC-0980 induced tumor stasis in the MPM line VAMT. In contrast to VAMT, the Ru19

MPM PDX was highly sensitive to MLN4924 and GDC-0980 monotherapies, suggesting that both compounds inhibit critical pathways in this cancer.

Chapter Six

Discussion and future directions

6.1: Merlin's nuclear and cortical tumor suppressor functions

The biochemical mechanisms underlying Merlin-mediated growth suppression are unraveling at an accelerating rate, with several critical observations occurring within the past five years. It is becoming increasingly clear that Merlin suppresses cell proliferation through two modes that are defined by functions at the cortex or in the nucleus. By linking Par3 to α-catenin at adherens junctions, Merlin promotes cell adhesions and thereby tissue organization in skin epithelium (60). At tight junctions, Merlin's binding to Angiomotin releases Rich, which inactivates Rac and thereby attenuates mitogenic signaling (7, 29). As Angiomotin directly suppresses Hippo signaling in the cytoplasm (123, 124, 126) and promotes YAP activity in the nucleus (127), further insight is needed to understand the contextual relevance of these observations as well as how Merlin may be involved. Moreover, as α-catenin inhibits YAP and Wnt-β-catenin signaling, Merlin's potential regulation of these pathways through interactions with α-catenin warrants investigation. In contrast to Merlin's cortex-specific roles that largely influence cell junctions and Rac signaling, intercellular and cortical cues lead to accumulation of dephosphorylated Merlin, which translocates to the nucleus and attenuates oncogenic gene expression via inhibition of $CRL4^{DCAF1}$ (30). As $CRL4^{DCAF1}$ regulates several proteins that broadly control transcription and epigenetics (100,

106, 108, 190), Merlin is poised to dramatically alter the expression of genes in response to adhesion signaling. Furthermore, Merlin's inhibition of $CRL4^{DCAF1}$ prevents this E3 ligase from ubiquitinating and inhibitiing the Lats kinases, maintaining a clamp to restrict Hippo signaling to YAP (129). Along with the findings that Merlin recruits Lats1 at the plasma membrane to promote Hippo signaling, these recently discovered mechanisms link Merlin to a pathway that has potent affects on cell proliferation, stemness, and contact inhibition (1, 116, 129, 132).

Recently, it was found that genetic ablation of Merlin promotes drug resistance in melanoma, suggesting that loss of Merlin can drive tumor evolution following initial cancer-causing oncogenic insults (191). Moreover, unpublished preliminary findings in our lab reveal that Merlin suppresses pancreatic cancer metastasis in the mouse. This finding reiterates Merlin's broad tumor suppressive role and highlights the need to establish Merlin's biochemical functions in normal tissue and to delineate the vital pathways dysregulated in Merlin-deficient tumorigenesis. The signaling pathways known to be regulated by Merlin lay as a cornerstone for understanding Merlin's functions in adhesion signaling and tumor suppression. Research to define the importance and hierarchy of these pathways, particularly in the pursuit of drugable targets in Merlin-deficient tumors, can be expected in the near future. While *in vivo* models will be paramount in identifying and alleviating pathogenic aberrations resulting from Merlin loss, biochemical investigations including a more detailed analysis of the inactive and active forms of Merlin as well as the Merlin-$CRL4^{DCAF1}$ interaction will shed light

on Merlin's normal function and guide the advent of therapies targeting Merlin-deficient malignancies.

6.2: Mouse models of Merlin-deficient tumorigenesis

The development of germline mouse models to address pathogenically relevant Merlin-deficient tumors has been hampered by various roadblocks. Differences in the kinetics and tissue specificity of loss of heterozygosity in *Nf2*$^{+/-}$ mice leads to the development of tumors that are not seen in NF2 patients (135). NF2 tumors including schwannomas have been difficult to effectively model since they are slow-growing (136) and multiple cooperating oncogenic lesions are required to drive tumorigenesis in the mouse mesothelium (139). *Nf2* loss in the liver leads to a highly penetrant and reproducible phenotype (24, 140), but ultimately this model is not pathogenically relevant since Merlin does not appear to be substantially lost in liver cancers. The development and unique regenerative potential of the liver adds further complexity to the interpretation of genetic experiments. *Nf2* loss in the liver increases a bipotential hepatobiliary niche during early development of the liver (24), strongly suggesting genetic manipulations driven by *Albumin-Cre* are not isolated to mature hepatocytes but are instead shared with a population of progenitors whose origins remain elusive.

In order to develop a pathogenically relevant Merlin-deficient mouse model, I set out to induce Merlin-deficient MPM using viruses to simultaneously recombine conditional alleles and inhibit or delete cooperating tumor suppressors. Preliminary efforts using RNAi-mediated knockdown of tumor

suppressors was unsuccessful *in vivo*, presumably due to the lack of complete knockdown. To address this shortcoming, I developed a strategy to somatically mutate cooperating MPM tumor suppressor genes using virally delivered CRISPR/Cas9 constructs. Based on the ease and versatility of current somatic genome engineer approaches as well as the success of Merlin-deficient MPM models using compound conditional alleles (139), I am optimistic that this strategy will lead to a flexible and pathogenically relevant MPM mouse model to explore *Nf2* genetics. Furthermore, this model could provide a genetically defined Merlin-deficient model to explore the pre-clinical efficacy of novel therapeutics.

6.3: Mechanism-based therapies for Merlin-deficient malignancies

Preliminary *in vitro* and *in vivo* experiments revealed that inhibition of dysregulated $CRL4^{DCAF1}$ in Merlin-deficient malignancies restrains oncogenic signaling pathways sustaining tumor development (30, 129). I found that the NEDD8 Activating Enzyme (NAE) inhibitor MLN4924 blocks full activation of $CRL4^{DCAF1}$ and suppresses its ubiquitin conjugating activity. MLN4924 blocks the proliferation of *NF2*-mutant MPM cells and significantly delays the growth of Merlin-deficient MPM xenografts. Traditional front-line chemotherapy with cisplatin and pemetrexed cooperates with MLN4924 in tumor killing, in part through inducing DNA damage in cells where MLN4924 has abrogated DNA repair pathways. MLN4924 cooperates more extensively with the dual mTOR/PI3K inhibitor GDC-0980, revealing that inhibition of two key oncogenic signaling pathways in *NF2*-mutant MPM shows extraordinary pre-clinical efficacy.

For the vast majority of patients, MPM is a death sentence. Traditional chemotherapy extends patient survival by only a matter of months. The observation of tumor stasis in a Merlin-deficient MPM PDX is quite remarkable, and raises a very real possibility for clinical trials. Notably, MLN4924 is in Phase I clinical trials while GDC-0980 is already in Phase II trials. Newer mTOR inhibitors and second generation NAE inhibitors may also soon be available, although a combined therapy trial with MLN4924 and GDC-0980 is closer to fruition since both drugs are already in the clinic.

It will be important to address the role of mechanism-based therapeutics in other Merlin-deficient tumors such as thyroid carcinoma, renal carcinoma, gliomas, as well as canonical NF2 tumors including schwannomas, meningiomas, and ependymomas. NF2 tumors are mostly slow growing and may be far less susceptible to the chemotherapeutic effects of MLN4924 or the proliferation-inhibiting effects of GDC-0980. Tumor onset in NF2 often occurs during adolescence or early adulthood. It may be particularly difficult for young patients to tolerate these drugs, particularly in a combination therapy that is more likely to cause toxicity. Additionally, drugging *NF2*-mutant intracranial tumors - such as glioblastomas - faces the added complexity of surpassing the blood-brain barrier. GDC-0980 unfortunately has low brain penetrance, although a derivative of the compound was optimized for brain penetrance and could be a viable alternative in this case (192, 193). While the brain penetrance of MLN4924 has not been directly tested, its ability to pass the blood-brain barrier was inferred based on its low molecular weight and high lipid solubility (194).

As the predominant oncogenic signaling pathways regulated in NF2-mutant malignancies and patients are uncovered, we will be better able to tailor rational mechanism-based therapies. Although NF2-related tumors and early stage Merlin-deficient mesotheliomas are particularly difficult to treat, these tumors tend to be non-metastatic. Since these cancers are limited to the primary site, they are genetically homogenous relative to disseminated metastatic cancers and patients receiving mechanism-based therapies are more likely to respond effectively to treatment. $CRL4^{DCAF1}$ controls a large portion of the oncogenic gene expression in Merlin-deficient tumors (30, 129) and therapies targeting $CRL4^{DCAF1}$ or its most pertinent downstream oncogenic effectors in these cases may elicit a strong clinical outcome.

Chapter 7

Materials and methods

7.1: Materials

7.1.1: Antibodies

See Table 7.1 for antibodies used in these studies. The DCAF1 antibody produced in our lab was described in (30). The Myc 9E11 antibody used was produced in the Sloan Kettering Monoclonal Antibody Core Facility.

7.1.2: Cell lines

Human mesothelioma cell lines 211H, H2452, H28, H-Meso, JMN, Meso-9, Meso-10, Meso-37, VAMT, and H2051 were cultured as previously described (19). LP9 and Met5A immortalized mesothelial cells and Merlin-deficient mesothelioma Meso-33 cells were cultured in MCDB 110:199 Earle's supplemented with EGF (10 ng/ml, Invitrogen #PHG0311), Hydrocortisone (50 µg/ml, CalBioChem #3867), ITS (1%, Invitrogen #I2521), antibiotics (1%, Gemini Bio # 400-101), Fetal Bovine Serum (FBS, 15%, Invitrogen #10437-028), and L-Glutamine (2 mM, Invitrogen # 25030-081). LP9 and Met5a were also cultured in RPMI 1640 supplemented with 10% FBS, antibiotics, and L-Glutamine. COS-7, 293FT, AND 293T cells were cultured in DMEM-HG supplemented with antibiotics, 10% FBS, and L-Glutamine. To generate FC-1801 *Nf2*$^{-/-}$ mouse Schwannoma cells, primary mouse Schwann cell cultures from E12.5 *Nf2*$^{Flox/Flox}$

Table 7.1: Antibodies

Antigen	Product	Company	Application
β Actin	A3376	Sigma	WB
BAP1	SC-28383	Santa Cruz	WB
CDT1	8064	Cell Signaling	WB
Chk1	SC-8408	Santa Cruz	WB
p-Chk1 Ser345	2348	Cell Signaling	WB
Cytokeratin 19	TROMA-III	DSHB	IHC, 1.2 µg/ml
Cre	MAB3120	Millipore	WB
CTGF	SC-14939	Santa Cruz	WB
Cyr61	SC-13100	Santa Cruz	WB
DCAF1	In-house	In-house	WB
DCAF1	14966	Cell Signaling	WB, IHC (7.5 µg/ml)
DDB1	A300-462A	Bethyl	WB
Erk2	SC-154	Santa Cruz	WB
p-Erk Thr202/Tyr204	9106	Cell Signaling	WB
FAK	05-537	Millipore	WB
p-FAK Tyr397	44624G	Invitrogen	WB
GFP	1814460	Roche	WB
HA	MMS-101R	Covance	WB
p-H2AX Ser139	2577	Cell Signaling	WB
p-Histone H3 Ser10	9701	Cell Signaling	WB
Merlin	SC-332	Santa Cruz	WB
Merlin	ab88957	Abcam	WB
Merlin	12888	Cell Signaling	WB
Myc	clone 9E11	In-house	WB
NEDD8	1571-1	Abcam	WB
p16	SC-1207	Santa Cruz	WB
p19	7543	Millipore	WB
p21	SC-6246	Santa Cruz	WB
p53	2524	Cell Signaling	WB
p70S6K	2708	Cell Signaling	WB
p-p70S6K Thr389	9206	Cell Signaling	WB
RhoGDI	SC-360	Santa Cruz	WB
Rb	554136	BD	WB
p-Rb Ser807/811	9308	Cell Signaling	WB
S6 Ribosomal Protein	SC-74459	Santa Cruz	WB
p-S6 Ser240/244	2215	Cell Signaling	WB

Table 7.1 (continued)

Antigen	Product	Company	Application
SOX9	AB5535	Millipore	IHC (0.5 µg/ml)
TdTomato (dsRed)	6324	Clontech	WB
Tubulin	T6074	Sigma	WB
Biotin (Strep-HRP)	RPN1231V	Sigma	WB
YAP	4912	Cell Signaling	WB
YAP	12395	Cell Signaling	WB
YAP	14074	Cell Signaling	WB, IHC (0.05 µg/ml)
p-YAP Ser127	4911	Cell Signaling	WB
Lats1	3477	Cell Signaling	WB
Lats2	5888	Cell Signaling	WB
Lats2	13646	Cell Signaling	WB

embryos were infected with adenoviral Cre (Ad5CMVCre, University of Iowa Gene Transfer Vector Core, Iowa City, IA, USA) and immortalized *in vitro* (195). Human schwannoma cells were kindly provided by NF2 patients after informed consent. Primary human Schwann cells and schwannoma cells were isolated and cultured as previously described (15). E13.5 fetal liver progenitor cells (LPCs) were isolated from conditional mice as described previously (149). LPCs were immortalized using retrovirus expressing MSCV-Myc (generously provided by Scott Lowe) and pHAGE-GFP-shp53-Cre lentivirus described below. Cas9-expressing MEFs were produced by infecting them with lentivirus produced from lentiCas9-Blast (Addgene #52962). Unless otherwise indicated, experiments were performed on cells grown to 70-90% confluency in complete medium.

7.1.3: Mice

Animal studies were conducted in accordance with protocols approved by the Institutional Animal Care and Use Committee of MSKCC. Drug efficacy experiments using xenografts were managed by Elisa de Stanchina and performed by Qi Li at the Sloan Kettering Antitumor Assessment Facility. Sub-capsular liver injections of LPCs were carried out in collaboration with the Antitumor Assessment Facility essentially as described previously (149). *Albumin-Cre* mice were obtained from The Jackson Laboratory (Stock 003574). *Nf2*$^{Flox/Flox}$ mice were obtained from Tyler Jacks. *LSL-Luciferase* and *LSL-TdTomato* mice were a generously provided by Scott Lowe. These alleles were originally obtained from The Jackson Laboratory and backcrossed to B6.

The *Dcaf1* conditional allele was produced in collaboration with the Rockefeller University Gene Targeting Resource Center and the Sloan Kettering Transgenic Mouse Core. With preliminary help from Laetitia Kasprzyk, I designed a targeting construct based on pKOII from Nabeel Bardeesy. The pKOII-Dcaf1 targeting construct comprises a deletion region consisting of exon 14 of *Dcaf1* (*VprBp*) flanked by LoxP sites for Cre-mediated recombination and distal long and short arms of homology with a 3' Diptheria Toxin (DT) cassette. An additional 5' DT cassette was provided by Willie Mark and was PCR cloned between the AatII and NotI sites. A long arm of homology comprising 7295 bp and corresponding to genomic sequence 28228-35522 was PCR cloned from mouse BAC clone RP23-201C3 between NotI and SalI. The 5' LoxP site was cloned in between XmaI and SmaI. The deletion region comprising 1890 bp corresponding to genomic sequence 35523-37412 was cloned from CY2.4 mouse genomic DNA between SacII and BamHI. The short arm of homology comprising 4632 bp corresponding to genomic sequence 37413-42022 was also PCR cloned from CY2.4 mouse DNA between XhoI and KpnI. The final construct was transformed into STBL2 bacteria and analyzed by restriction analysis for plasmid integrity. pKOII-Dcaf1 was linearized using AatII prior to ES cell electroporation. Electroporation, clone isolation, and initial screening was performed by Ekatarina Zafranskaia at the Rockefeller University Gene Targeting Resource Center directed by Chingwen Yang. With help from Chingwen Yang and Peter Romanienko, I designed a Southern blotting strategy to confirm 3' homologous recombination using a probe hybridizing to *Dcaf1* bp 44,423-45,656 on genomic

DNA digested with BglI. The expected hybridized DNA fragment size was 17.3 kb for the WT allele and 8.4 kb for the successfully targeted conditional allele. I designed a second strategy to confirm 5' homologous recombination using probes hybridizing to *Dcaf1* bp 25604-26083, 25674-26024, or 25254-25491 on genomic DNA digested with EcoRI. Expected hybridized DNA fragment size was 26 kb for the WT allele and 12.5 kb for the successfully targeted conditional allele. Positively targeted clones were further confirmed using a probe hybridizing the Neomycin cassette. Positive clones were injected into albino blastocysts by the MSKCC Mouse Genetics Core. Highly chimeric mice were used to produce founders which were then crossed with *Flp* mice to remove the Neomycin cassette. Loss of the Neomycin cassette was confirmed by genotyping. *Dcaf1*$^{F/F}$ mice were bred to homozygosity without issue and confirmed using genotyping primers amplifying genomic DNA between bp 35,285-35,575:

Forward primer 5'-ACTTTTAGCCCAAGCTTGCCTT-3'

Reverse primer: 5'- GGCATCAAGCCTAAGAACTGACA-3'

The WT allele yielded a band of ~300 bp, the conditional allele yields a band of ~400 bp. *Dcaf1*$^{F/F}$ mice were kept in a stably breeding colony and sperm from a confirmed fertile male was frozen for long-term storage.

7.1.4: Plasmids

To generate a vector encoding Merlin bearing an amino-terminal Flag-HA tag, a cDNA encoding the Flag peptide was subcloned upstream of the sequences encoding the HA tag in pXJ40-HA-Merlin and the resulting cDNA

encoding Flag-HA-Merlin was subcloned in pRK5. To generate point mutations in Merlin, the resulting expression vector, pRK5-FH-Merlin, was subjected to site-directed mutagenesis using the Quickchange mutagenesis Kit (Stratagene). To generate pRK5-Merlin-FH, which encodes Merlin bearing a carboxy-terminal Flag-HA tag, PCR products encoding Merlin and the Flag-HA tag were subcloned in pRK5. pRK5-Myc-DCAF1 was constructed by subcloning a cDNA encoding human DCAF1 (ATCC) in pRK5-Myc. To generate pRK5-FH-DCAF1, we replaced the sequences encoding the Myc epitope in pRK5-Myc-DCAF1 with sequences encoding the Flag-HA tag. His-Myc-Ubiquitin was generously provided by Michele Pagano (Department of Pathology, NYU School of Medicine, New York, NY). pHA-Ub was described previously (196) and was generously provided by Pengbo Zhou (Pathology and Laboratory Medicine, Weill Cornell Medical College)

Constructs encoding truncation mutants of DCAF1 were generated by subcloning PCR products of a cDNA encoding human DCAF1 in pRK5-Myc and pRK5-FH. Retroviral vectors encoding FH-DCAF1 and mutants thereof were generated by subcloning the corresponding cDNAs in pBabe-hygro. Lentiviral vectors encoding Merlin-WT and Merlin-L64P were generated by subcloning the corresponding cDNAs in pLenti6/V5-D-TOPO (Invitrogen). pcDNA3-Myc-Lats1 and pcDNA3-Myc-Lats2 were generously provided by DJ Pan. To generate a vector encoding Lats1 or Lats2 bearing an amino-terminal HA or Flag-HA tag, the cDNA encoding Lats1 or Lats2 from the above pcDNA3 constructs was subcloned downstream of the sequences encoding the HA or Flag-HA tag in

pRK5-HA or pRK5-Flag-HA vector. Site-directed mutagenesis was used to generate phosphorylation site mutants of Lats1. Constructs encoding truncation mutants of DCAF1 and Lats1 were generated by subcloning PCR products of a cDNA encoding human DCAF1 or human Lats1 from the above vectors in pRK5-Myc, pRK5-FH, or pGEX vectors.

pHAGE-GFP-miR30-Cre and pHAGE-GFP-miRE-Cre vectors containing shRNAs targeting Renilla luciferase (control), p53, and p16/p19 were cloned from a parental pHAGE vector kindly provided by Jae Shim of Weill Cornell Medical College. Briefly, a miR30 or miRE cassette provided by the Scott Lowe lab at MSKCC was cloned into pHAGE-GFP upstream of the GFP cDNA between a SalI and MluI site. A PGK promoter was cloned between MluI and NheI. Cre was cloned between NheI and NdeI. To insert miR30-based shRNAs into this vector, the entire miR30 cassette containing the shRNA from a MLP vector (Scott Lowe lab) was cut out with XhoI and MluI and cloned into the linear pHAGE-GFP-miR30-Cre vector cut with the same enzymes. The pHAGE vectors carrying tandem shRNAs were designed based on a tandem-miRE MLP vector (MLPtE) with help from Chun-Hao Huang of the Scott Lowe lab. A miRtE cassette containing a shRNA of interest could be cut out of MLPtE with SbfI and MluI and cloned into the recipient miRtE-containing plasmid (either MLPtE or pHAGE-miRtE-Cre) digested with BstXI and MluI.

pX33Cre was cloned by swapping out Cre in place of Cas9 in pX333 (Addgene #64073). sgRNAs targeting *Trp53* and *Cdkn2a* were cloned into

pX33Cre in the same manner as for pX333, as described previously (157). sgRNA sequences were as follows:

sg*Cdkn2a*: 5'-TGCGATATTTGCGTTCCGCTGGG-3'

sg*Trp53*: 5'-GACCCTGTCACCGAGACCCCTGG-3'

7.1.5: Compounds

MG132 was obtained from Calbiochem (#474790), solubilized in DMSO, and used at a working concentration of 10-25 μM. MLN4924 was generously provided by Takeda Pharmaceutical Company and solubilized in DMSO for *in vitro* experiments or 10% Captisol for *in vivo* experiments. GDC-0980 was generously provided by Genentech and was solubilized in DMSO for *in vitro* experiments or 0.5% methylcellulose with 0.1% Tween-80 for *in vivo* experiments. Cisplatin was obtained from the Sloan Kettering Pharmacy and solubilized in saline for *in vivo* experiments or from Sigma and solubilized in DMF for *in vitro* experiments. Pemetrexed (Alimta) was obtained from the Sloan Kettering Pharmacy and solubilized in saline for *in vivo* experiments.

7.2: Methods

7.2.1: Apoptosis assay

Meso-33 and VAMT treated with cisplatin and MLN4924 were subjected to a Annexin-V/PI apoptosis assay using the Annexin V : FITC Apoptosis Detection Kit II (BD #556570) according to manufacturer's instructions. Annexin V- and PI-

positive cells were determined using FACS by the MSKCC Flow Cytometry Core Facility using a BD FACSCalibur Cell Analyzer.

7.2.2: Bioluminescent imaging

Mice were anesthetized using isoflurane and injected retro-orbitally with 1.5 mg (75 mg/kg) of D-luciferin. Animals were imaged in an IVIS 100 chamber within 5 minutes of luciferin injection and data were collected using Living Image software from Xenogen. To calculate average photon flux, a circular region of interest encompassing the pleural cavity was measured. Background luminescence was subtracted.

7.2.3: BrdU incorporation assay

Unless otherwise indicated, Meso-33 and Met5A cells were plated at 2.5 x 10^4 per cm^2 on fibronectin-coated coverslips and were deprived of growth factors for 24 hours. They were then incubated with complete medium supplemented with BrdU for 24 hours. After fixation with 100% cold methanol, cells were stained with BrdU Labeling and Detection Kit I (Roche). When indicated, cells were lysed in SDS-boiling buffer (10 mM Tris ph 7.5, 1% SDS, 50 mM NaF, 1 mM $NaVO_4$) and subjected to SDS-PAGE and immunoblotting.

7.2.4: Gene expression and silencing

Transient transfections in COS-7 and 293T were performed using Lipofectamine 2000 or Oligofectamine (Invitrogen). MEFs and Meso-33 were

transfected using the Lonza HUVEC Nucleofector Kit and Amaxa Nucleofector Device with program A-034. Retroviral and lentiviral vectors encoding recombinant proteins or shRNAs targeting Merlin (#1: RHS3979-97079645 and #2: RHS3979-97079647 from Open Biosystems) or DCAF1 (#1: TRCN0000129909; #2: TRCN0000129831 from Open Biosystems) were generated as previously described (197). DCAF1 GIPZ miR30-based shRNAs were obtained from Dharmacon (#1: V2THS_255610; #2: V2THS_74081) and subcloned into pTRIPZ along with a non-targeting control shRNA. Cells were incubated with infectious particles in the presence of 10 μg/ml Polybrene (Sigma) overnight. After recovery in complete medium for 24 hours, Meso-33 cells and FC-1801 cells were placed under selection medium containing 2 μg/ml puromycin, 200 μg/ml hygromycin, 500 μg/ml G418, or 10 μg/ml blasticidin. Meso-33 and Met5A cells were transfected with 75 pmol of ON-TARGETplus SMARTpool against DCAF1 or ON-TARGETplus siCONTROL Non-targeting pool (Dharmacon).

7.2.5: GI_{50} calculations

GI_{50} values were calculated based on the 72-hour growth of cells in 96-well plates following DMSO or MLN4924 treatment as assessed by MTT assay (ThermoFisher #M6494). Fresh media containing DMSO or MLN4924 was replaced daily. Drug-treated samples were normalized to DMSO-treated controls. Data from three biological replicates with three technical replicates each were used to derive a nonlinear regression curve using GraphPad Prism software. The

IC_{50} value for each curve was established using the dose-response equation log(inhibitor) vs. response – Variable slope (four parameters).

7.2.6: GST pull down assay

GST fusion proteins containing the FERM domain of Merlin and mutants thereof (WT, L46R, F62S, L64P, L141P, G197C, A211D, E270G) were expressed in BL21 (DE3) competent cells (Invitrogen C6000-03) and purified from lysates using glutathione-Sepharose 4B beads (GE Healthcare 17-0756-01). A TnT SP6 High-Yield Expression System (Promega L3261) was used to transcribe and translate DCAF1 in the presence of biotinylated lysine tRNA (Promega L5061). Ten µl of the TnT reaction, containing less than or equal to 1 µg of DCAF1, was diluted in 0.5 ml of Binding Buffer (20 mM Tris pH7.5, 100 mM NaCl, 2 mM EDTA, 10% Glycerol, 0.05% NP-40, 0.5 mM DTT, and protease inhibitors) and incubated with 0.5 µg, 1 µg, or 2 µg of each GST-FERM fusion protein immobilized on Sepharose-Glutathione for 2 hours at 4°C. After washing with Binding Buffer, the samples were analyzed by SDS-PAGE and immunoblotting. GST fusion proteins containing Lats1 residues 598-1054 (GST-Lats1-Kinase Domain) or 598-1130 (GST-Lats1-Cterm) were expressed and purified in the same manner. The same expression system was used to transcribe and translate DCAF1 or Merlin in the presence of biotinylated lysine tRNA. 10 µl of the TnT reaction, containing less than or equal to 1 µg of DCAF1 or Merlin, was diluted in 0.5 ml of Binding Buffer and incubated with GST-Lats1 fragment fusion protein immobilized on Sepharose-Glutathione for 2 hours at

4°C. After washing with Binding Buffer, the samples were analyzed by SDS-PAGE and immunoblotting.

7.2.7: Immunohistochemistry

Immunohistochemistry protocols for DCAF1, YAP, Cytokeratin 19 (CK19), and Sox9 were optimized in collaboration with Afsar Barlas at the MSKCC Molecular Cytology Core. Immunostaining was performed on 4% paraformaldehyde-fixed paraffin-embedded tissue on a Ventana Benchmark XT automated immunohistochemistry instrument. Antibody catalog numbers and working concentrations are shown in Table 7.1. For YAP, DCAF1, and Sox-9, primary antibody was incubated for 5 hours and secondary antibody (7.5 µg/ml biotinylated goat anti-rabbit IgG, Vector Labs #PK6101) was incubated for 1 hour. CK19 primary was incubated for 6 hours and secondary antibody (1:200 biotinylated rabbit anti-rat IgG, Vector Labs #BA-4000) was incubated for 52 minutes.

7.2.8: Immunoprecipitation and immunoblotting

293FT or 293T cells in 6-well plates were transiently transfected with 1 µg of pRK5 plasmids expressing tagged DCAF1 and 1 µg of pRK5 plasmids expressing tagged Lats1 or Lats2 using Lipofectamine 2000 (Invitrogen) or Polyethylenimine (PEI) and were lysed 24 hours later with RIPA buffer or RIPA buffer without SDS as indicated. To isolate Flag-HA-DCAF1, extracts were pre-cleared with Mouse IgG-Agarose (Sigma A0919) for one hour and then incubated

with anti-FLAG M2 Affinity Gel (Sigma) at 4°C for 2 hours. Immunoprecipitates were washed three or four times with RIPA buffer or RIPA buffer without SDS as indicated, and bound proteins were dissociated in 20 µL 1x SDS sample buffer (25 mM Tris pH 6.8, 4% SDS, 5% Glycerol, bromophenol blue). Eluted proteins were separated on 4-12% Bis-Tris SDS-PAGE gels (Invitrogen) and transferred to nitrocellulose or Immobilon-P membranes (Millipore). Membranes were incubated in blocking buffer (5% skim milk, 0.1% Tween, 10 mM Tris at pH 7.6, 100 mM NaCl) for 0.5-1 hour at room temperature and then with primary antibodies diluted in blocking buffer for another hour at the same temperature or overnight at 4°C. After three washes, the membranes were incubated with goat anti Rabbit HRP-conjugated antibody (1:10,000; Santa Cruz sc-2054) or goat anti-mouse HRP-conjugated antibody (1:10,000; Santa Cruz sc-2005) at room temperature for 1 hour and subjected to chemiluminescence using ECL (Pierce #1856136). When indicated, cells were lysed in SDS-boiling buffer (10 mM Tris pH 7.5, 1% SDS, 50 mM NaF, 1 mM NaVO4) and subjected to SDS-PAGE and immunoblotting.

7.2.9: Intrapleural injections

Intrapleural injections of lentivirus were carried out as described previously (198). The mouse was anesthetized using isoflurane and the right side was shaved from hind limb to forelimb to expose the ribcage. The fully anesthetized mouse was placed on its left side with the right side of the ribcage facing upwards and made slightly convex by placing a small tube or other small object

underneath the mouse. A 1 cm incision was made through the skin exposing the ribcage at the level of the diaphragm where the border between the liver and lungs can be clearly identifited. Scissors or forceps were used to gently spread the connective tissue surrounding the incision to allow for access and visualization of the injection site. Counting two to three ribs above the liver/lung border, a insulin syringe was inserted between the ribs resting on the top of a rib at an angle of ~40° towards the head of the animal. The syringe was inserted when the animal exhaled so that the lungs receded from the chest wall and the syringe was less likely to puncture the lung. After pushing the syringe into the pleural cavity, the needle head was quickly but smartly angled upwards so as to avoid piercing the lung. Immediately after positioning the needle head, the plunger of the syringe was carefully pushed down to inject ~250 µl of virus concentrate in ~3-5 seconds. A successful injection was often accompanied by a distinct fluttering motion of the lung, presumably due to the pressure differential introduced by the addition of liquid into the pleural cavity.

7.2.10: Lats *in vivo* ubiquitylation assay

293T cells in 6-well plates were transfected using Lipofectamine 2000 (Invitrogen) with 1 µg of pHis-Myc-Ub and 0.5 µg of pRK5-HA-Lats1, 1 µg of pRK5-Myc-DCAF1, and 0.25 µg pRK5-Myc-Merlin. Cells were treated with 10 µM MG132 for 4 hours and ±MLN4924 at the indicated concentrations before harvest. 24 hours after transfection, cells were scraped into cold PBS and 10% of the sample was lysed in SDS lysis buffer and reserved for immunoblotting of the

total lysate. The remaining 90% of each sample was lysed in 1 ml of Guanidinium chloride lysis buffer (6 M Guanidinium-HCL, 0.1 M NaHPO4, 0.01 M Tris/HCL, pH 8.0, 20 mM Imidazole, 10 mM β-mercaptoethanol), sonicated, and centrifuged to. Equal quantities of cleared protein lysates, as extrapolated from the quantified SDS aliquots, were incubated with 100 µl Ni-NTA magnetic beads (Qiagen #36111) for 2 hours at room temperature. After incubation, Ni-NTA magnetic beads were washed once with each of Guanidinium washing buffer (6 M Guanidinium-HCL, 0.1 M NaHPO4, 0.01 M Tris/HCL, pH 8.0, 10 mM β-mercaptoethanol, 0.2% Triton X-100), Urea washing buffer I (8 M Urea, 0.1 M NaHPO4, 0.01 M Tris/HCL, pH 8.0, 10 mM β-mercaptoethanol, 0.2% Triton X-100), Urea washing buffer II (8 M Urea, 0.1 M NaHPO4, 0.01 M Tris/HCL, pH 6.3, 10 mM β-mercaptoethanol, 0.2% Triton X-100) and Urea washing buffer III (8 M Urea, 0.1 M NaHPO4, 0.01 M Tris/HCL, pH 6.3, 10 mM β-mercaptoethanol, 0.1% Triton X-100). Bound proteins were dissociated in 20 µL SDS sample/elution buffer supplemented with 250 mM Imidazole and 5% β-mercaptoethanol and immunoblotted as indicated.

7.2.11: Preclinical efficacy in Merlin-deficient xenografts

Preclinical xenograft experiments were performed in collaboration with the MSKCC Antitumor Assessment Facility. VAMT, Meso-10, and Ru19 xenografts were implanted in the rear flank of female NOD-*scid* IL2Rgamma^{null} (NSG) mice obtained from the MSKCC Genomics Core. VAMT and Meso-10 received bilateral injections whereas Ru19 received unilateral injections due to the

heterogeneous growth of PDXs. Drug treatments begun once tumors reached approximately 100mm^3. Tumors were measured by caliper every 3-4 days and mice were sacrificed if tumors reached 1000mm^3 or if they began to ulcerate.

7.2.12: Soft agar and tumorigenicity assay

For soft agar assay, cells were trypsinized, resuspended in complete medium, and plated in 0.34% low gelling temperature agarose (Sigma A9414) in complete medium at 2x10^4 (Meso-33 cells), 1.2x10^4 (FC-1801 cells), or 1.5x10^4 (LPCs) per well in 24-well Ultra Low Cluster Plates (Costar). For the FC-1801 tumorigenicity assay, 1×10^6 cells were suspended in PBS and injected subcutaneously into the right flank of nude mice. Tumor volumes were determined by caliper measurement. Animal studies were conducted in accordance with protocols approved by the Institutional Animal Care and Use Committee of MSKCC.

7.2.13: Statistical methods

Statistical significance was determined by Student's t-test unless indicated otherwise.

7.2.14: T7E1 assay

Analysis of genomic alterations induced by CRISPR/Cas9 was determined using a T7E1 assay essentially as previously described (199). Briefly, the

genomic region surrounding the CRISPR/Cas9 cleavage site was amplified by PCR.

For the *Trp53* locus, the primers used were:

Forward: 5'- CAGAAGATATCCTGGTAAGG-3'

Reverse: 5'- CTACAGGCTGAAGAGGAACC-3'

For the *Cdkn2a* locus, the primers used were:

Forward: 5'-ATCCGAGTAGTTAACAGCGG-3'

Reverse: 5'- GGTGGGTAAAATGGGAACTT-3'

The amplicons were subjected to a cycle of melting and re-annealing to hybridize putatively heterogeneous amplicons (i.e. sense strand with WT sequence, antisense strand with an altered sequence) and then digested with T7E1, which recognizes and cleaves DNA at mismatched regions. Amplicons were run on a 2.5% agarose gel.

7.2.15: Ubiquitylation assay

Ten cm diameter plates of COS-7 cells were transfected using Lipofectamine 2000 with 3 µg of pRK5-Flag-HA-DCAF1 and 2 µg of pHis-Myc-Ub in combination with indicated quantities of pRK5-HA-Merlin, or with 3 µg of pRK5-Flag-HA-DCAF1 and 2 µg of pHA-Ub in combination with 3 µg of pRK5-Myc-Merlin-WT, pRK5-Myc-Merlin1-339, pRK5-Myc-Ezrin or empty vector. When indicated, cells were treated with 25 µM MG132 for 6 hours. Lysates containing 0.5 mg of proteins were subjected to immunoprecipitations and western blotting as already described.

REFERENCES

1. McClatchey AI, and Yap AS. Contact inhibition (of proliferation) redux. *Current opinion in cell biology.* 2012;24(5):685-94.

2. Hanahan D, and Weinberg RA. Hallmarks of cancer: the next generation. *Cell.* 2011;144(5):646-74.

3. Rouleau GA, Merel P, Lutchman M, Sanson M, Zucman J, Marineau C, Hoang-Xuan K, Demczuk S, Desmaze C, Plougastel B, et al. Alteration in a new gene encoding a putative membrane-organizing protein causes neuro-fibromatosis type 2. *Nature.* 1993;363(6429):515-21.

4. Trofatter J, MacCollin M, Rutter J, Murrell J, Duyao M, Parry D, Eldridge R, Kley N, Menon A, and Pulaski K. A novel moesin-, ezrin-, radixin-like gene is a candidate for the neurofibromatosis 2 tumor suppressor. *Cell.* 1993;75(4):826.

5. Lallemand D, Curto M, Saotome I, Giovannini M, and McClatchey AI. NF2 deficiency promotes tumorigenesis and metastasis by destabilizing adherens junctions. *Genes Dev.* 2003;17(9):1090-100.

6. Morrison H, Sherman LS, Legg J, Banine F, Isacke C, Haipek CA, Gutmann DH, Ponta H, and Herrlich P. The NF2 tumor suppressor gene product, merlin, mediates contact inhibition of growth through interactions with CD44. *Genes Dev.* 2001;15(8):968-80.

7. Okada T, Lopez-Lago M, and Giancotti FG. Merlin/NF-2 mediates contact inhibition of growth by suppressing recruitment of Rac to the plasma membrane. *J Cell Biol.* 2005;171(2):361-71.

8. Cheng JQ, Lee WC, Klein MA, Cheng GZ, Jhanwar SC, and Testa JR. Frequent mutations of NF2 and allelic loss from chromosome band 22q12 in malignant mesothelioma: evidence for a two-hit mechanism of NF2 inactivation. *Genes, chromosomes & cancer.* 1999;24(3):238-42.

9. Bott M, Brevet M, Taylor BS, Shimizu S, Ito T, Wang L, Creaney J, Lake RA, Zakowski MF, Reva B, et al. The nuclear deubiquitinase BAP1 is commonly inactivated by somatic mutations and 3p21.1 losses in malignant pleural mesothelioma. *Nature genetics.* 2011;43(7):668-72.

10. Bianchi AB, Hara T, Ramesh V, Gao J, Klein-Szanto AJ, Morin F, Menon AG, Trofatter JA, Gusella JF, Seizinger BR, et al. Mutations in transcript isoforms of the neurofibromatosis 2 gene in multiple human tumour types. *Nature genetics.* 1994;6(2):185-92.

11. Dalgliesh GL, Furge K, Greenman C, Chen L, Bignell G, Butler A, Davies H, Edkins S, Hardy C, Latimer C, et al. Systematic sequencing of renal carcinoma reveals inactivation of histone modifying genes. *Nature.* 2010;463(7279):360-3.

12. Lau YK, Murray LB, Houshmandi SS, Xu Y, Gutmann DH, and Yu Q. Merlin is a potent inhibitor of glioma growth. *Cancer Res.* 2008;68(14):5733-42.

13. Rustgi AK, Xu L, Pinney D, Sterner C, Beauchamp R, Schmidt S, Gusella JF, and Ramesh V. Neurofibromatosis 2 gene in human colorectal cancer. *Cancer genetics and cytogenetics.* 1995;84(1):24-6.

14. McClatchey AI, and Fehon RG. Merlin and the ERM proteins--regulators of receptor distribution and signaling at the cell cortex. *Trends Cell Biol.* 2009;19(5):198-206.

15. Kaempchen K, Mielke K, Utermark T, Langmesser S, and Hanemann CO. Upregulation of the Rac1/JNK signaling pathway in primary human schwannoma cells. *Hum Mol Genet.* 2003;12(11):1211-21.

16. Kissil JL, Wilker EW, Johnson KC, Eckman MS, Yaffe MB, and Jacks T. Merlin, the product of the Nf2 tumor suppressor gene, is an inhibitor of the p21-activated kinase, Pak1. *Mol Cell.* 2003;12(4):841-9.

17. Shaw RJ, Paez JG, Curto M, Yaktine A, Pruitt WM, Saotome I, O'Bryan JP, Gupta V, Ratner N, Der CJ, et al. The Nf2 tumor suppressor, merlin, functions in Rac-dependent signaling. *Dev Cell.* 2001;1(1):63-72.

18. James MF, Han S, Polizzano C, Plotkin SR, Manning BD, Stemmer-Rachamimov AO, Gusella JF, and Ramesh V. NF2/merlin is a novel negative regulator of mTOR complex 1, and activation of mTORC1 is associated with meningioma and schwannoma growth. *Mol Cell Biol.* 2009;29(15):4250-61.

19. Lopez-Lago MA, Okada T, Murillo MM, Socci N, and Giancotti FG. Loss of the tumor suppressor gene NF2, encoding merlin, constitutively activates integrin-dependent mTORC1 signaling. *Mol Cell Biol.* 2009;29(15):4235-49.

20. Rong R, Tang X, Gutmann DH, and Ye K. Neurofibromatosis 2 (NF2) tumor suppressor merlin inhibits phosphatidylinositol 3-kinase through binding to PIKE-L. *Proc Natl Acad Sci U S A.* 2004;101(52):18200-5.

21. Poulikakos PI, Xiao GH, Gallagher R, Jablonski S, Jhanwar SC, and Testa JR. Re-expression of the tumor suppressor NF2/merlin inhibits

invasiveness in mesothelioma cells and negatively regulates FAK. *Oncogene.* 2006;25(44):5960-8.

22. Jin H, Sperka T, Herrlich P, and Morrison H. Tumorigenic transformation by CPI-17 through inhibition of a merlin phosphatase. *Nature.* 2006;442(7102):576-9.

23. Ammoun S, Flaiz C, Ristic N, Schuldt J, and Hanemann CO. Dissecting and targeting the growth factor-dependent and growth factor-independent extracellular signal-regulated kinase pathway in human schwannoma. *Cancer Res.* 2008;68(13):5236-45.

24. Zhang N, Bai H, David KK, Dong J, Zheng Y, Cai J, Giovannini M, Liu P, Anders RA, and Pan D. The Merlin/NF2 tumor suppressor functions through the YAP oncoprotein to regulate tissue homeostasis in mammals. *Dev Cell.* 2010;19(1):27-38.

25. Hamaratoglu F, Willecke M, Kango-Singh M, Nolo R, Hyun E, Tao C, Jafar-Nejad H, and Halder G. The tumour-suppressor genes NF2/Merlin and Expanded act through Hippo signalling to regulate cell proliferation and apoptosis. *Nat Cell Biol.* 2006;8(1):27-36.

26. Zhao B, Wei X, Li W, Udan RS, Yang Q, Kim J, Xie J, Ikenoue T, Yu J, Li L, et al. Inactivation of YAP oncoprotein by the Hippo pathway is involved in cell contact inhibition and tissue growth control. *Genes Dev.* 2007;21(21):2747-61.

27. Kieran FH, Xiaomeng Z, and David MT. The Hippo pathway and human cancer. *Nature Reviews Cancer.* 2013.

28. Sher I, Hanemann CO, Karplus PA, and Bretscher A. The tumor suppressor merlin controls growth in its open state, and phosphorylation converts it to a less-active more-closed state. *Dev Cell.* 2012;22(4):703-5.

29. Yi C, Troutman S, Fera D, Stemmer-Rachamimov A, Avila JL, Christian N, Persson NL, Shimono A, Speicher DW, Marmorstein R, et al. A tight junction-associated Merlin-angiomotin complex mediates Merlin's regulation of mitogenic signaling and tumor suppressive functions. *Cancer cell.* 2011;19(4):527-40.

30. Li W, You L, Cooper J, Schiavon G, Pepe-Caprio A, Zhou L, Ishii R, Giovannini M, Hanemann CO, Long SB, et al. Merlin/NF2 suppresses tumorigenesis by inhibiting the E3 ubiquitin ligase CRL4(DCAF1) in the nucleus. *Cell.* 2010;140(4):477-90.

31. Sherman L, Xu H, Geist R, Saporito-Irwin S, Howells N, Ponta H, Herrlich P, and Gutmann D. Interdomain binding mediates tumor growth suppression by the NF2 gene product. *Oncogene.* 1997;15(20):2505-9.

32. Gonzalez-Agosti C, Wiederhold T, Herndon ME, Gusella J, and Ramesh V. Interdomain interaction of merlin isoforms and its influence on intermolecular binding to NHE-RF. *J Biol Chem.* 1999;274(48):34438-42.

33. Lallemand D, Saint-Amaux AL, and Giovannini M. Tumor-suppression functions of merlin are independent of its role as an organizer of the actin cytoskeleton in Schwann cells. *J Cell Sci.* 2009;122(Pt 22):4141-9.

34. Zoch A, Mayerl S, Schulz A, Greither T, Frappart L, Rübsam J, Heuer H, Giovannini M, and Morrison H. Merlin Isoforms 1 and 2 Both Act as Tumour Suppressors and Are Required for Optimal Sperm Maturation. *PloS one.* 2015;10(8).

35. Ahronowitz I, Xin W, Kiely R, Sims K, MacCollin M, and Nunes FP. Mutational spectrum of the NF2 gene: a meta-analysis of 12 years of research and diagnostic laboratory findings. *Hum Mutat.* 2007;28(1):1-12.

36. Bretscher A, Edwards K, and Fehon RG. ERM proteins and merlin: integrators at the cell cortex. *Nat Rev Mol Cell Biol.* 2002;3(8):586-99.

37. Shimizu T, Seto A, Maita N, Hamada K, Tsukita S, Tsukita S, and Hakoshima T. Structural basis for neurofibromatosis type 2. Crystal structure of the merlin FERM domain. *J Biol Chem.* 2002;277(12):10332-6.

38. Johnson KC, Kissil JL, Fry JL, and Jacks T. Cellular transformation by a FERM domain mutant of the Nf2 tumor suppressor gene. *Oncogene.* 2002;21(39):5990-7.

39. LaJeunesse DR, McCartney BM, and Fehon RG. Structural analysis of Drosophila merlin reveals functional domains important for growth control and subcellular localization. *J Cell Biol.* 1998;141(7):1589-99.

40. Gary R, and Bretscher A. Ezrin self-association involves binding of an N-terminal domain to a normally masked C-terminal domain that includes the F-actin binding site. *Mol Biol Cell.* 1995;6(8):1061-75.

41. Li Q, Nance MR, Kulikauskas R, Nyberg K, Fehon R, Karplus PA, Bretscher A, and Tesmer JJ. Self-masking in an intact ERM-merlin protein: an active role for the central alpha-helical domain. *J Mol Biol.* 2007;365(5):1446-59.

42. Pearson MA, Reczek D, Bretscher A, and Karplus PA. Structure of the ERM protein moesin reveals the FERM domain fold masked by an extended actin binding tail domain. *Cell.* 2000;101(3):259-70.

43. Heiska L, Alfthan K, Grönholm M, Vilja P, Vaheri A, and Carpén O. Association of ezrin with intercellular adhesion molecule-1 and -2 (ICAM-1 and ICAM-2). Regulation by phosphatidylinositol 4, 5-bisphosphate. *J Biol Chem.* 1998;273(34):21893-900.

44. Tsukita S, Oishi K, Sato N, Sagara J, and Kawai A. ERM family members as molecular linkers between the cell surface glycoprotein CD44 and actin-based cytoskeletons. *J Cell Biol.* 1994;126(2):391-401.

45. Nguyen R, Reczek D, and Bretscher A. Hierarchy of merlin and ezrin N- and C-terminal domain interactions in homo- and heterotypic associations and their relationship to binding of scaffolding proteins EBP50 and E3KARP. *J Biol Chem.* 2001;276(10):7621-9.

46. Gutmann DH, Haipek CA, and Hoang Lu K. Neurofibromatosis 2 tumor suppressor protein, merlin, forms two functionally important intramolecular associations. *J Neurosci Res.* 1999;58(5):706-16.

47. Meng JJ, Lowrie DJ, Sun H, Dorsey E, Pelton PD, Bashour AM, Groden J, Ratner N, and Ip W. Interaction between two isoforms of the NF2 tumor suppressor protein, merlin, and between merlin and ezrin, suggests modulation of ERM proteins by merlin. *J Neurosci Res.* 2000;62(4):491-502.

48. Rong R, Surace EI, Haipek CA, Gutmann DH, and Ye K. Serine 518 phosphorylation modulates merlin intramolecular association and binding to critical effectors important for NF2 growth suppression. *Oncogene.* 2004;23(52):8447-54.

49. Surace EI, Haipek CA, and Gutmann DH. Effect of merlin phosphorylation on neurofibromatosis 2 (NF2) gene function. *Oncogene.* 2004;23(2):580-7.

50. Hennigan RF, Foster LA, Chaiken MF, Mani T, Gomes MM, Herr AB, and Ip W. Fluorescence resonance energy transfer analysis of merlin conformational changes. *Mol Cell Biol.* 2010;30(1):54-67.

51. Kissil JL, Johnson KC, Eckman MS, and Jacks T. Merlin phosphorylation by p21-activated kinase 2 and effects of phosphorylation on merlin localization. *J Biol Chem.* 2002;277(12):10394-9.

52. Serrano I, McDonald PC, Lock F, Muller WJ, and Dedhar S. Inactivation of the Hippo tumour suppressor pathway by integrin-linked kinase. *Nat Commun.* 2013;4(2976.

53. Shaw RJ, McClatchey AI, and Jacks T. Regulation of the neurofibromatosis type 2 tumor suppressor protein, merlin, by adhesion and growth arrest stimuli. *J Biol Chem.* 1998;273(13):7757-64.

54. Laulajainen M, Muranen T, Carpen O, and Gronholm M. Protein kinase A-mediated phosphorylation of the NF2 tumor suppressor protein merlin at serine 10 affects the actin cytoskeleton. *Oncogene.* 2008;27(23):3233-43.

55. Alfthan K, Heiska L, Gronholm M, Renkema GH, and Carpen O. Cyclic AMP-dependent protein kinase phosphorylates merlin at serine 518 independently of p21-activated kinase and promotes merlin-ezrin heterodimerization. *J Biol Chem.* 2004;279(18):18559-66.

56. Kim HA, DeClue JE, and Ratner N. cAMP-dependent protein kinase A is required for Schwann cell growth: interactions between the cAMP and neuregulin/tyrosine kinase pathways. *J Neurosci Res.* 1997;49(2):236-47.

57. Tang X, Jang SW, Wang X, Liu Z, Bahr SM, Sun SY, Brat D, Gutmann DH, and Ye K. Akt phosphorylation regulates the tumour-suppressor merlin through ubiquitination and degradation. *Nat Cell Biol.* 2007;9(10):1199-207.

58. Qi Q, Liu X, Brat DJ, and Ye K. Merlin sumoylation is required for its tumor suppressor activity. *Oncogene.* 2013.

59. McClatchey AI, and Giovannini M. Membrane organization and tumorigenesis--the NF2 tumor suppressor, Merlin. *Genes Dev.* 2005;19(19):2265-77.

60. Gladden AB, Hebert AM, Schneeberger EE, and McClatchey AI. The NF2 tumor suppressor, Merlin, regulates epidermal development through the establishment of a junctional polarity complex. *Dev Cell.* 2010;19(5):727-39.

61. Sainio M, Zhao F, Heiska L, Turunen O, den Bakker M, Zwarthoff E, Lutchman M, Rouleau GA, Jaaskelainen J, Vaheri A, et al. Neurofibromatosis 2 tumor suppressor protein colocalizes with ezrin and CD44 and associates with actin-containing cytoskeleton. *J Cell Sci.* 1997;110 (Pt 18)(2249-60.

62. McCartney BM, and Fehon RG. Distinct cellular and subcellular patterns of expression imply distinct functions for the Drosophila homologues of moesin and the neurofibromatosis 2 tumor suppressor, merlin. *J Cell Biol.* 1996;133(4):843-52.

63. Shaw RJ, McClatchey AI, and Jacks T. Localization and functional domains of the neurofibromatosis type II tumor suppressor, merlin. *Cell Growth Differ.* 1998;9(4):287-96.

64. Gonzalez-Agosti C, Xu L, Pinney D, Beauchamp R, Hobbs W, Gusella J, and Ramesh V. The merlin tumor suppressor localizes preferentially in membrane ruffles. *Oncogene.* 1996;13(6):1239-47.

65. Scherer S, and Gutmann D. Expression of the neurofibromatosis 2 tumor suppressor gene product, merlin, in Schwann cells. *Journal of neuroscience research.* 1996;46(5):595-605.

66. Murthy A, Gonzalez-Agosti C, Cordero E, Pinney D, Candia C, Solomon F, Gusella J, and Ramesh V. NHE-RF, a regulatory cofactor for Na(+)-H+ exchange, is a common interactor for merlin and ERM (MERM) proteins. *J Biol Chem.* 1998;273(3):1273-6.

67. Schlegelmilch K, Mohseni M, Kirak O, Pruszak J, Rodriguez JR, Zhou D, Kreger BT, Vasioukhin V, Avruch J, Brummelkamp TR, et al. Yap1 acts downstream of alpha-catenin to control epidermal proliferation. *Cell.* 2011;144(5):782-95.

68. Silvis MR, Kreger BT, Lien WH, Klezovitch O, Rudakova GM, Camargo FD, Lantz DM, Seykora JT, and Vasioukhin V. alpha-catenin is a tumor suppressor that controls cell accumulation by regulating the localization and activity of the transcriptional coactivator Yap1. *Science signaling.* 2011;4(174):ra33.

69. Choi SH, Estarás C, Moresco JJ, Yates JR, and Jones KA. α-Catenin interacts with APC to regulate β-catenin proteolysis and transcriptional repression of Wnt target genes. *Genes Dev.* 2013;27(22):2473-88.

70. Jessica SB, and Stephen PJ. Ubiquitylation, neddylation and the DNA damage response. *Open Biology.* 2015.

71. Ernkvist M, Luna Persson N, Audebert S, Lecine P, Sinha I, Liu M, Schlueter M, Horowitz A, Aase K, Weide T, et al. The Amot/Patj/Syx signaling complex spatially controls RhoA GTPase activity in migrating endothelial cells. *Blood.* 2009;113(1):244-53.

72. Stickney JT, Bacon WC, Rojas M, Ratner N, and Ip W. Activation of the tumor suppressor merlin modulates its interaction with lipid rafts. *Cancer Res.* 2004;64(8):2717-24.

73. Mani T, Hennigan RF, Foster LA, Conrady DG, Herr AB, and Ip W. FERM domain phosphoinositide binding targets merlin to the membrane and is

essential for its growth-suppressive function. *Mol Cell Biol.* 2011;31(10):1983-96.

74. Okada M, Wang Y, Jang SW, Tang X, Neri LM, and Ye K. Akt phosphorylation of merlin enhances its binding to phosphatidylinositols and inhibits the tumor-suppressive activities of merlin. *Cancer Res.* 2009;69(9):4043-51.

75. Brault E, Gautreau A, Lamarine M, Callebaut I, Thomas G, and Goutebroze L. Normal membrane localization and actin association of the NF2 tumor suppressor protein are dependent on folding of its N-terminal domain. *J Cell Sci.* 2001;114(Pt 10):1901-12.

76. Bensenor LB, Barlan K, Rice SE, Fehon RG, and Gelfand VI. Microtubule-mediated transport of the tumor-suppressor protein Merlin and its mutants. *Proc Natl Acad Sci U S A.* 2010;107(16):7311-6.

77. Xu HM, and Gutmann DH. Merlin differentially associates with the microtubule and actin cytoskeleton. *J Neurosci Res.* 1998;51(3):403-15.

78. Smole Z, Thoma CR, Applegate KT, Duda M, Gutbrodt KL, Danuser G, and Krek W. Tumor Suppressor NF2/Merlin Is a Microtubule Stabilizer. *Cancer Res.* 2014;74(1):353-62.

79. Hennigan R, Moon C, Parysek L, Monk K, Morfini G, Berth S, Brady S, and Ratner N. The NF2 tumor suppressor regulates microtubule-based vesicle trafficking via a novel Rac, MLK and p38(SAPK) pathway. *Oncogene.* 2012.

80. Lee J, and Zhou P. DCAFs, the missing link of the CUL4-DDB1 ubiquitin ligase. *Mol Cell.* 2007;26(6):775-80.

81. O'Connell BC, and Harper JW. Ubiquitin proteasome system (UPS): what can chromatin do for you? *Current opinion in cell biology.* 2007;19(2):206-14.

82. Muranen T, Gronholm M, Renkema GH, and Carpen O. Cell cycle-dependent nucleocytoplasmic shuttling of the neurofibromatosis 2 tumour suppressor merlin. *Oncogene.* 2005;24(7):1150-8.

83. Kressel M, and Schmucker B. Nucleocytoplasmic transfer of the NF2 tumor suppressor protein merlin is regulated by exon 2 and a CRM1-dependent nuclear export signal in exon 15. *Human Molecular Genetics.* 2002;11(19):2269-78.

84. Zhang S, Feng Y, Narayan O, and Zhao LJ. Cytoplasmic retention of HIV-1 regulatory protein Vpr by protein-protein interaction with a novel human cytoplasmic protein VprBP. *Gene.* 2001;263(1-2):131-40.

85. Zhao LJ, Mukherjee S, and Narayan O. Biochemical mechanism of HIV-I Vpr function. Specific interaction with a cellular protein. *J Biol Chem.* 1994;269(22):15577-82.

86. Angers S, Li T, Yi X, MacCoss MJ, Moon RT, and Zheng N. Molecular architecture and assembly of the DDB1-CUL4A ubiquitin ligase machinery. *Nature.* 2006;443(7111):590-3.

87. Hrecka K, Gierszewska M, Srivastava S, Kozaczkiewicz L, Swanson S, Florens L, Washburn M, and Skowronski J. Lentiviral Vpr usurps Cul4-DDB1[VprBP] E3 ubiquitin ligase to modulate cell cycle. *Proceedings of the National Academy of Sciences of the United States of America.* 2007;104(28):11778-83.

88. Le Rouzic E, Belaidouni N, Estrabaud E, Morel M, Rain JC, Transy C, and Margottin-Goguet F. HIV1 Vpr arrests the cell cycle by recruiting DCAF1/VprBP, a receptor of the Cul4-DDB1 ubiquitin ligase. *Cell Cycle.* 2007;6(2):182-8.

89. Li T, Robert EI, van Breugel PC, Strubin M, and Zheng N. A promiscuous alpha-helical motif anchors viral hijackers and substrate receptors to the CUL4-DDB1 ubiquitin ligase machinery. *Nature structural & molecular biology.* 2010;17(1):105-11.

90. Li T, Chen X, Garbutt KC, Zhou P, and Zheng N. Structure of DDB1 in complex with a paramyxovirus V protein: viral hijack of a propeller cluster in ubiquitin ligase. *Cell.* 2006;124(1):105-17.

91. Petroski MD, and Deshaies RJ. Function and regulation of cullin-RING ubiquitin ligases. *Nat Rev Mol Cell Biol.* 2005;6(1):9-20.

92. Maitra S, Kulikauskas RM, Gavilan H, and Fehon RG. The tumor suppressors Merlin and Expanded function cooperatively to modulate receptor endocytosis and signaling. *Current biology : CB.* 2006;16(7):702-9.

93. Conlon I, and Raff M. Size control in animal development. *Cell.* 1999;96(2):235-44.

94. Lloyd AC. The regulation of cell size. *Cell.* 2013;154(6):1194-205.

95. Ahn J, Hao C, Yan J, DeLucia M, Mehrens J, Wang C, Gronenborn A, and Skowronski J. HIV/simian immunodeficiency virus (SIV) accessory

virulence factor Vpx loads the host cell restriction factor SAMHD1 onto the E3 ubiquitin ligase complex CRL4DCAF1. *The Journal of biological chemistry.* 2012;287(15):12550-8.

96. Yu J, Zheng Y, Dong J, Klusza S, Deng WM, and Pan D. Kibra functions as a tumor suppressor protein that regulates Hippo signaling in conjunction with Merlin and Expanded. *Dev Cell.* 2010;18(2):288-99.

97. Chen CL, Gajewski KM, Hamaratoglu F, Bossuyt W, Sansores-Garcia L, Tao C, and Halder G. The apical-basal cell polarity determinant Crumbs regulates Hippo signaling in Drosophila. *Proc Natl Acad Sci U S A.* 2010;107(36):15810-5.

98. Schwefel D, Groom HC, Boucherit VC, Christodoulou E, Walker PA, Stoye JP, Bishop KN, and Taylor IA. Structural basis of lentiviral subversion of a cellular protein degradation pathway. *Nature.* 2013.

99. Lee J, Lee J, Kim H, Kim K, Park H, Kim J-Y, Lee S, Kim I, Kim J, Lee M, et al. EZH2 generates a methyl degron that is recognized by the DCAF1/DDB1/CUL4 E3 ubiquitin ligase complex. *Molecular cell.* 2012;48(4):572-86.

100. Kim K, Kim JM, Kim JS, Choi J, Lee YS, Neamati N, Song JS, Heo K, and An W. VprBP has intrinsic kinase activity targeting histone H2A and represses gene transcription. *Mol Cell.* 2013;52(3):459-67.

101. Ahn J, Vu T, Novince Z, Guerrero-Santoro J, Rapic-Otrin V, and Gronenborn AM. HIV-1 Vpr loads uracil DNA glycosylase-2 onto DCAF1, a substrate recognition subunit of a cullin 4A-ring E3 ubiquitin ligase for proteasome-dependent degradation. *J Biol Chem.* 2010;285(48):37333-41.

102. Laguette N, Bregnard C, Hue P, Basbous J, Yatim A, Larroque M, Kirchhoff F, Constantinou A, Sobhian B, and Benkirane M. Premature Activation of the SLX4 Complex by Vpr Promotes G2/M Arrest and Escape from Innate Immune Sensing. *Cell.* 2014;156(1-2):134-45.

103. Tamori Y, Bialucha CU, Tian AG, Kajita M, Huang YC, Norman M, Harrison N, Poulton J, Ivanovitch K, Disch L, et al. Involvement of Lgl and Mahjong/VprBP in cell competition. *PLoS biology.* 2010;8(7):e1000422.

104. Kassmeier MD, Mondal K, Palmer VL, Raval P, Kumar S, Perry GA, Anderson DK, Ciborowski P, Jackson S, Xiong Y, et al. VprBP binds full-length RAG1 and is required for B-cell development and V(D)J recombination fidelity. *The EMBO journal.* 2012;31(4):945-58.

105. Kaur M, Khan M, Kar A, Sharma A, and Saxena S. CRL4-DDB1-VPRBP ubiquitin ligase mediates the stress triggered proteolysis of Mcm10. *Nucleic acids research.* 2012;40(15):7332-46.

106. Kim K, Heo K, Choi J, Jackson S, Kim H, Xiong Y, and An W. Vpr-binding protein antagonizes p53-mediated transcription via direct interaction with H3 tail. *Mol Cell Biol.* 2012;32(4):783-96.

107. Chao Y, Shu-Yan J, Qian-Qian S, Qing-Yuan S, and Heng-Yu F. CRL4-DCAF1 ubiquitin E3 ligase directs protein phosphatase 2A degradation to control oocyte meiotic maturation. *Nature Communications.* 2015;6(8017.

108. Yu C, Zhang YL, Pan WW, Li XM, Wang ZW, Ge ZJ, Zhou JJ, Cang Y, Tong C, Sun QY, et al. CRL4 complex regulates mammalian oocyte survival and reprogramming by activation of TET proteins. *Science.* 2013;342(6165):1518-21.

109. Tan L, and Shi YG. Tet family proteins and 5-hydroxymethylcytosine in development and disease. *Development.* 2012;139(11):1895-902.

110. Pan D. The hippo signaling pathway in development and cancer. *Dev Cell.* 2010;19(4):491-505.

111. Zhao B, Tumaneng K, and Guan KL. The Hippo pathway in organ size control, tissue regeneration and stem cell self-renewal. *Nat Cell Biol.* 2011;13(8):877-83.

112. Zhou D, Conrad C, Xia F, Park JS, Payer B, Yin Y, Lauwers GY, Thasler W, Lee JT, Avruch J, et al. Mst1 and Mst2 maintain hepatocyte quiescence and suppress hepatocellular carcinoma development through inactivation of the Yap1 oncogene. *Cancer cell.* 2009;16(5):425-38.

113. Lee KP, Lee JH, Kim TS, Kim TH, Park HD, Byun JS, Kim MC, Jeong WI, Calvisi DF, Kim JM, et al. The Hippo-Salvador pathway restrains hepatic oval cell proliferation, liver size, and liver tumorigenesis. *Proc Natl Acad Sci U S A.* 2010;107(18):8248-53.

114. Lu L, Li Y, Kim SM, Bossuyt W, Liu P, Qiu Q, Wang Y, Halder G, Finegold MJ, Lee JS, et al. Hippo signaling is a potent in vivo growth and tumor suppressor pathway in the mammalian liver. *Proc Natl Acad Sci U S A.* 2010;107(4):1437-42.

115. Song H, Mak KK, Topol L, Yun K, Hu J, Garrett L, Chen Y, Park O, Chang J, Simpson RM, et al. Mammalian Mst1 and Mst2 kinases play essential roles in organ size control and tumor suppression. *Proc Natl Acad Sci U S A.* 2010;107(4):1431-6.

116. Johnson R, and Halder G. The two faces of Hippo: targeting the Hippo pathway for regenerative medicine and cancer treatment. *Nature reviews Drug discovery.* 2014;13(1):63-79.

117. Harvey K, and Tapon N. The Salvador-Warts-Hippo pathway - an emerging tumour-suppressor network. *Nat Rev Cancer.* 2007;7(3):182-91.

118. Grusche FA, Richardson HE, and Harvey KF. Upstream regulation of the hippo size control pathway. *Current biology : CB.* 2010;20(13):R574-82.

119. Saburi S, Hester I, Fischer E, Pontoglio M, Eremina V, Gessler M, Quaggin SE, Harrison R, Mount R, and McNeill H. Loss of Fat4 disrupts PCP signaling and oriented cell division and leads to cystic kidney disease. *Nature genetics.* 2008;40(8):1010-5.

120. Mao Y, Mulvaney J, Zakaria S, Yu T, Morgan KM, Allen S, Basson MA, Francis-West P, and Irvine KD. Characterization of a Dchs1 mutant mouse reveals requirements for Dchs1-Fat4 signaling during mammalian development. *Development.* 2011;138(5):947-57.

121. Visser-Grieve S, Hao Y, and Yang X. Human homolog of Drosophila expanded, hEx, functions as a putative tumor suppressor in human cancer cell lines independently of the Hippo pathway. *Oncogene.* 2012;31(9):1189-95.

122. Vanessa SR-O, Sarat C, Nen CP, Poulikos IP, Maurizio S, Elizabeth M, José B, Sylvie G, and Neal R. mTOR Kinase Inhibition Causes Feedback-Dependent Biphasic Regulation of AKT Signaling. *Cancer Discovery.* 2011;1(3):248-59.

123. Chan SW, Lim CJ, Chong YF, Pobbati AV, Huang C, and Hong W. Hippo pathway-independent restriction of TAZ and YAP by angiomotin. *J Biol Chem.* 2011;286(9):7018-26.

124. Paramasivam M, Sarkeshik A, Yates JR, Fernandes MJ, and McCollum D. Angiomotin family proteins are novel activators of the LATS2 kinase tumor suppressor. *Mol Biol Cell.* 2011;22(19):3725-33.

125. Wang W, Huang J, and Chen J. Angiomotin-like proteins associate with and negatively regulate YAP1. *J Biol Chem.* 2011;286(6):4364-70.

126. Zhao B, Li L, Lu Q, Wang LH, Liu CY, Lei Q, and Guan KL. Angiomotin is a novel Hippo pathway component that inhibits YAP oncoprotein. *Genes Dev.* 2011;25(1):51-63.

127. Yi C, Shen Z, Stemmer-Rachamimov A, Dawany N, Troutman S, Showe LC, Liu Q, Shimono A, Sudol M, Holmgren L, et al. The p130 isoform of

angiomotin is required for Yap-mediated hepatic epithelial cell proliferation and tumorigenesis. *Science signaling.* 2013;6(291):ra77.

128. Li Y, Wei Z, Zhang J, Yang Z, and Zhang M. Structural basis of the binding of Merlin FERM domain to the E3 ubiquitin ligase substrate adaptor DCAF1. *The Journal of biological chemistry.* 2014;289(21):14674-81.

129. Li W, Cooper J, Zhou L, Yang C, Erdjument-Bromage H, Zagzag D, Snuderl M, Ladanyi M, Hanemann CO, Zhou P, et al. Merlin/NF2 loss-driven tumorigenesis linked to CRL4(DCAF1)-mediated inhibition of the hippo pathway kinases Lats1 and 2 in the nucleus. *Cancer cell.* 2014;26(1):48-60.

130. Jin J, Arias EE, Chen J, Harper JW, and Walter JC. A family of diverse Cul4-Ddb1-interacting proteins includes Cdt2, which is required for S phase destruction of the replication factor Cdt1. *Mol Cell.* 2006;23(5):709-21.

131. Youjun L, Hao Z, Fengzhi L, Siew Wee C, Zhijie L, Zhiyi W, Zhou Y, Fusheng G, Chun Jye L, Wancai X, et al. Angiomotin binding-induced activation of Merlin/NF2 in the Hippo pathway. *Cell Research.* 2015;25(7):801-17.

132. Yin F, Yu J, Zheng Y, Chen Q, Zhang N, and Pan D. Spatial organization of Hippo signaling at the plasma membrane mediated by the tumor suppressor Merlin/NF2. *Cell.* 2013;154(6):1342-55.

133. Toji S, Yabuta N, Hosomi T, Nishihara S, Kobayashi T, Suzuki S, Tamai K, and Nojima H. The centrosomal protein Lats2 is a phosphorylation target of Aurora-A kinase. *Genes to cells : devoted to molecular & cellular mechanisms.* 2004;9(5):383-97.

134. Yang X, Yu K, Hao Y, Li DM, Stewart R, Insogna KL, and Xu T. LATS1 tumour suppressor affects cytokinesis by inhibiting LIMK1. *Nat Cell Biol.* 2004;6(7):609-17.

135. McClatchey AI, Saotome I, Mercer K, Crowley D, Gusella JF, Bronson RT, and Jacks T. Mice heterozygous for a mutation at the Nf2 tumor suppressor locus develop a range of highly metastatic tumors. *Genes Dev.* 1998;12(8):1121-33.

136. Giovannini M, Robanus-Maandag E, van der Valk M, Niwa-Kawakita M, Abramowski V, Goutebroze L, Woodruff JM, Berns A, and Thomas G. Conditional biallelic Nf2 mutation in the mouse promotes manifestations of human neurofibromatosis type 2. *Genes Dev.* 2000;14(13):1617-30.

137. Kalamarides M, Niwa-Kawakita M, Leblois H, Abramowski V, Perricaudet M, Janin A, Thomas G, Gutmann DH, and Giovannini M. Nf2 gene inactivation in arachnoidal cells is rate-limiting for meningioma development in the mouse. *Genes Dev.* 2002;16(9):1060-5.

138. Fleury-Feith J, Lecomte C, Renier A, Matrat M, Kheuang L, Abramowski V, Levy F, Janin A, Giovannini M, and Jaurand MC. Hemizygosity of Nf2 is associated with increased susceptibility to asbestos-induced peritoneal tumours. *Oncogene.* 2003;22(24):3799-805.

139. Jongsma J, van Montfort E, Vooijs M, Zevenhoven J, Krimpenfort P, van der Valk M, van de Vijver M, and Berns A. A conditional mouse model for malignant mesothelioma. *Cancer cell.* 2008;13(3):261-71.

140. Benhamouche S, Curto M, Saotome I, Gladden AB, Liu CH, Giovannini M, and McClatchey AI. Nf2/Merlin controls progenitor homeostasis and tumorigenesis in the liver. *Genes Dev.* 2010;24(16):1718-30.

141. Zhang N, Bai H, David KK, Dong J, Zheng Y, Cai J, Giovannini M, Liu P, Anders RA, and Pan D. The Merlin/NF2 Tumor Suppressor Functions through the YAP Oncoprotein to Regulate Tissue Homeostasis in Mammals. *Dev Cell.* 2010;19(1):27-38.

142. Breuhahn K, and Schirmacher P. A Cellular View of Nf2 in Liver Homeostasis and Tumorigenesis. *Developmental Cell.* 2010;19(3):363-4.

143. Yimlamai D, Christodoulou C, Galli GG, Yanger K, Pepe-Mooney B, Gurung B, Shrestha K, Cahan P, Stanger BZ, and Camargo FD. Hippo pathway activity influences liver cell fate. *Cell.* 2014;157(6):1324-38.

144. Fischer ES, Scrima A, Bohm K, Matsumoto S, Lingaraju GM, Faty M, Yasuda T, Cavadini S, Wakasugi M, Hanaoka F, et al. The molecular basis of CRL4DDB2/CSA ubiquitin ligase architecture, targeting, and activation. *Cell.* 2011;147(5):1024-39.

145. Zender L, Xue W, Cordon-Cardo C, Hannon GJ, Lucito R, Powers S, Flemming P, Spector MS, and Lowe SW. Generation and analysis of genetically defined liver carcinomas derived from bipotential liver progenitors. *Cold Spring Harb Symp Quant Biol.* 2005;70(251-61.

146. Zender L, Xue W, Zuber J, Semighini CP, Krasnitz A, Ma B, Zender P, Kubicka S, Luk JM, Schirmacher P, et al. An oncogenomics-based in vivo RNAi screen identifies tumor suppressors in liver cancer. *Cell.* 2008;135(5):852-64.

147. Zender L, Spector MS, Xue W, Flemming P, Cordon-Cardo C, Silke J, Fan ST, Luk JM, Wigler M, Hannon GJ, et al. Identification and validation of

oncogenes in liver cancer using an integrative oncogenomic approach. *Cell.* 2006;125(7):1253-67.

148. Huang CH, Lujambio A, Zuber J, Tschaharganeh DF, Doran MG, Evans MJ, Kitzing T, Zhu N, de Stanchina E, Sawyers CL, et al. CDK9-mediated transcription elongation is required for MYC addiction in hepatocellular carcinoma. *Genes Dev.* 2014;28(16):1800-14.

149. Saborowski A, Saborowski M, Davare MA, Druker BJ, Klimstra DS, and Lowe SW. Mouse model of intrahepatic cholangiocarcinoma validates FIG-ROS as a potent fusion oncogene and therapeutic target. *Proc Natl Acad Sci U S A.* 2013;110(48):19513-8.

150. Postic C, Shiota M, Niswender KD, Jetton TL, Chen Y, Moates JM, Shelton KD, Lindner J, Cherrington AD, and Magnuson MA. Dual roles for glucokinase in glucose homeostasis as determined by liver and pancreatic beta cell-specific gene knock-outs using Cre recombinase. *J Biol Chem.* 1999;274(1):305-15.

151. Weisend CM, Kundert JA, Suvorova ES, Prigge JR, and Schmidt EE. Cre activity in fetal albCre mouse hepatocytes: Utility for developmental studies. *Genesis.* 2009;47(12):789-92.

152. Fitamant J, Kottakis F, Benhamouche S, Tian HS, Chuvin N, Parachoniak CA, Nagle JM, Perera RM, Lapouge M, Deshpande V, et al. YAP Inhibition Restores Hepatocyte Differentiation in Advanced HCC, Leading to Tumor Regression. *Cell reports.* 2015.

153. Font-Burgada J, Shalapour S, Ramaswamy S, Hsueh B, Rossell D, Umemura A, Taniguchi K, Nakagawa H, Valasek MA, Ye L, et al. Hybrid Periportal Hepatocytes Regenerate the Injured Liver without Giving Rise to Cancer. *Cell.* 2015;162(4):766-79.

154. Pasmant E, Louvrier C, Luscan A, Cohen J, Laurendeau I, Vidaud M, Vidaud D, Goutagny S, Kalamarides M, and Parfait B. Neurofibromatosis type 2 French cohort analysis using a comprehensive NF2 molecular diagnostic strategy. *Neuro-Chirurgie.* 2015.

155. Dickins RA, Hemann MT, Zilfou JT, Simpson DR, Ibarra I, Hannon GJ, and Lowe SW. Probing tumor phenotypes using stable and regulated synthetic microRNA precursors. *Nature genetics.* 2005;37(11):1289-95.

156. Fellmann C, Hoffmann T, Sridhar V, Hopfgartner B, Muhar M, Roth M, Lai DY, Barbosa IA, Kwon JS, Guan Y, et al. An optimized microRNA backbone for effective single-copy RNAi. *Cell reports.* 2013;5(6):1704-13.

157. Maddalo D, Manchado E, Concepcion CP, Bonetti C, Vidigal JA, Han YC, Ogrodowski P, Crippa A, Rekhtman N, de Stanchina E, et al. In vivo engineering of oncogenic chromosomal rearrangements with the CRISPR/Cas9 system. *Nature.* 2014;516(7531):423-7.

158. Yamashita K, Ide M, Furukawa KT, Suzuki A, Hirano H, and Ohno S. Tumor suppressor protein Lgl mediates G1 cell cycle arrest at high cell density by forming an Lgl-VprBP-DDB1 complex. *Molecular biology of the cell.* 2015.

159. Michalopoulos G. Liver regeneration. *Journal of cellular physiology.* 2007;213(2):286-300.

160. Vidigal JA, and Ventura A. Rapid and efficient one-step generation of paired gRNA CRISPR-Cas9 libraries. *Nat Commun.* 2015;6(8083.

161. Miyanaga A, Masuda M, Tsuta K, Kawasaki K, Nakamura Y, Sakuma T, Asamura H, Gemma A, and Yamada T. Hippo pathway gene mutations in malignant mesothelioma: revealed by RNA and targeted exon sequencing. *Journal of thoracic oncology : official publication of the International Association for the Study of Lung Cancer.* 2015;10(5):844-51.

162. Murakami H, Mizuno T, Taniguchi T, Fujii M, Ishiguro F, Fukui T, Akatsuka S, Horio Y, Hida T, Kondo Y, et al. LATS2 is a tumor suppressor gene of malignant mesothelioma. *Cancer Res.* 2011;71(3):873-83.

163. Yingxiang L, Angela IP, Haiwei M, Cansu C, Aizhan B, Elliot A-G, Nik J, Eric AH, David F, Hao Y, et al. A versatile reporter system for CRISPR-mediated chromosomal rearrangements. *Genome Biology.* 2015.

164. Cooper J, and Giancotti FG. Molecular insights into NF2/Merlin tumor suppressor function. *FEBS letters.* 2014;588(16):2743-52.

165. Li W, Cooper J, Karajannis MA, and Giancotti FG. Merlin: a tumour suppressor with functions at the cell cortex and in the nucleus. *EMBO reports.* 2012.

166. Matthew WS, Karen EK, Anne FF, Marc FD, Bernard EW, Anthony NI, and Erik SK. BRG-1 is required for RB-mediated cell cycle arrest. *Proceedings of the National Academy of Sciences.* 2000.

167. Anbarasi K, Kathirvel G, Bhaskar K, David R, and Steve MP. Downregulation of SWI/SNF chromatin remodeling factor subunits modulates cisplatin cytotoxicity. *Experimental Cell Research.* 2012.

168. Ladanyi M, Zauderer M, Krug L, Ito T, McMillan R, Bott M, and Giancotti F. New Strategies in Pleural Mesothelioma: BAP1 and NF2 as novel targets

for therapeutic development and risk assessment. *Clinical cancer research : an official journal of the American Association for Cancer Research.* 2012.

169. Soucy TA, Smith PG, Milhollen MA, Berger AJ, Gavin JM, Adhikari S, Brownell JE, Burke KE, Cardin DP, Critchley S, et al. An inhibitor of NEDD8-activating enzyme as a new approach to treat cancer. *Nature.* 2009;458(7239):732-6.

170. David MD, Laura AB, Daniel CS, Harold WH, Michal H, and Brenda AS. Structural insights into NEDD8 activation of cullin-RING ligases: conformational control of conjugation. *Cell.* 2008;134(6):995-1006.

171. Saha A, and Deshaies RJ. Multimodal activation of the ubiquitin ligase SCF by Nedd8 conjugation. *Molecular cell.* 2008.

172. Bennett EJ, Rush J, Gygi SP, and Harper JW. Dynamics of cullin-RING ubiquitin ligase network revealed by systematic quantitative proteomics. *Cell.* 2010;143(6):951-65.

173. Wei-Wei P, Jian-Jie Z, Chao Y, Ying X, Lian-Jun G, Hai-Yi Z, Dawang Z, Fang-Zhou S, and Heng-Yu F. Ubiquitin E3 ligase CRL4(CDT2/DCAF2) as a potential chemotherapeutic target for ovarian surface epithelial cancer. *The Journal of biological chemistry.* 201341):29680-91.

174. Lin JJ, Milhollen MA, Smith PG, Narayanan U, and Dutta A. NEDD8-targeting drug MLN4924 elicits DNA rereplication by stabilizing Cdt1 in S phase, triggering checkpoint activation, apoptosis, and senescence in cancer cells. *Cancer Res.* 2010;70(24):10310-20.

175. Jessica SB, Natalia L, Matylda S-C, Sébastien B, Carlos le S, Patrick C, Petra B, Yaron G, and Stephen PJ. Neddylation Promotes Ubiquitylation and Release of Ku from DNA-Damage Sites. *Cell reports.* 2015.

176. Steffan TN, Kevin RK, Peter GS, Claudia ME, Anthony P, Sean AB, Michael M, Stephen B, Michael T, Allison B, et al. Disrupting Protein NEDDylation with MLN4924 Is a Novel Strategy to Target Cisplatin Resistance in Ovarian Cancer. *Clinical Cancer Research.* 2013;19(13):3577-90.

177. Amir AJ, Etsuko S, Jonghoon P, Jennifer LB, Mark RC, Susan CM, Peter GS, Michael AM, Allison JB, and Anindya D. Overcoming platinum resistance in preclinical models of ovarian cancer using the neddylation inhibitor MLN4924. *Molecular cancer therapeutics.* 2013.

178. Garcia K, Blank JL, Bouck DC, Liu XJ, and Sappal DS. Nedd8-activating enzyme inhibitor MLN4924 provides synergy with mitomycin C through

interactions with ATR, BRCA1/BRCA2, and chromatin dynamics pathways. *Molecular cancer ….* 2014.

179. Kee Y, Huang M, Chang S, Moreau LA, and Park E. Inhibition of the Nedd8 system sensitizes cells to DNA interstrand cross-linking agents. *Molecular Cancer ….* 2012.

180. Courtois-Cox S, Genther Williams SM, Reczek EE, Johnson BW, McGillicuddy LT, Johannessen CM, Hollstein PE, MacCollin M, and Cichowski K. A negative feedback signaling network underlies oncogene-induced senescence. *Cancer cell.* 2006;10(6):459-72.

181. O'Reilly KE, Rojo F, She QB, Solit D, Mills GB, and Smith D. mTOR inhibition induces upstream receptor tyrosine kinase signaling and activates Akt. *Cancer research.* 2006.

182. Tremblay F, Brûlé S, Um SH, and Li Y. Identification of IRS-1 Ser-1101 as a target of S6K1 in nutrient-and obesity-induced insulin resistance. *Proceedings of the ….* 2007.

183. Shi Y, Yan H, Frost P, Gera J, and Lichtenstein A. Mammalian target of rapamycin inhibitors activate the AKT kinase in multiple myeloma cells by up-regulating the insulin-like growth factor receptor/insulin receptor …. *Molecular cancer therapeutics.* 2005.

184. Yu Y, Yoon S-OO, Poulogiannis G, Yang Q, Ma XM, Villén J, Kubica N, Hoffman GR, Cantley LC, Gygi SP, et al. Phosphoproteomic analysis identifies Grb10 as an mTORC1 substrate that negatively regulates insulin signaling. *Science (New York, NY).* 2011;332(6035):1322-6.

185. Wallin J, Edgar K, Guan J, Berry M, Prior W, Lee L, Lesnick J, Lewis C, Nonomiya J, Pang J, et al. GDC-0980 is a novel class I PI3K/mTOR kinase inhibitor with robust activity in cancer models driven by the PI3K pathway. *Molecular cancer therapeutics.* 2011;10(12):2426-36.

186. Testa JR, Cheung M, Pei J, Below JE, Tan Y, Sementino E, Cox NJ, Dogan AU, Pass HI, Trusa S, et al. Germline BAP1 mutations predispose to malignant mesothelioma. *Nature genetics.* 2011;43(10):1022-5.

187. Wiesner T, Obenauf AC, Murali R, Fried I, Griewank KG, Ulz P, Windpassinger C, Wackernagel W, Loy S, Wolf I, et al. Germline mutations in BAP1 predispose to melanocytic tumors. *Nature genetics.* 2011;43(10):1018-21.

188. Harbour JW, Onken MD, Roberson ED, Duan S, Cao L, Worley LA, Council ML, Matatall KA, Helms C, and Bowcock AM. Frequent mutation

of BAP1 in metastasizing uveal melanomas. *Science.* 2010;330(6009):1410-3.

189. Fousteri M, Vermeulen W, van Zeeland AA, and Mullenders LH. Cockayne syndrome A and B proteins differentially regulate recruitment of chromatin remodeling and repair factors to stalled RNA polymerase II in vivo. *Molecular cell.* 2006;23(4):471-82.

190. Yoshizawa T, Karim MF, Sato Y, Senokuchi T, Miyata K, Fukuda T, Go C, Tasaki M, Uchimura K, Kadomatsu T, et al. SIRT7 controls hepatic lipid metabolism by regulating the ubiquitin-proteasome pathway. *Cell metabolism.* 2014;19(4):712-21.

191. Shalem O, Sanjana NE, Hartenian E, Shi X, Scott DA, Mikkelsen TS, Heckl D, Ebert BL, Root DE, Doench JG, et al. Genome-scale CRISPR-Cas9 knockout screening in human cells. *Science.* 2014;343(6166):84-7.

192. Becker CM, Oberoi RK, McFarren SJ, Muldoon DM, Pafundi DH, Pokorny JL, Brinkmann DH, Ohlfest JR, Sarkaria JN, Largaespada DA, et al. Decreased affinity for efflux transporters increases brain penetrance and molecular targeting of a PI3K/mTOR inhibitor in a mouse model of glioblastoma. *Neuro-Oncology.* 2015.

193. Heffron TP, Salphati L, Alicke B, Cheong J, Dotson J, Edgar K, Goldsmith R, Gould SE, Lee LB, Lesnick JD, et al. The design and identification of brain penetrant inhibitors of phosphoinositide 3-kinase α. *Journal of medicinal chemistry.* 2012;55(18):8007-20.

194. Hua W, Li C, Yang Z, Li L, Jiang Y, Yu G, Zhu W, Liu Z, Duan S, Chu Y, et al. Suppression of glioblastoma by targeting the overactivated protein neddylation pathway. *Neuro Oncol.* 2015.

195. Lallemand D, Manent J, Couvelard A, Watilliaux A, Siena M, Chareyre F, Lampin A, Niwa-Kawakita M, Kalamarides M, and Giovannini M. Merlin regulates transmembrane receptor accumulation and signaling at the plasma membrane in primary mouse Schwann cells and in human schwannomas. *Oncogene.* 2008.

196. Treier M, Staszewski LM, and Bohmann D. Ubiquitin-dependent c-Jun degradation in vivo is mediated by the delta domain. *Cell.* 1994;78(5):787-98.

197. Pylayeva Y, Guo W, and Giancotti FG. Analysis of integrin signaling in genetically engineered mouse models of mammary tumor progression. *Methods Enzymol.* 2007;426(439-61.

198. Servais EL, Colovos C, Kachala SS, and Adusumilli PS. Pre-clinical mouse models of primary and metastatic pleural cancers of the lung and breast and the use of bioluminescent imaging to monitor pleural tumor burden. *Current protocols in pharmacology / editorial board, SJ Enna.* 2011;Chapter 14(Unit14 21.

199. Gonzalez F, Zhu Z, Shi ZD, Lelli K, Verma N, Li QV, and Huangfu D. An iCRISPR platform for rapid, multiplexable, and inducible genome editing in human pluripotent stem cells. *Cell stem cell.* 2014;15(2):215-26.